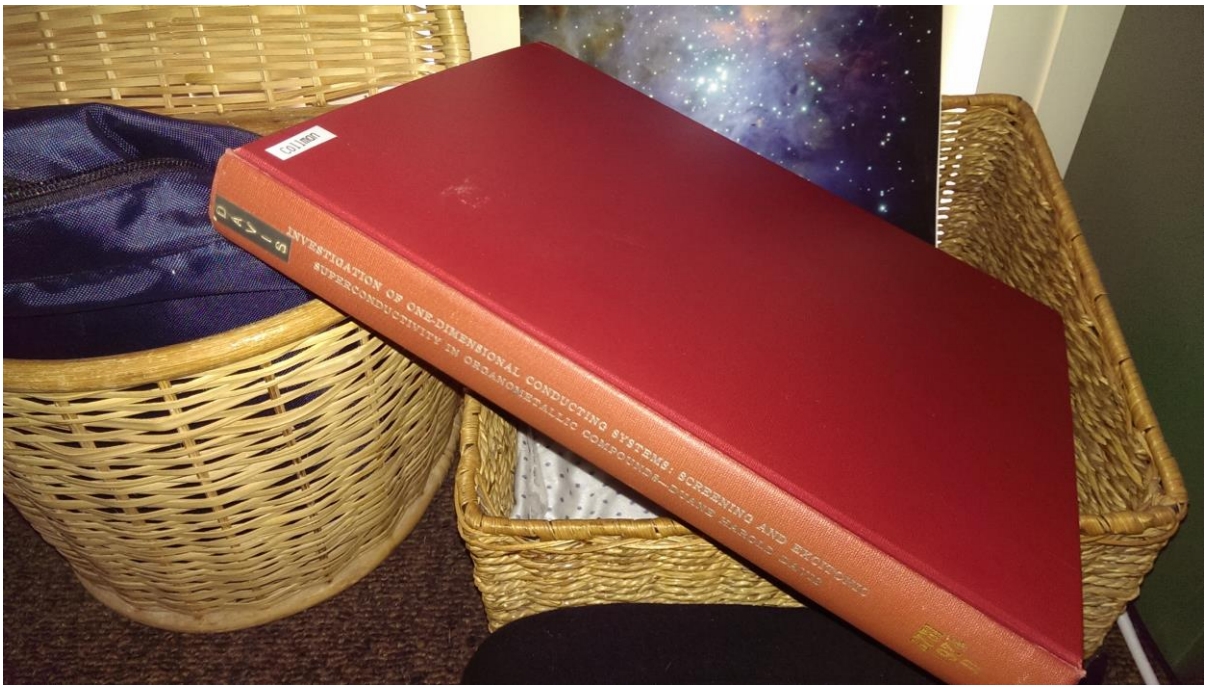

Investigation of One-Dimensional Conducting Systems: Screening and Excitonic Superconductivity in Organometallic Compounds

The Chemistry PhD Thesis of
Duane Harold Davis
August 1974

Stanford University

DAVIS

INVESTIGATION OF ONE-DIMENSIONAL CONDUCTING SYSTEMS: SCREENING AND EXCITONIC SUPERCONDUCTIVITY IN ORGANOMETALLIC COMPOUNDS—DUANE HAROLD DAVIS

INVESTIGATION OF ONE-DIMENSIONAL CONDUCTING SYSTEMS: SCREENING AND EXCITONIC SUPERCONDUCTIVITY IN ORGANOMETALLIC COMPOUNDS

A DISSERTATION

SUBMITTED TO THE DEPARTMENT OF CHEMISTRY

AND THE COMMITTEE ON GRADUATE STUDIES

OF STANFORD UNIVERSITY

IN PARTIAL FULFILLMENT OF THE REQUIREMENTS

FOR THE DEGREE OF

DOCTOR OF PHILOSOPHY

By

Duane Harold Davis

August 1974

I certify that I have read this thesis and that in my opinion it is fully adequate, in scope and quality, as a dissertation for the degree of Doctor of Philosophy.

James P. Collman
(Principal Adviser)

I certify that I have read this thesis and that in my opinion it is fully adequate, in scope and quality, as a dissertation for the degree of Doctor of Philosophy.

William A Little

I certify that I have read this thesis and that in my opinion it is fully adequate, in scope and quality, as a dissertation for the degree of Doctor of Philosophy.

Approved for the University Committee on Graduate Studies:

Dean of Graduate Studies

ACKNOWLEDGEMENTS

It is a pleasure to acknowledge the continued support, guidance, and invaluable suggestions of Dr. William A. Little, Professor of Physics. Unbeknown to Professor Little, an article entitled "Superconductivity at Room Temperature" published for laymen, generated the initial enthusiasm for this investigation many years before the author embarked on graduate study. Nor did this writer anticipate that the author of that article would be his advisor.

Certainly a debt of gratitude is owed to Dr. James P. Collman, Professor of Chemistry, whose encouragement to pursue this interdisciplinary study has always been greatly appreciated.

The author would also like to thank the National Science Foundation for its financial support.

"In all your ways acknowledge Him,
And He will make your paths straight."

Proverbs 3:6

TABLE OF CONTENTS

TABLE OF CONTENTS (continued)

LIST OF TABLES

LIST OF FIGURES

LIST OF FIGURES (continued)

Page

Figure

I. INTRODUCTION

The advances in cryogenic techniques at the beginning of the Twentieth Century gave impetus to the investigation of the low-temperature electrical properties of conducting systems. It was generally thought at that time that the resistance of a metal should increase as the temperature was lowered and the electron vapor froze to the atoms. However, investigations using precious metals – gold, silver and platinum – showed that the resistance near absolute zero attained a constant value which depended upon the residual impurities of the sample. In an effort to produce metallic wires of exceedingly high purity, Kamerlingh Onnes selected elemental mercury which could be distilled repeatedly *in vacuo*. In December 1911, Onnes observed the catastrophic loss of resistance that characterized the superconducting state.[1*]

Following two decades of cataloguing the transition temperatures of various materials, Meissner and Ochsenfeld observed a second fundamental property of superconductors: on cooling below the transition temperature, a weak magnetic field is expelled from the interior of a bulk superconductor.[2†] Several other experimental observations such as the specific heat[3] and isotope effect[4,5] also preceded the development of the first successful microscopic theory of superconductivity -- that of Bardeen, Cooper, and Schrieffer[6] --

---

*All references are listed at the end.

†The Meissner effect is characteristic of Type I superconductors. Type II superconductors were later discovered which show a mixed state in which the magnetic field may penetrate the bulk material.

in 1957. With the theoretical understanding came a variety of new experimental observations -- flux quantization,[7,8] tunneling,[9] and others.

The wealth of practical applications for superconducting materials was recognized from the beginning, and the list grew as new properties of the superconducting state were found. The ultimate drawback to the realization of most of these applications, however, was the necessity for elaborate, costly refrigeration. By 1930 the element with the highest transition temperature, niobium (9.2°K), had been catalogued.[10] Searches for higher-temperature superconductors focused on alloys, particularly those of niobium; four decades of research produced the material Nb_3Ge in thin film form with a transition temperature of 22.3°K,[11] the highest currently known.*

As the effort to obtain materials with higher transition temperatures brought diminishing returns, a new era of investigation was dramatically opened in 1964 when Little proposed that superconductivity should occur as a result of exciton-induced electron-electron attraction in the same manner as for the phonon mechanism.[13] Because of the significantly larger energies characteristic of the molecular excitons envisioned by Little compared with common Debye energies, a correspondingly higher transition temperature could be expected. Soon after a similar proposal was advanced by Ginsburg.[14,15]

The models proposed by Little and Ginsburg entail the juxtaposition of a conducting or semiconducting medium with a highly polarizable material such as a dye. In the Little model a filament of carbon or transition metal atoms known as the "spine" is surrounded by

*Recent work on the same material raises the critical temperature to 23.3°K.[12]

covalently bonded or complexed dye molecules as shown in Figure 1. Direct interaction of electrons on the spine is supplemented by indirect interaction through the excitation of the polarizable side chains. Under favorable conditions the attractive region of the exciton interaction may be sufficiently strong to dominate the Coulomb repulsion between spine electrons. That such an attractive interaction does exist is supported by the observation that highly polarizable cyanine dyes substituted on the methine bridges of copper porphin result in shifts of the near-ultraviolet "Soret" absorption band to lower energies -- up to 0.5 electron volt shift -- compared with the unsubstituted copper porphins.[16]

The Ginsburg model uses similar ingredients, but it differs in the spatial arrangement. The surface of a conducting material is coated with the polarizable material; or alternatively, alternate layers of metal and dielectric are placed on a substrate. The Little and Ginsburg models became known as one- and two-dimensional excitonic superconductors, respectively.

Soon after the proposals for these low-dimensional superconductors were published, a theoretical objection arose. Noting that at finite temperatures thermodynamic fluctuations in one-dimensional systems with short-range forces preclude the existence of a phase transition to a state with long-range order, Ferrell,[17] Rice,[18] and Hohenberg[19] concluded that such systems could not exhibit superconductivity. In response Little proposed that persistent currents still might occur in truly one-dimensional systems even in the absence of a sharp phase transition.[20] In the Ginsburg-Landau

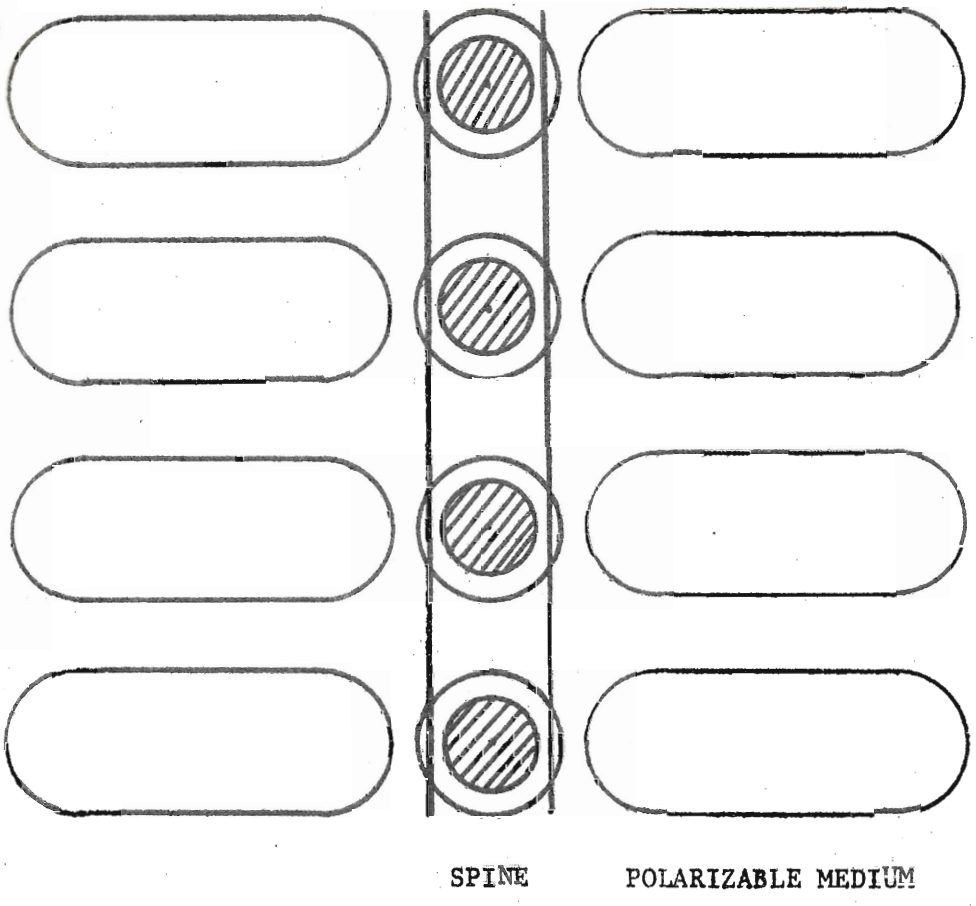

Figure 1 Proposed one-dimensional excitonic superconductor model.

theory, the supercurrent is given by $(\psi^*\nabla\psi - \psi\nabla\psi^*)$, where ψ is the quantized order parameter. To dissipate a supercurrent, it is necessary that the amplitude of ψ must become zero. While fluctuations of ψ in one dimension destroy long-range phase coherence, amplitude fluctuations are highly restricted. Studies along this line were later reported by Langer.[21] A further response, and one more in keeping with the nature of real systems, was presented by Dzyaloshinskii and Katz.[22] They proposed an array of filamentary structures with sufficient space between filaments for an excitonic medium and concluded that such a system would be a superconductor of the second type.

A further objection to the Little model was raised by Kuper.[23] On considering the lack of screening of charges in a filamentary conductor, he concluded that the strength of the excitonic attractive interaction would be insufficient to dominate the unscreened Coulomb repulsion. Extending the model calculation of Kuper by accounting for neighboring filaments, Davis found that static screening does occur for such systems.[24]

As originally proposed, the spine in the filamentary model would consist of carbon atoms with alternate double bonds. Ideally in such a structure the resonance of the bonds would give a half-filled conduction band. In the absence of a stabilizing interaction caused by the surrounding environment, however, the alternate double bonds would tend to localize. This same phenomenon is observed in a second class of compounds that serve as our primary spine models for the investigation of one-dimensional excitonic superconductivity. These are the partially oxidized platinum chain compounds investigated independently

by Krogmann.[25] Early theoretical arguments proposed and recent experimental evidence confirms that these linear chain compounds, which are metallic conductors at room temperature, are subject to a periodic distortion along the chain similar to the localization in the carbon chain and known as the Peierls distortion (see Chapter II). Such a distortion, which occurs at low temperatures, results in an energy gap in the conduction band and thus competes with Cooper pair formation for the ground state. The excitonic interaction must be sufficiently attractive to overcome this competing mechanism.

One final objection with regard to the lattice stability may be noted. On calculating the maximum transition temperature to be expected when phonon attraction and Coulomb repulsion are accounted for, as in the two square-well model of McMillan,[26] Cohen and Anderson found that the highest transition temperatures would not result from using the largest excitation energies possible (i.e., molecular excitons); rather, the typical phonon energies were more nearly the optimum energy.[27] This analysis was based on the stability requirement that the static effective interaction for any wave vector must necessarily be non-negative in order for the lattice to be stable against deformation of that wave vector. The strength of the electron-phonon coupling would be limited by the strength of the Coulomb pseudopotential, which would apply similarly to the exciton case. Cohen and Anderson went on to show, however, that such a limitation would not apply if Umklapp processes, that is, short-range scattering through wave vectors lying outside the first Brillouin zone, were allowed. Such processes occur in the Little model where

the polarization of the dyes occurs over regions in space smaller than the lattice dimensions. Similarly, Allender, Bray, and Bardeen have investigated the two-dimensional model of Ginsburg and find that the strength of the electron-exciton coupling can be greater than that of the Coulomb pseudopotential.[28] This occurs in their model under favorable conditions.

The organization of the investigation of these one-dimensional model systems as presented in this thesis is as follows. In Chapter II we review the current experimental data on the platinum chain compounds that are used to model the spine. We consider in detail the static screening calculation mentioned above. Chapter III deals with the calculation of the electronic properties of individual dye molecules and of various arrays of dyes about the spine. The development of superconductivity theory is briefly reviewed in Chapter IV and the recent theory of Kirzhnits, Maksimov, and Khomskii[29] which is used in the calculations is developed in detail. Finally, Chapter V presents the numerical method and results of these calculations, discusses the dependence of the transition temperature on the various parameters, and indicates areas of this investigation that allow for further study.

II. SCREENING

A. Metal Atom Chains

The chain of metal atoms, or "spine", serves three basic functions. These are 1) to provide a point of attachment (atom for complexation) for the dye units, 2) to provide a conducting pathway for electron flow in the superconducting state, and 3) to screen the Coulomb interaction between charges on the spine and those in the dye molecule.

Investigation of the first function is in the domain of organometallic synthesis. Much novel synthetic work has been stimulated by the request for such a metal-atom-dye system.[30,31] Figure 2 shows two ligand systems developed for this purpose.[32] While such work has

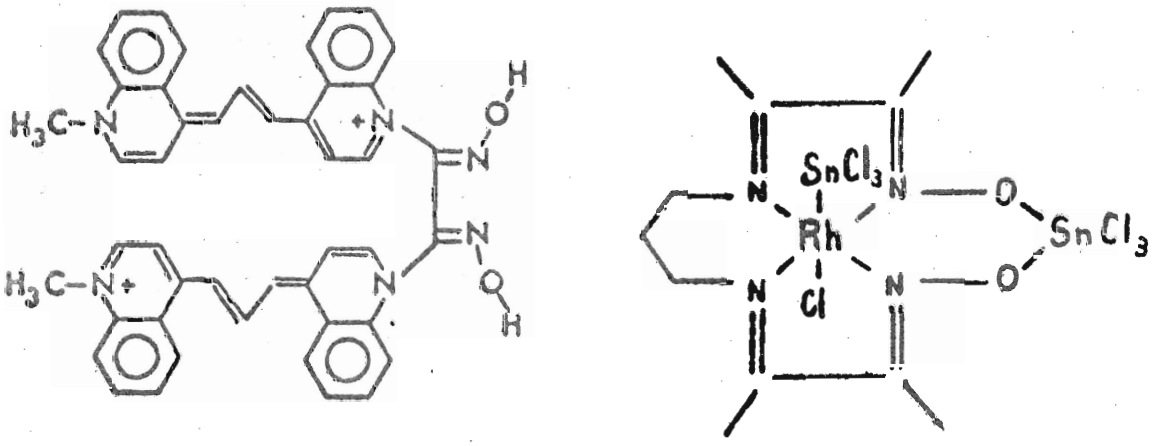

Figure 2 Ligands for metal-atom-dye systems.

produced several new discoveries in organometallic chemistry,[33] the compounds used as models in the theoretical calculations of this work are the partially oxidized platinum cyanide complexes, in particular $K_2Pt(CN)_4Cl_{0.32}\cdot 2.6H_2O$ (KCP-Cl) and $K_2Pt(CN)_4Br_{0.30}\cdot 2.3H_2O$ (KCP-Br). MVP is used to designate these partially oxidized compounds in general. As discussed later, the important discovery that dye molecules could be complexed directly to the platinum atom reaffirmed the choice of these compounds for the prototype,[32,34] and we may expect to have some freedom in the manipulation of these structures.

The ability of MVP compounds to fulfill the second function is even better established. We shall review the properties of these materials, but it may be noted in passing that the spine for a model excitonic superconductor need not be a metallic conductor in the normal phase. A semiconductor with a gap E_g may become superconducting provided the superconducting gap Δ_o is sufficiently large that the conduction band becomes populated. Using the simple BCS formulation, a superconducting phase should be found for $E_g < \Delta_o$ in the calculation by Little,[13] or $E_g < \Delta_o/2$ in the calculation by Davis.[30]

Theoretical investigation of the electrical properties of one-dimensional conducting systems began soon after the foundation was laid by Bloch in 1928 for three-dimensional materials.[35] The well-known Kronig-Penny model[36] represented the potential at each nucleus by a delta function. Matching the wave functions at each nucleus gave the eigenvalues. Using the tight-binding approximation, a simple cosine band shape, $E(k) = (E_o/2)(1 - \cos(ka))$, can be obtained for a linear array of atoms. We shall see below that this result is a good approximation to the band structure in these platinum chain compounds.

The early experimental work on one-dimensional systems began with Magnus Green Salt (MGS) which attracted attention because its deep green color could not be explained from the colors of the anion (usually red in salts and solutions) or the cation (colorless). The crystal structure was determined early (1932),[37] but the nature of the absorption was not investigated until 1951 when Yamada measured the unusual dichroism of MGS[38] and other platinum cyanide complexes.[39] He related the changes in wavelength and sharpness of the characteristic absorption band for light polarized parallel to the platinum chain on changing the cation (Mg, Ca, Ba) to the changes in the distance and strength of interaction of the platinum atoms rather than to the interaction of the platinum complex with the cation. Rundle[40] developed the platinum-platinum interaction theory using molecular orbital theory, and by 1961 a review of the metal-metal interactions in square-planar complexes was written by Miller.[41]

The assignment of the various 5d orbitals to the observed transitions in the visible spectra of square planar platinum complexes was undertaken by several investigators with conflicting results for the ordering of the energy levels.[42-45] The work of Fenske et. al.[43] included the first application of ligand field theory to these complexes. In the square planar environment the platinum 5d orbitals are split into four groups:

$$d_{xy}\ (b_{2g}),\quad d_{xz}, d_{yz}\ (e_g),\quad d_{z^2}\ (a_{1g}),\quad d_{x^2-y^2}\ (b_{1g}).$$

On investigation of a wide variety of these complexes, Miller[46] concluded that the $5d_{z^2}$ orbital would be the highest filled level and proposed a band picture using this as the valence band and the $6p_z$ as

the conduction band. At the same time Day et. al.[45] suggested the possibility of narrow band semiconduction and reported the first electrical measurement.

Other early measurements on MGS and $Ir(CO)_2acac$ (dicarbonylacetylacetoiridium) were reported by Collman[47] who noted the significant anisotropic nature of the conductivity. Atkinson, et. al.[48] studied a variety of MGS analogues reporting approximate ohmic behavior and an activation energy calculated from the expression $R = A\ e^{-E/kT}$. Extending the electrical measurements to a wider selection of compounds, Monteith, et. al.[49] measured square planar complexes of palladium, nickel, iridium, copper, and rhodium. They observed that the conductivity of nd^8 systems generally increased in the order $n=3$ to $n=5$ for analogous complexes as had been suggested by Collman.[47]

In 1969 an excellent review of the square planar complexes containing metal-metal bonds was published by Krogmann.[25] He noted that the $d_{x^2-y^2}$ orbital should lie highest, and the metal d orbitals (specifically the d_{xz} and d_{yz}[50]) should be involved in back π-bonding with the ligand molecular orbitals. More importantly he drew attention to the new class of compounds which could be formed by partial oxidation of the platinum cyanide and oxalate complexes.[51-57] Krogmann recognized that the removal of antibonding electrons from the $5d_{z^2}$ orbital on oxidation with Cl_2 or Br_2 resulted not only in stronger Pt-Pt bonding but also in metallic and paramagnetic behavior.[51] Thus began a period of intensive investigation of MVP materials. Experiments included reflection and absorption spectroscopy, magnetic circular dichroism, dc and ac conductivity, x-ray and diffuse x-ray analysis,

specific heat, Mossbauer spectroscopy, inelastic neutron scattering, NMR, and EPR.

The ordering of the 5d orbitals was soon established by Piepho et. al.[58] on measuring the magnetic circular dichroism. Their ordering is as follows:

$$d_{xy} < d_{xz}, d_{yz} \lesssim d_{z^2} \ll d_{x^2-y^2}$$

In contrast to the semiconductor behavior of the unoxidized compounds, early results of electrical measurements indicated metallic behavior in one-dimension for MVP compounds. Krogmann reported conductivities up to 10^{-2} $(\text{ohm-cm})^{-1}$ in the chain direction using a two probe technique. Minot and Perlstein[59] reported a dc conductivity of 4 $(\text{ohm-cm})^{-1}$ for KCP-Br at room temperature compared with 5×10^{-7} for $K_2Pt(CN)_4$ using a four probe technique in both cases. They also reported a Seebeck coefficient of $+12\mu v/^{o}K$ indicating "a degenerate gas of holes." Noting the random occupation by bromine atoms of 3/5 the total Br sites crystallographically available, Minot and Perlstein introduced the question of the effect of this disorder on the periodic potential which would give rise to the d-band structure. The screening calculation of this work responds in part to this question.

A second report on conductivity in KCP-Br by Berenblyum et. al.[60] gave information on the ac conductivity as well as temperature dependence. Measurements for frequencies up to 10^{10} Hz gave the same conductivity as dc measurements above $100^{o}K$ – a room temperature conductivity of $(3.5 \pm 0.5) \times 10^{2}$ $(\text{ohm-cm})^{-1}$ being reported. On lowering the temperature σ_{dc} and σ_{hf} fell off exponentially, the slope being

larger for σ_{dc} and low-temperature activation energies of 800°K and 160°K were reported for σ_{dc} and σ_{hf} respectively. This unexpected result was interpreted as indicating a nonmetallic hopping transport mechanism.

In reply to this assertion, the Interrupted Strand Model (ISM) was introduced by Kuse and Zeller.[61] In real crystals metal atom chains are interrupted by impurities, vacancies, dislocations, etc. Each strand is assumed metallic, but current flow between strands may require an activation energy at low frequencies; at higher frequencies the interruptions are short-circuited by their capacitance. Experimental observation of the optical reflectivity of KCP-Br was used to support this view. A Drude (free-electron)[62] absorption edge was found for light polarized parallel to the crystal axis with a plasma frequency $h\nu_p = 2.88$ e.v., and collision time $\tau = 7.3 \times 10^{-15}$ sec. In addition the temperature-dependent longitudinal conductivity extrapolated to $T = \infty$ gave $\sigma = 1.2 \times 10^{4} (\text{ohm-cm})^{-1}$ which can be compared with the optical data using the formula $\sigma = \pi\tau\nu_p^2$.[63] Gesereich et. al.[64] found similar results and more recently far infrared[65] and very low temperature[66] measurements have been made.

In addition to the ISM, other hypotheses were advanced nearly simultaneously. The parallel work on NMP-TCNQ (N-methyl phenazinium tetracyanoquinodimethan) led Epstein et. al.[67] to apply the Mott-Hubbard model to these one-dimensional systems. In 1949 Mott discussed the process whereby electronic states of a metal would become localized as the lattice separation increased.[68] In the metal-to-insulator transition the decrease in electronic kinetic energy is balanced by an increase in

the electron-electron Coulomb energy. The Hubbard model[69] explicitly takes into account the electron correlation effects. These one-dimensional conducting systems became model compounds for comparison of theory and experiment.[70-73] We shall not discuss this model in detail, but only note one result: an insulating ground state is predicted for a half-filled one-dimensional band. The TCNQ compounds have insulating ground states and several have half-filled bands. The KCP compounds, while possessing insulating ground states, do not have half-filled bands.

Mossbauer studies (^{195}Pt) on KCP-Br by Ruegg et. al.[74] later confirmed the fact that the electrons are not localized on an atomic scale even at low temperatures. Such localization would result in a double salt, $\{0.85[K_2Pt^{(II)}(CN)_4] + 0.15[K_2Pt^{(IV)}(CN)_4Br_2]\}\cdot 3H_2O$, and two overlapping lines in the Mossbauer spectrum. Only one Lorentzian line could be fit to the data thus eliminating charge localization models.

Bloch et. al.[75] focused on the disorder in the system noted by Minot and Perlstein who also developed this theory. The random occupation by Br atoms adds a non-periodic contribution to the potential along the spine. The result is localization of the electron states to within distances on the order of 30c (c = Pt-Pt distance).[76,77] Conduction occurs along the chain via phonon-assisted hopping[78] and the temperature dependence of the conductivity would be $\ln\sigma \sim -(T_o/T)^{\mu}$ with $\mu = 1/2$ for the one-dimensional systems. A replotting of the $\sigma(T)$ data of Kuse and Zeller for KCP-Br showed a significantly better fit for $\mu = 1/2$ than for $\mu = 1$ over 13 orders of magnitude in the conductivity.[79]

Greene and Little measured the low-temperature (1.5 to 6.5°K) specific heat of KCP-Cl.[80] A least squares fit of the data using the expression $C = \gamma T + \beta T^3 + \delta T^5$ showed a very small value for γ ($.51 \times 10^{-4}$ J/mole°K) and thus a small value for the density of states at the Fermi level: $\mathcal{N}(0) \leq 7.6 \times 10^{19} cm^{-3}\ ev^{-1}$. This result was nevertheless reconcilable with both the ISM and WL (weak-localization) models which predicted $\mathcal{N}(0)$ to be of the order $2\text{-}5 \times 10^{20} cm^{-3} ev^{-1}$. In the WL model the time required for the system to come to equilibrium at these temperatures greatly exceeds the measurement period. In the interrupted strand model if the conduction is assumed to occur only along the chains, then the crystal will appear as a distribution of Schottky anomalies, and no term linear in T is expected. On the other hand, if conduction around the interruptions occurs via hopping to neighboring chains, the slow response time again accounts for the lack of the linear term.

The mechanism for transport between strands was at that time under investigation by Bernasconi, Kuse, Rice, and Zeller[81-83] in an enlargement of the interrupted strand model. The following observations were recorded for KCP-Br: 1) $\sigma_{||}$ and $\sigma_{\perp}$ (conductivities parallel and perpendicular to the chain, respectively) were found to have the same temperature dependence (same μ), and 2) $\sigma_{||}$ (300°K) varied widely with sample while $\sigma_{\perp}$ (300°K) was independent of the sample used in the measurement. They concluded that the interstrand transition limited the conductivity, $\sigma_{||}$ being determined by $\sigma_{\perp}$ and the average strand length ℓ_o. This ruled out the WL model in the

form developed by Bloch et. al., but does allow for weak localization in general. In addition the ISM had to be revised to allow for hopping between strands using the formalism of Mott.

At this time there was a growing awareness of the applicability of a general theorem due to Peierls.[84] In a solid it is possible to produce a gap in the electron energy spectrum at wave vector $\vec{k}$ by introducing a static lattice distortion of wave vector $2\vec{k}$, so that the Brillouin zone boundaries are redefined at $\vec{k}$. There is no overall gain in energy unless the discontinuity occurs at or near the Fermi level. In three dimensions this is generally of little consequence since a reduction in translational symmetry results in an energy gap which is planar in k-space so that the intersection with the Fermi surface would occur only in a small region. In one dimension, however, both the gap and Fermi level could involve the same singular region so that the gain in energy on distortion could be substantial.

In a similar way a dynamic distortion first postulated by Kohn for three-dimensional metals can occur in a much exaggerated form in one dimension.[85] This arises from the energy conserving scattering of electrons from the singular Fermi points at $+k_f$ and $-k_f$ and leads to a divergence of the dielectric function $\epsilon(k)$ at $k = 2k_f$. Renker et. al. observed a giant Kohn anomaly in KCP-Br using coherent inelastic neutron scattering at room temperature.[86]

Shortly thereafter theoretical treatments of the Peierls instability in one dimension were reported.[87,88] Two reviews of one-dimensional conducting systems were also published by Shchegolev[89] and by Zeller.[90]

Several recent experiments provide confirmational evidence for the Peierls-Kohn instability. Comes et. al. measured the diffuse x-ray scattering from KCP-Br.[91] At room temperature they found a linear superlattice distortion of periodicity 6×2.88 Å in which the platinum atoms varied from the average position by a longitudinal sinusoidal displacement. The wave vector for such a period has the value $2k_f$. When the temperature was lowered, the diffuse x-ray scattering progressively lost its one-dimensional character below $120^{\circ}K$, and it was concluded that a phase transition would occur below $77^{\circ}K$ (the lowest temperature at which measurements were made) leading to a unit cell $3c \times 2a \times 2a$. They suggested that the soft phonon mode of a room temperature giant "Kohn anomaly" transforms to a static Peierls distortion at low temperatures.

Similarly, a comparison of room temperature NMR experiments with low temperature ones supports the Peierls-Kohn instability. At room temperature Rupp found a Knight shift between oxidized and unoxidized compounds.[92] However, at low temperatures ($1.5 - 110^{\circ}K$) no shift is observed for KCP-Br by Niedoba et. al.[93] Their observation of a single, narrow, temperature-independent NMR line suggested the compound to be a band insulator in the ground state.

Most recently, EPR experiments by Mehran and Scott[94] on KCP-Br showed g factors characteristic of d_{z^2}-like hole states as they had previously found for MGS.[95] They conclude that the temperature variation of the line intensities cannot be reconciled to either the ISM or the WL model, but canbe explained in terms of the Peierls-Kohn instability model.

A band structure calculation has been carried out by Abarbanel[96] for one-dimensional systems by using the multiple-scattering technique of Johnson.[97] A linear array of $PtCl_4^{=}$ ions was used; the 45° staggering of neighboring complexes was not included. Preliminary results indicated a simple cosine $5d_{z^2}$ band with band width of approximately 3 ev.* This may be compared with the analysis of the optical data of Bernasconi et. al.[98] On evaluating the effective number of electrons contributing to the oscillator strength as a function of energy, they found $N_{eff}(\omega)$ to saturate at 1.67 electrons per platinum at $\hbar\omega$ = 2ev and to remain constant up to 5ev. This puts an upper limit on the $5d_{z^2}$ band width which is comparable with that calculated by Abarbanel for the oxidized compounds.

In summary, the mixed valency compounds exhibit metallic behavior at room temperature with a dynamic lattice instability, and at lower temperatures a phase transition occurs with a static distortion. The details of the transition are not yet clear nor is the zero order band structure entirely resolved.

The third function of the spine in the Little model for an excitonic superconductor is to screen the Coulomb interaction between charges on the spine and those in the dye molecules. This will result in a smaller repulsion between the spine electrons and the negative charge induced in the far end of the dye molecules. A model calculation has been performed to evaluate the extent of this screening.

---

*More recent results give a band width of 2.3 e.v.

B. Thomas-Fermi Screening

The nature of screening in compounds which have less than three-dimensional freedom of motion for the conduction electrons has been treated by several authors.[22,23,99-101] The one-dimensional case is treated by Kuper[23] using a single-filament model and by Dzyaloshinskii and Katz[22] using an array of filaments. Recently an extensive investigation of the dynamical nature of the screening in one-dimensional and nearly one-dimensional systems by Bush[99] has extended the present calculation.

We consider two models in the present treatment. The first is that of Kuper which involves a single filament of radius R_1 lying along the z axis. The region within the filament is designated as metallic and in the absence of source charges has a uniform electron density N_o, matched by an equal uniform positive background. The region outside the filament has zero charge density and is designated as empty. This model neglects the contribution to the screening of the Coulomb field which arises from the movement of charge in the neighboring filaments. Our second model attempts to correct this by including the average effect of these filaments. This is done by adding to the first model another metallic region with electron density N_o' and corresponding positive background. This third region is coaxial with the inner filament and extends from an inner radius R_2 to infinity, thus limiting the extent of the empty region in the radial direction to the region from R_1 to R_2. See Figure 3. N_o' is chosen to represent the mean density of screening electrons in the bulk material. It

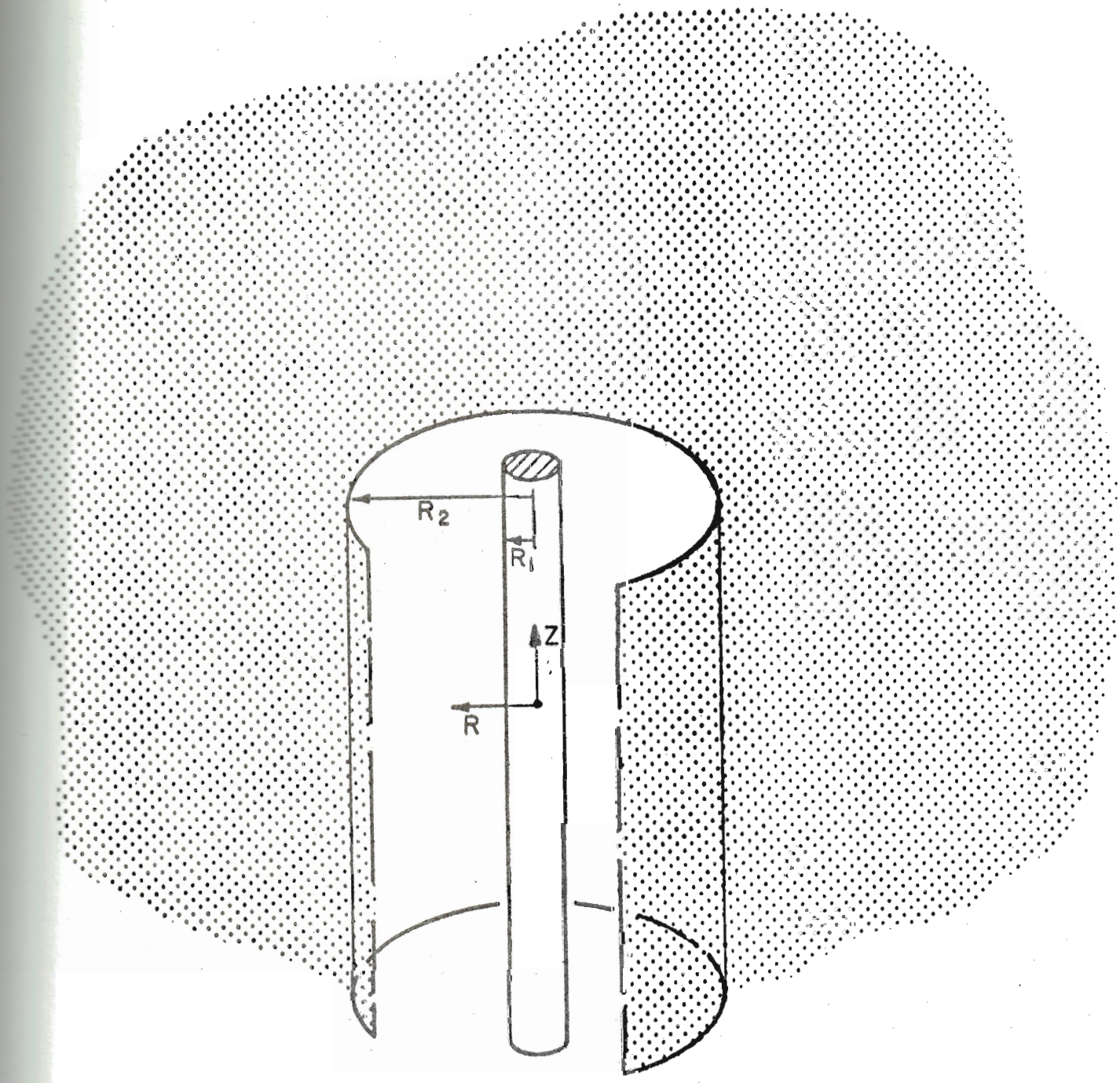

Figure 3 Screening region geometry.

is convenient to define ρ , the linear density of screening electrons in the z direction, which is also characteristic of the filamentary compound being represented; $\rho = abN_o'$, where a and b are the lattice constants in the x and y directions, respectively. The density of electrons in the inner filament is then related by $N_o = \rho/\pi R_1^2$. For systems we are considering, a representative value for R_1 would be the covalent radius of platinum, and for R_2 we would use the distance between metal-atom chains a for compounds with tetragonal unit cells such as KCP-Cl, or the geometrical mean distance $(ab)^{1/2}$ for compounds with rhombic unit cells such as $Mg_{0.82}Pt(C_2O_4)_2 \cdot 5.3H_2O$ (see Table 1).

TABLE 1. Parameters for partially oxidized compounds (Refs. 25,51-57)

Compound	Lattice Constants (Å) a	b	c	Effective R_2 (Å) $\sqrt{(ab)}$	Linear Density Carriers/Å
$K_2Pt(CN)_4Cl_{0.32} \cdot 2.6H_2O$	9.87	9.87	2.89	9.87	0.111
$MgPt(CN)_4Cl_{0.28} \cdot 7H_2O$	14.66	14.66	2.985	14.66	0.094
$Mg_{0.82}Pt(C_2O_4)_2 \cdot 5.3H_2O$	16.56	14.27	2.85	15.37	0.126
$K_{1.74}Pt(CN)_4 \cdot 1.8H_2O$	15.59	10.01	2.96	12.49	0.088

Inside bulk materials the Coulomb interaction between conduction electrons is modified by a wave-vector- and frequency-dependent dielectric constant $\epsilon(k,\omega)$, such that the Fourier transform of the

potential due to a source charge q has the form

$$\Phi = 4\pi q/k^2\epsilon(k,\omega) .$$

The evaluation of $\epsilon(k,\omega)$ is a major task in itself, and for present purposes we shall use the results of the Thomas-Fermi approximation. This leads to a static screening constant of the form $\epsilon = 1+\kappa^2/k^2$, where κ^{-1} is the screening length. The results of our treatment can be expected to give a good description in the static limit. In our second model the radial movement of charge is permitted in the outer coaxial region corresponding to the movement of charge between metal-atom chains in the actual compounds by hopping or tunneling. Characteristic times for such movement, however, may be long and thus may place a low limit on the frequencies for which we can expect this model to give valid results. We expect our model to give best results for static screening.

We chose not to use the random-phase approximation (RPA) to evaluate the dielectric constant because of the difficulty one can encounter in these one-dimensional systems from a variety of instabilities to which such linear systems are prone. In particular, the use of an unstable Hartree-Fock state as the starting point in an RPA calculation leads to imaginary excitation energies resulting in a screened interaction which would be unphysical.[102] The Thomas-Fermi method is less sensitive to these instabilities and gives physically reasonable results which depend principally upon the density of the assumed ground state.

This Thomas-Fermi quasiclassical treatment of electron interactions is based on the assumptions that the system is in its lowest quantum state and that the spatial variation of the electrostatic potential is small over distances comparable to the mean electron wavelength.[103,104] The application of these assumptions is made in the following manner. We consider the source charge q to be located at the origin, and we denote by $\Phi(\vec{r})$ the electrostatic potential at $\vec{r}$. The electron density is modified by the presence of the charge so that the new maximum kinetic energy $E_f + e\Phi(\vec{r})$, which varies in the metallic region, gives rise to a variation of the charge density,

$$N(\vec{r}) = -e(8\pi/3h^3)[2m(e\Phi+E_f)]^{3/2} .$$

Poisson's equation then gives the second relationship necessary to determine $N(\vec{r})$,

$$\nabla^2\Phi = -4\pi[N(\vec{r})-N_o] - 4\pi q\delta(r) .$$

Expanding for small values of Φ compared with E_f, we have

$$\nabla^2\Phi = \kappa^2\Phi - 4\pi q\delta(r) ,$$

where

$$\kappa^2 \equiv \frac{2e^2}{\pi}(2m/\hbar^2)^{3/2} E_f^{1/2} = \frac{4me^2}{\hbar^2}(3N_o/\pi)^{1/3}$$

or more generally

$$\kappa^2 = 4\pi e^2 \mathcal{N}(0) ,$$

where $\mathcal{N}(0)$ is the density of states at the Fermi surface.

The basic problem is to find solutions to the differential equation

$$\nabla^2\Phi = \kappa^2\Phi \qquad (1)$$

subject to boundary conditions which will depend upon the particular model. Since both models have cylindrical and reflection symmetry we use cylindrical coordinates, and (1) becomes

$$\frac{\partial^2\Phi}{\partial R^2} + \frac{1}{R}\frac{\partial\Phi}{\partial R} + \frac{\partial^2\Phi}{\partial z^2} = \kappa^2\Phi \quad , \qquad (2)$$

which is independent of the angular coordinate and is separable in R and z :

$$\Phi(R,z) = \mathcal{R}(R)\, Z(z).$$

Thus,

$$\frac{1}{Z(z)}\frac{\partial^2 Z}{\partial z^2} = -\alpha^2$$

and

$$\frac{1}{\mathcal{R}(R)}\left(\frac{\partial^2\mathcal{R}}{\partial R^2} + \frac{1}{R}\frac{\partial\mathcal{R}}{\partial R}\right) - (\kappa^2+\alpha^2) = 0 \; .$$

Solutions for the z coordinate are

$$Z(z) = \cos\alpha z \; ,$$

which are even functions of z due to reflection symmetry through the $z=0$ plane. Solutions of the radial equation are the modified Bessel functions of order zero, $I_o(\beta R)$ and $K_o(\beta R)$, where $\beta^2 = \kappa^2+\alpha^2$.

Each value of α gives a linearly independent solution to (2), and the general solution for a metallic region is the integral

$$\Phi(R,z) = \int_0^\infty [A_I(\alpha)I_o(\beta R) + B_I(\alpha)K_o(\beta R)] \cos\alpha z d\alpha \ .$$

In the case of the metallic region of the coaxial surrounding cylinder we replace β by $\beta' = (\kappa'^2 + \alpha^2)^{1/2}$, using the initial uniform density of electrons appropriate for this region to determine κ' ; the coefficients are then $A_{III}(\alpha)$ and $B_{III}(\alpha)$. For the empty region $\kappa = 0$, and we have the general soletion

$$\Phi(R,z) = \int_0^\infty [A_{II}(\alpha)I_o(\alpha R) + B_{II}(\alpha)K_o(\alpha R)] \cos\alpha z d\alpha \ .$$

We determine the various coefficients A_i and B_i by applying the boundary conditions. For both models we require the limiting form of the potential as $r = 0$ to be

$$\lim_{r\to 0} r\Phi(r) = q \ ,$$

where $r = (R^2 + z^2)^{1/2}$. In this limit $I_o(\beta R) \to 1$, and the potential reduces to the second term

$$\lim_{r\to 0} r\Phi(r) \to r\int_0^\infty B_I(\alpha)K_o(\beta R) \cos\alpha z d\alpha \ .$$

Choosing $B_I(\alpha)$ to be independent of α gives[105]

$$r\Phi(R,z) = B_I \pi e^{-\kappa r}/2 \ ,$$

so that

$$\lim_{r\to 0} r\Phi(R,z) = B_I \pi/2 \quad .$$

Thus $B_I(\alpha) = 2q/\pi$. The solution $\Phi(R,z)$ scales with q and for our calculations we use $q = 1$ throughout.

The behavior as $r \to \infty$ is also the same in both models, and we require that $\Phi \to 0$ as $r \to \infty$. Since I_o is unbounded as its argument increases, we must have $A_i(\alpha) = 0$, where $i = II$ for the filament model and $i = III$ for the extended model.

The application of the remaining boundary conditions requires a separate treatment in each case although the general requirement can easily be stated, that is, we require the potential and its normal derivative to be continuous across each boundary.

In the single filament case requiring Φ and $\partial\Phi/\partial R$ to be continuous at R_1 gives a pair of linear equations to be solved for $A_I(\alpha)$ and $B_{II}(\alpha)$:

$$I_o(\beta R_1)A_I(\alpha) - K_o(\alpha R_1)B_{II}(\alpha) = -(2q/\pi)K_o(\beta R_1) ,$$

$$\beta I_1(\beta R_1)A_I(\alpha) + \alpha K_1(\alpha R_1)B_{II}(\alpha) = \beta(2q/\pi)K_1(\beta R_1) \quad .$$

The solutions are

$$A_I(\alpha) = \frac{2q}{\pi} \frac{\beta K_o(\alpha R_1)K_1(\beta R_1) - \alpha K_o(\beta R_1)K_1(\alpha R_1)}{\beta K_o(\alpha R_1)I_1(\beta R_1) + \alpha K_1(\alpha R_1)I_o(\beta R_1)} ,$$

$$B_{II}(\alpha) = \frac{2q}{\pi} \frac{\beta I_o(\beta R_1)K_1(\beta R_1) + \beta K_o(\beta R_1)I_1(\beta R_1)}{K_o(\alpha R_1)I_1(\beta R_1) + \alpha K_1(\alpha R_1)I_o(\beta R_1)} .$$

In the case of the filament and coaxial cylinder there are two boundaries and thus four linear equations for the coefficients $A_I(\alpha)$,

$A_{II}(\alpha)$, $B_{II}(\alpha)$, and $B_{III}(\alpha)$. The solutions are

$$A_I(\alpha) = \frac{1}{M(\alpha)} \begin{vmatrix} -\frac{2q}{\pi} K_o(\beta R_1) & -I_o(\alpha R_1) & -K_o(\alpha R_1) & 0 \\ \frac{2q}{\pi} \beta K_1(\beta R_1) & -\alpha I_1(\alpha R_1) & \alpha K_1(\alpha R_1) & 0 \\ 0 & I_o(\alpha R_2) & K_o(\alpha R_2) & -K_o(\beta' R_2) \\ 0 & \alpha I_1(\alpha R_2) & -\alpha K_1(\alpha R_2) & \beta' K_1(\beta' R_2) \end{vmatrix}$$

$$A_{II}(\alpha) = \frac{1}{M(\alpha)} \begin{vmatrix} I_o(\beta R_1) & -\frac{2q}{\pi} K_o(\beta R_1) & -K_o(\alpha R_1) & 0 \\ \beta I_1(\beta R_1) & \frac{2q}{\pi} \beta K_1(\beta R_1) & \alpha K_1(\alpha R_1) & 0 \\ 0 & 0 & K_o(\alpha R_2) & -K_o(\beta' R_2) \\ 0 & 0 & -\alpha K_1(\alpha R_2) & \beta' K_1(\beta' R_2) \end{vmatrix}$$

$$B_{II}(\alpha) = \frac{1}{M(\alpha)} \begin{vmatrix} I_o(\beta R_1) & -I_o(\alpha R_1) & -\frac{2q}{\pi} K_o(\beta R_1) & 0 \\ \beta I_1(\beta R_1) & -\alpha I_1(\alpha R_1) & \frac{2q}{\pi} \beta K_1(\beta R_1) & 0 \\ 0 & I_o(\alpha R_2) & 0 & -K_o(\beta' R_2) \\ 0 & \alpha I_1(\alpha R_2) & 0 & \beta' K_1(\beta' R_2) \end{vmatrix}$$

$$B_{III}(\alpha) = \frac{1}{M(\alpha)} \begin{vmatrix} I_o(\beta R_1) & -I_o(\alpha R_1) & -K_o(\alpha R_1) & -\frac{2q}{\pi} K_o(\beta R_1) \\ \beta I_1(\beta R_1) & -\alpha I_1(\alpha R_1) & \alpha K_1(\alpha R_1) & \frac{2q}{\pi} \beta K_1(\beta R_1) \\ 0 & I_o(\alpha R_2) & K_o(\alpha R_2) & 0 \\ 0 & \alpha I_1(\alpha R_2) & -\alpha K_1(\alpha R_2) & 0 \end{vmatrix}$$

where

$$M(\alpha) \equiv \begin{vmatrix} I_o(\beta R_1) & -I_o(\alpha R_1) & -K_o(\alpha R_1) & 0 \\ \beta I_1(\beta R_1) & -\alpha I_1(\alpha R_1) & \alpha K_1(\alpha R_1) & 0 \\ 0 & I_o(\alpha R_2) & K_o(\alpha R_2) & -K_o(\beta' R_2) \\ 0 & \alpha I_1(\alpha R_2) & -\alpha K_1(\alpha R_2) & \beta' K_1(\beta' R_2) \end{vmatrix}$$

The integrals involved in the computation of the potential were performed by numerical quadrature. The lower limit of zero was replaced by $10^{-5}\kappa$. For small values of α the integrand is well behaved for regions in which $\kappa \neq 0$. In the empty regions the integrand is dominated by the $B_{II}(\alpha)K_o(\alpha R)$ term for small α, since $K_o(\alpha R) \propto -\ln\alpha R$. The coefficient $B_{II}(\alpha)$, however, varies as $(-\ln\alpha R_1)^{-1}$ so that in this case the integrand is well behaved also, and we can cut off at the lower limit $10^{-5}\kappa$. For large α, the $A_i(\alpha)I_o(\alpha R)$ or $A_i(\alpha)I_o(\beta R)$ term

dominates for $i = I$ or II . One finds that $A_i(\alpha) \propto e^{-2\alpha R_i}$, so that the product varies as $A_i(\alpha) I_o(\alpha R)\, e^{-\alpha(2R_i - R)}$, which is less than or equal to $e^{-\alpha R}$ since $R_i \geq R$. The portion of the integral for $\alpha > 5\kappa$ contributes approximately

$$\int_{5\kappa}^{\infty} e^{-\alpha R}\, d\alpha = (1/R)\, e^{-5\kappa R} .$$

For $R > \kappa^{-1}$ this will be negligible.

The integral from $10^{-5}\kappa$ to 5κ was calculated using Simpson's rule. In addition the integral was bounded above and below by rectangles whose areas were also computed. In this way error limits could easily be placed on the value for the integral. Typically a grid of 1100 points was used whose spacing was constant throughout a given section, there being generally ten contiguous sections chosen to minimize the computation time while retaining sufficient accuracy. Maximum error for the integral was less than 5% for most cases; the error increased as z increased. Calculations with very fine grids (10,000 points) showed that the actual error was generally less than 0.1%.

KCP-Cl is a typical compound which we hope to describe by this method. The lattice is tetragonal with lattice constants $a = b = 9.87$ Å and $c = 2.89$ Å .[25] The formal oxidation state of the platinum is +2.32 giving 0.32 holes/Pt for screening. Thus in a chain of platinum atoms the linear density is $\rho = 0.111$ holes/Å . For a filament of radius $R_1 = 1.295$ Å this gives a density $N_o = 21.2 \times 10^{21}$ holes/cm^3 and $\kappa = 1.14$ Å^{-1} . In the bulk material where there is one platinum chain in a cross section of 97.4 Å^2 the resulting density is much lower, $N_o' = 1.14 \times 10^{21}$ holes/cm^3 giving $\kappa' = 0.88$ Å^{-1} . This is the value

for the reciprocal of the screening length in the bulk material, that is, in the metallic region which extends outward from an inner radius $R_2 = 9.87$ Å, the distance between platinum chains.

A different "effective" charge density could also be used if one wished to take into account the effect of the random distribution of the chloride ions. Their random distribution should result in an increase in the bandwidth of the partially filled $5d_{z^2}$ band of the platinum atoms, thereby giving a smaller density of states at the Fermi level $\mathcal{N}(0)$, effectively reducing the density of screening charges in the material, and resulting in proportionate decreases in κ^2 and κ'^2. One could also superimpose a uniform background dielectric constant ϵ_o by including it in the substituted Poisson's equation

$$\epsilon_o \nabla^2 \Phi = \kappa^2 \Phi - 4\pi q \delta(\mathbf{r}) \quad .$$

Thus κ^2 would be replaced by κ^2/ϵ_o, or equivalently the effective linear charge density would be given by ρ/ϵ_o^3, since κ^2 varies as the cube root of ρ. The source charge q would then be replaced by q/ϵ_o.

Preliminary calculations, using the covalent radius of platinum for R_1, confirmed Kuper's suggestion that an effective radius smaller than the covalent radius should be used to account for the absence of screening within the filament due to radial or azimuthal adjustment of the electron gas. The physical system has the source charge distributed throughout this region in the atomic orbitals of platinum rather than concentrated at the center, and thus there should be only a slight reduction in the potential from the Coulomb value at R_1, the surface

of the cylinder. The effect of reducing the radius of the filament below the covalent radius (1.295 Å) was examined by computing the screening for the smaller values of R_1: 0.1, 0.01, 0.001, 0.0001 Å. In each case the linear density ρ remained constant giving increasing values of κ with decreasing filament radius. Using values of R_1 less than 0.1 Å resulted in a potential at $R = 1.295$ Å which was less than the Coulomb potential by about 10% for both models. All calculations were repeated using values of R_1 from 0.1 to 0.001 Å. The results for $R_1 = 0.01$, 0.001, and 0.0001 Å were found to be essentially identical. In this manner we are able to take into account the contribution from screening due to movement along the filament while excluding that due to transverse motion.

We have calculated the screened potential in the $z = 0$ plane for a large range of radial distances for both models. The results are shown in Figure 4. The potential screened by the filament alone lies just below the unscreened Coulomb potential and shows no exponential decay outside the filament. On the other hand, the potential screened by both the filament and the outer cylinder falls away from the Coulomb potential in the region between the filament and cylinder even though $\kappa = 0$ in this region. The potential was found approximately to fit the function

$$\Phi(R,0) = Ae^{-\kappa_{eff}^{z=0} R}/R$$

in this empty region, with $\kappa_{eff}^{z=0} = 0.111$ Å^{-1}. The fully screened potential shown in Figure 4 is the usual result for the bulk material. It can be seen that the potential screened by both regions lies between

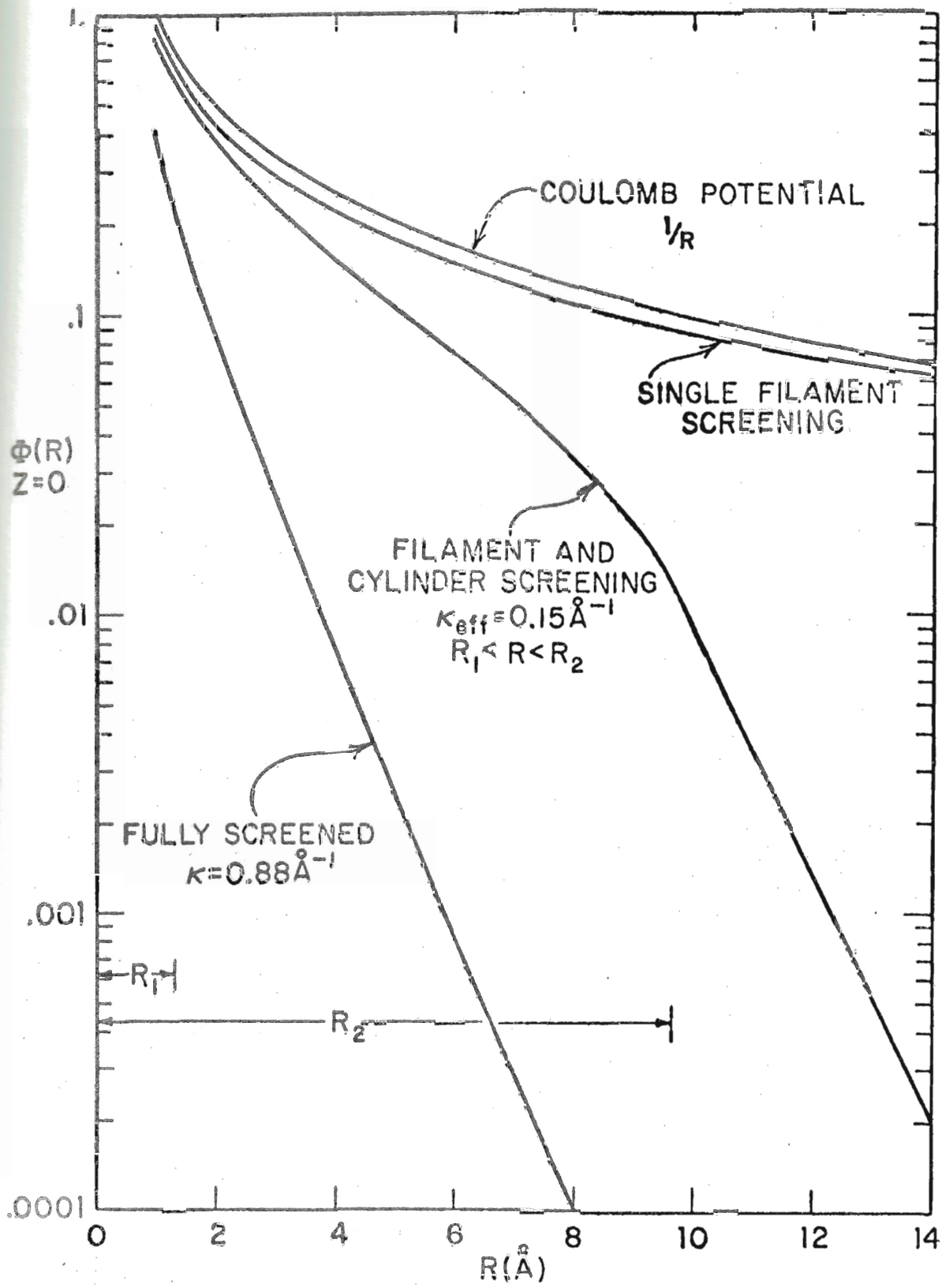

Figure 4 Potentials in the z = 0 plane.

the Coulomb potential and the fully screened potential.

The remainder of the calculations were done only with the extended model, since the Kuper single-screening-region model showed results qualitatively very similar to the unscreened Coulomb potential. The extended model, which accounts for the presence of the neighboring chains, is expected to give results more directly applicable to the calculation of the effective interaction as given in Chapter III.

The anisotropy of the potential in the extended model was investigated by calculating the potential at a grid of 80 points with R in the range 1.295 - 5 Å and z in the range 0 - 15 Å. These results were fitted by least squares to the function

$$\Phi(R,z) = Ae^{-\kappa_{eff}r}/r \quad ,$$

where $r = (R^2 + z^2)^{1/2}$. It was found that this isotropic function provided an excellent fit with error generally less than 5% and nearly always less than 15% throughout the region. Table 2 shows the results for KCP-Cl. The insensitivity of the effective reciprocal screening length to orders-of-magnitude changes in R_1 is clearly evident. Thus the screened potential due to a unit source charge in a platinum chain can be described by the equation

$$\Phi(r) = 1.18\ e^{-0.135r}/r \quad ,$$

for the region between chains.

TABLE 2. Screening in $K_2Pt(CN)_4Cl_{0.32}\cdot 2.6H_2O$

($\rho = 0.111$ holes/cm^3 $\quad \kappa' = 0.88$ Å^{-1} $\quad R_2 = 9.87$ Å)

R_1	κ	A	κ_{eff}
0.1	3.368	0.952	0.1421
0.01	7.256	1.168	0.1356
0.001	15.633	1.183	0.1344
0.0001	33.680	1.186	0.1346

Other compounds similar to KCP-Cl are known which have different values for the formal oxidation state of Pt and also different lattice constants. Table 1 gives several examples. In order to investigate the effect of varying the linear density and the nearest-chain distance, we computed the potentials at the same spatial grid of points for values of ρ varying from 0.08 to 0.10 carriers/Å and R_2 varying from 10 to 15 Å. Table 3 shows the results for $\bar{\kappa}_{eff}$ obtained by least-squares fit and averaged over the three smallest values of R_1. We see that the variation of ρ has little effect on the screened potential, at least within this small range. Of course, as $\rho \to 0$ the potential must approach the Coulomb potential, $\kappa_{eff} \to 0$. Variation of the interchain distance has a more pronounced effect; as the distance increases by 50%, the average effective reciprocal screening length decreases by 50%. The variation is smooth and is describable by the function

$$\bar{\kappa}_{eff} = 0.1318 - 0.01549(R_2 - 10) + 0.001009(R_2 - 10)^2 .$$

TABLE 3. $\bar{\kappa}_{eff}$ for Extended Model

ρ	R_2 (Å)					
Carriers/Å	10	11	12	13	14	15
0.08	0.132	0.116	0.104	0.094	0.086	0.079
0.09	0.132	0.117	0.105	0.094	0.086	0.079
0.10	0.132	0.117	0.105	0.095	0.086	0.079

For the compounds with unequal lattice constants a and b , the geometrical mean can be used for R_2 , thus giving the correct density of screening charges in the bulk region N_o' .

A third model was also investigated to a limited extent. In this we attempted to take into account only the four nearest-neighbor filaments by replacing them by a metallic cylinder of finite extent in the radial direction. The inner radius $R_2 = 9.7$ Å and outer radius $R_3 = 10.04$ Å were chosen so that the cylinder's average radius was the interchain distance and the cross-sectional area was four times that of a filament with covalent radius. The value of κ appropriate for the platinum chain was used in both the filament and the finite cylinder. It was found that screening in the finite cylinder reduced the potential below that of the filament alone by about 5%, but did not result in the exponential decay found for screening by a filament and infinite cylinder. It appears that the addition of a large number of concentric finite cylinders would result in the screening produced by the infinite cylinder.

Screening in materials which are characteristically one-dimensional cannot be described by results from models which ignore the three-dimensional nature of the bulk material. Instead, screening is intermediate between that for a single filament and that for bulk screening. The close relationship to bulk screening is shown by the isotropic form of the screened potential, as has also been observed by Visscher and Falicov[99] in the two-dimensional case. As mentioned above this result bears directly on the problem of finding the field due to a random distribution of charges such as the chloride ions in KCP-Cl. A much narrower potential distribution is expected in the case where screening is substantial, since in that case only nearest-neighbor contributions would be significant rather than Coulomb contributions from sites located many cells away.

In the investigation of the superconducting transition temperatures for model organometallic systems composed of a spine surrounded by dye molecules, we shall employ the results of this chapter to account for screening of the Coulomb interaction due to neighboring spines. We shall compare the transition temperatures of these cases to those for which the neighboring spines are neglected.

III. EXCITONIC SYSTEMS

A. Individual Dye Molecules

The dye molecules which surround the spine in the Little model for an excitonic superconductor modify the direct Coulomb interaction due to the virtual excitation of the dyes. In this chapter the method for calculating the new effective interaction, $V_{eff}(q,\omega)$, will be described. Parts of this method have been discussed in the literature.[1-6-111]

The wave function for the n^{th} eigenstate of a dye may be written $\psi_n(r_1,r_2,\ldots)$. When combined with other dyes in an array the dye-dye interaction results in a band of energy levels for the system whose ground state wave function may be written in the form

$$\Psi_o(q) = \frac{1}{\sqrt{N}} \sum_j e^{iqR_j} \psi_o(r_1-R_j,r_2-R_j,\ldots) .$$

The ground state and low-lying excited states of the system are used to calculate the effective interaction. The method for calculating single dye wave functions will be described first, followed by the method and results for the array of dyes.

The cyanine dyes under consideration are large conjugated molecules whose polarizability arises from the extended π-electron system. See Figure 5. The total number of atoms ranges from 27 to $\sim$ 60 with each dye having 2 (in some cases 4) nitrogen atoms and approximately equal numbers of carbon and hydrogen. Since the relevant electronic properties arise primarily from the π-electrons we wish to treat these

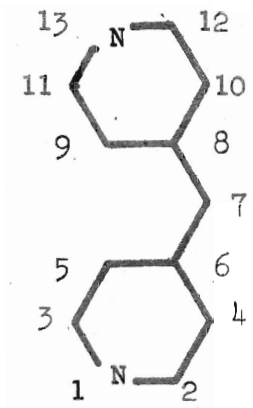

Pyridine cyanine

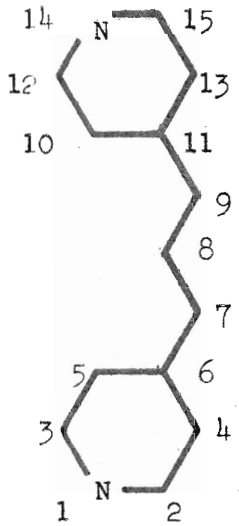

Pyridine Carbocyanine

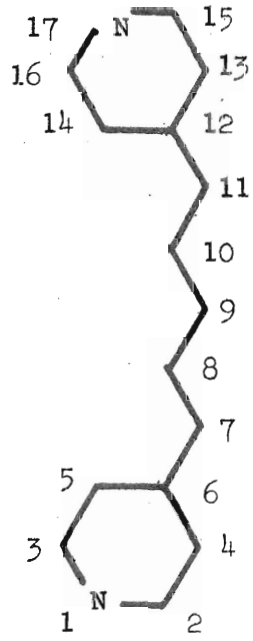

Pyridine Dicarbocyanine

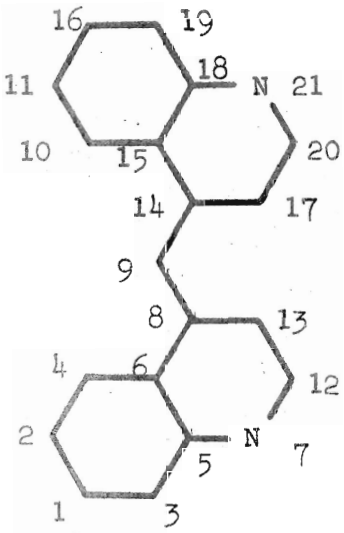

Cyanine

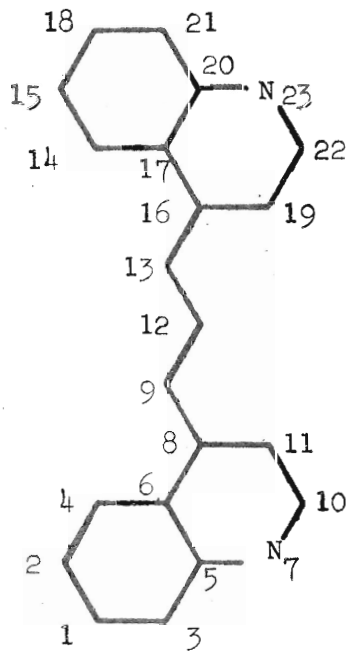

Carbocyanine

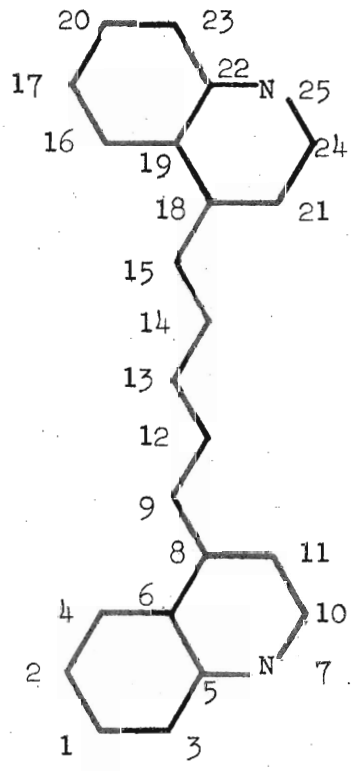

Dicarbocyanine

Figure 5 Dye molecules used in model system.

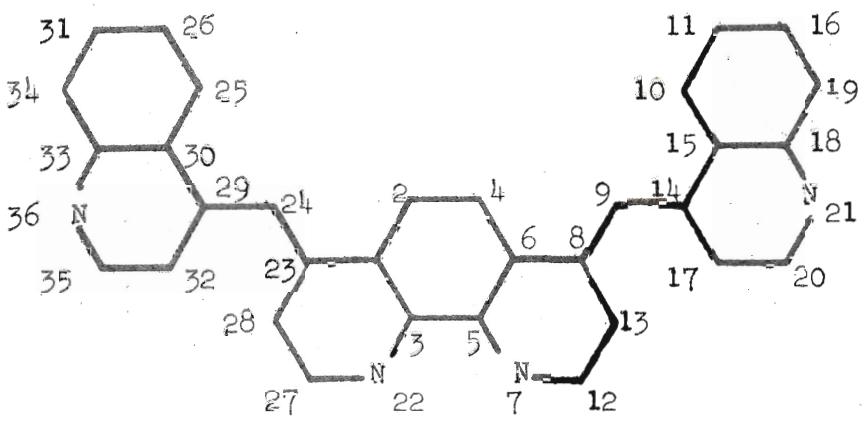

Phenanthroline Cyanine

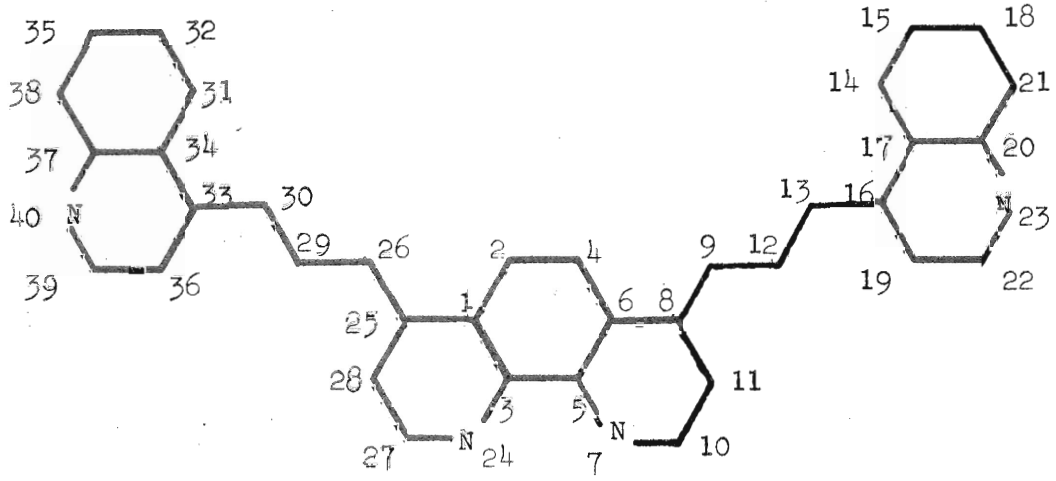

Phenanthroline Carbocyanine

Figure 5 (continued)

electrons in as accurate a manner as is computationally feasible. We begin by assuming a fixed nuclear configuration and σ-π separability.

The calculation of the ground state and low-lying excited states proceeds in three separable stages. The initial stage is a Huckel calculation for the molecular orbitals using a Linear Combination of Atomic Orbitals (LCAO) basis set built from atomic $2p_z$ orbitals. The second stage is a Zero-Differential-Overlap (ZDO) approximation, modified to account for many-body π-electron correlation effects. The final step is a configuration interaction (CI) calculation involving generally 4 or 16 configurations. The methods and parameters for each of these will now be described briefly paying particular attention to the many-body modification of the second stage.

The Huckel method is a single particle approach in which the molecular orbitals are eigenvectors of an effective Hamiltonian:

$$H_{eff}(r) = -(\hbar^2/2m)\nabla^2 + V_{eff}(r) .$$

The potential seen by the electron accounts for the attraction due to the nuclei plus the repulsion due to an average distribution of all the electrons. The Hamiltonian is characterized by its matrix elements which are related to empirical quantities. The Coulomb integrals, $\alpha = H_{ii}$, are taken as the sum:[112] $\alpha_i = -W_i + \gamma_{ii}V_i/2$ where W_i is the ionization potential, γ_{ii} is the repulsion integral for two π-electrons on the same atom, and V_i is the valence. Throughout this work the following values have been used: $W_C = 11.2$, $W_N = 24.7$, $\gamma_C = 10.6$, and $\gamma_N = 13.3$ all in e.v. Also $V_C = 1$ and $V_N = 2$.

Thus $\alpha_C = -5.9$ and $\alpha_N = -11.4$ e.v. for the Huckel calculation. The resonance integrals, $\beta = H_{rs}$, are taken to be zero for non-bonded atoms r and s. For bonded atoms variation of β with environment is taken into account. In the aromatic rings the resonance integrals are $\beta_{CC,ring} = -2.30$ and $\beta_{CN} = -1.80$ e.v. The twisting of the rings[113] relative to one another lowers the $\beta_{CC,chain}$ integral. The expression $\beta = \beta_o \cos\theta$[114] can be used to approximate the resulting integral. In this work $\beta_{CC,chain} = -1.40$ e.v. was found to give good agreement for the simplest cyanine dye and was used in all cases. This corresponds to a twist of $\sim 50^\circ$ at each chain carbon.

Zeroth order molecular orbitals determined in the Huckel calculation were then used in the ZDO calculation of the second stage. The closed shell Fock Hamiltonian for π-electrons is given by $F_{rs} = H_{rs}^{core} + 2J_{rs} - K_{rs}$, or more explicitly:

$$F_{rs} = H_{rs}^{core} + \sum_t \sum_u p_{tu} \Big| \langle \phi_r^*(1)\phi_s(1) | e^2/r_{12} | \phi_t^*(2)\phi_u(2) \rangle - (1/2)\langle \phi_r^*(1)\phi_t(1) | e^2/r_{12} | \phi_s^*(2)\phi_u(2) \rangle \Big|$$

where H_{rs}^{core} includes the nuclei plus σ-electrons, $p_{tu} \equiv 2\sum c_{kt} c_{ku}$ is the bond order, $\langle \phi_r^*(1)\phi_s(1) | e^2/r_{12} | \phi_t^*(2)\phi_u(2) \rangle$ is the two-electron Coulomb integral, and $\langle \phi_r^*(1)\phi_t(1) | e^2/r_{12} | \phi_s^*(2)\phi_u(2) \rangle$ is the two-electron exchange integral.

The ZDO method introduced independently by Pariser and Parr[115,116] and by Pople[117] employs the following simplifying assumptions:[112]

1) Atomic overlap is neglected, $S_{rs} = \delta_{rs}$.

2) $H_{rs}^{core} = \beta_{rs}^{core}$ $(r \neq s)$ is neglected if r and s are not bonded atoms. In theory the core integrals differ from the resonance integrals of Huckel theory since the latter include a contribution from the potential of the smoothed-out distribution of π-electrons. For this work, however, we set $\beta_{rs}^{core} = \beta_{rs}$ using the different values for chain, ring, and heteroatom bonds.

3) $\langle \phi_r^*(1)\phi_s(1)|e^2/r_{12}|\phi_t^*(2)\phi_u(2)\rangle = \delta_{rs}\delta_{tu}\gamma_{rt}$. Two-electron integrals which depend on overlapping charge distributions of atomic orbitals on different atoms are neglected. Thus off-diagonal Coulomb integrals vanish as do the "proper" atomic exchange integrals.

With these assumptions the off-diagonal Fock operator becomes

$$F_{rs}\ (r \neq s) = \beta_{rs} - (1/2)\, p_{rs}\gamma_{rs} \qquad r \text{ and } s \text{ bonded},$$
$$= -(1/2)\, p_{rs}\gamma_{rs} \qquad r \text{ and } s \text{ not bonded}.$$

The diagonal elements are then

$$F_{rr} = H_{rr}^{core} + \sum_t \sum_u p_{tu}\Big[\delta_{tu}\langle\phi_r^*(1)\phi_r(1)|e^2/r_{12}|\phi_t^*(2)\phi_u(2)\rangle - (1/2)\delta_{tr}\delta_{ur}\langle\phi_r^*(1)\phi_t(1)|e^2/r_{12}|\phi_r^*(2)\phi_u(2)\rangle\Big]$$

$$= H_{rr}^{core} + (1/2)q_r\gamma_r + \sum_{t\neq r} q_t\gamma_{rt}$$

where $q_r \equiv p_{rr}$ is the charge density at atom r, and H_{rr}^{core} includes the kinetic energy plus the potential due to the nuclei and σ-electrons. H_{rr}^{core} can be split into two parts as was done for the Huckel calculation. The first term, $-W_i$, is the kinetic energy plus

the core potential (nucleus, inner shell and σ-electrons) at atom i. The second term gives the potential due to the cores of all other atoms, j. From a distance these will appear as localized positive charges of magnitude given by the valence, V_j. Their contribution is

$$-\sum_{j\neq i} V_j\gamma_{ij} \quad , \quad \text{so that} \quad H_{ii}^{core} = -W_i - \sum_{j\neq i} V_j\gamma_{ij} \; .$$

The basic equations are then

$$F_{ii} = -W_i + (1/2)q_i\gamma_{ii} + \sum_{j\neq i} (q_i - V_i)\gamma_{jj}$$

$$F_{ij} = \Delta_{ij}\beta_{ij} - (1/2)\gamma_{ij}P_{ij}$$

where $\Delta_{ij} = 1$ if i and j are bonded

$= 0$ otherwise.

The secular equations are

$$(F_{ii} - E_k)c_{ki} + \sum_{j\neq i} F_{ij}c_{kj} = 0$$

Empirical values for W_i and β_{ij} are the same as used in the Huckel calculation.

It is at this point, where empirical values for the γ_{ii} and empirical expressions for the γ_{ij} are introduced, that a modification of the ZDO procedure is made. Expressions for γ_{ij} such as the Pariser-Parr polynomial interpolation formula[116] and the simple $e^2/(r_{ij} + a)$ expression of Nishimoto and Mataga[118] attempt to account for σ-screening of the interaction between π-electrons on different

atoms. However, in the large conjugated systems which are under consideration, π-electron screening must also be taken into account in a consistent manner.

The importance of many-body π-electron correlation effects has been demonstrated by Little in the following way. A test charge was placed at r_1 within the boundary of a large conjugated molecule, resulting in charges being induced on the atoms r'. See Figure 6.

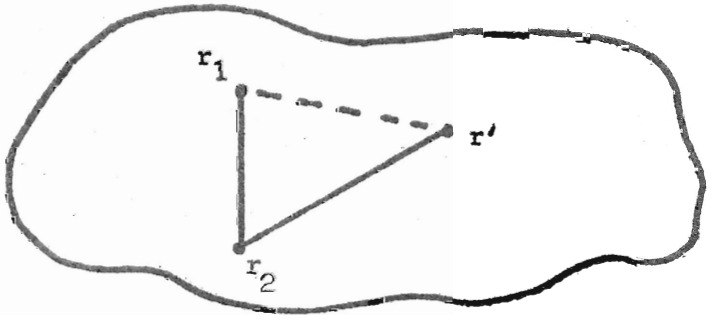

Figure 6 Induced charges in conjugated molecules.

The net potential at point r_2 is then given by the sum of the potential due to the test charge and induced charges which were determined by a standard ZDO-SCF-MO calculation using Mataga's expression for γ_{ij}. Due to the finite size of the molecule (lack of translational invariance), the effective potential, $V(r_1,r_2)$, depended on both r_1 and r_2 rather than $|r_1 - r_2|$. The effective potential determined in this manner was used in a subsequent calculation in place of Mataga's expression. Comparison of these results with observed spectra show substantially better agreement than results from using either Mataga's expression or the Pariser-Parr expression alone.

A straightforward procedure for incorporating this many-body correlation effect in a ZDO-SCF-MO calculation has been developed by Little and Gutfreund.[108-110] It is based on the Random Phase Approximation developed by Gell-Mann and others[119-121] for a dense electron gas. A brief physical description is given below.

The ground state of the system $|\Psi_o\rangle$ is first determined by the Huckel MO method. A limited set of excited states, formed by excitation of a particle from an occupied state α to an unoccupied state i, is used to expand the perturbed state $|\Psi\rangle$ which results from placing a test charge within the molecule at r_1:

$$|\Psi\rangle = |\Psi_o\rangle + 2 \sum_{i,\alpha} |\Psi_{i\alpha}\rangle \frac{\langle \Psi_{i\alpha}|V(r_1,r'')|\Psi\rangle}{-\epsilon_{i\alpha}} \quad . \qquad (3)$$

The factor 2 accounts for the sum over spins. Note that the net potential, given by

$$V(r_1,r_2) = V_o(r_1,r_2) + \sum_{r'} \delta q(r_1,r') V_o(r',r_2) \quad , \qquad (4)$$

is used in the matrix elements between Huckel states. ($V_o(r_i,r_j)$, the unscreened interaction between π-electrons at r_i and r_j, is given by Mataga's expression for γ_{ij} and thus includes σ-screening.) On using (3) to evaluate the induced charges we obtain

$$\delta q(r_1,r') = -4 \sum_{i,\alpha} \left[\int \Psi_i(r'') V(r_1,r'') \Psi_\alpha(r'') dr'' \right] (1/\epsilon_{i\alpha}) \Psi_i(r') \Psi_\alpha(r') \quad ,$$

where $\epsilon_{i\alpha} = \epsilon_i - \epsilon_\alpha$ is the excitation energy. Using the Huckel LCAO coefficients we may write this as

$$\delta q(r_1,r') = \sum_{r''} V(r_1,r'') \left[-4 \sum_{i,\alpha} \frac{(c_{ir''}c_{\alpha r''})(c_{ir'},c_{\alpha r'})}{\epsilon_i - \epsilon_\alpha} \right] \quad (5)$$

which gives

$$\delta q(r_1,r') = \sum_{r''} V(r_1,r'') \Pi (r'',r') \quad (6)$$

on substituting the expression for the mutual polarizability, $\Pi(r'',r')$. Using (5) in (4) we have

$$V(r_1,r_2) = V_o(r_1,r_2) + \sum_{r',r''} V(r_1,r'') \Pi (r'',r')V_o(r',r_2)$$

which can be rewritten

$$\sum_{r''} V(r_1,r'')\left[\delta_{r'',r_2} - \sum_{r'} \Pi(r'',r')V_o(r',r_2)\right] = V_o(r_1,r_2) .$$

Defining $R(r'',r_2)$ by the term in the brackets gives in matrix notation

$$V \cdot R = V_o$$

and thus

$$V = V_o \cdot R^{-1} .$$

Thus the effective interaction between π-electrons, $\tilde{\gamma}_{ij}$, used in the SCF-MO calculation is determined for all pairs of points from the bare interaction, V_o , and the effective dielectric function R . The expressions for the elements of the secular equation becomes

$$F_{ii} = -W_i + (1/2)q_i\tilde{\gamma}_{ii} + \sum_{j\neq i} (q_j - V_j)\tilde{\gamma}_{jj}$$

$$F_{ij} = \Delta_{ij}\beta_{ij} - (1/2)P_{ij}\tilde{\gamma}_{ij} .$$

Orbitals and excitation energies obtained in the modified ZDO-SCF-MO calculation are used in a configuration interaction calculation in the third stage. In the CI calculation the π-electron correlation effects are accounted for to a certain extent through the use of an interaction, $\tilde{V}$, screened by higher excitations. The effective interaction, V, was calculated in the static limit since the magnitude of the test charge was constant with time. In the calculation of the excited states an excited configuration mixed with the ground state corresponds to the oscillation of charge with frequency $\omega = \epsilon_{i\alpha}/\hbar$. Thus the frequency dependent mutual polarizability should be used in (6), and damping effects should be taken into account as well. In the CI method developed by Little and Gutfreund, a simplifying assumption is introduced in calculating the low-lying excited states. Generally only the lowest-lying excited singlet state is required for present purposes. Transition dipoles for other excited states are too small to give a substantial contribution. Thus the configurations may be divided into two sets, the first containing low-lying single-particle configurations, the second containing all other configurations. The interaction between members of the first set is then calculated by allowing for virtual excitations in the second set only. The frequencies of these higher excitations will be sufficiently large that the static mutual polarizability, calculated by summing only over excitations of the second set, can be used.

Using this effective interaction, the energies of the low-lying excited states were calculated along with the transition densities for each of the dyes considered in this investigation. Table 4 shows the

results for the lowest-lying excited state only. Due to the symmetry of the phenanthroline molecules the lowest-lying state results in the nitrogens of the phenanthroline ring having opposite charges. This will give negligible contribution to the effective interaction. The second and fourth excited states, both of which are listed in Table 4, result in like charges on these nitrogens. Examination of the dipole moments shows that the higher of these two has the larger moment, and only this state is used in subsequent calculations.

B. Arrays of Dye Molecules

With the wave functions, energies, and transition densities of the individual dye units, a calculation of the band of energies resulting from dye-dye interactions between dyes placed along the linear spine can be made. The wave functions for an excitation in a periodic array of N unit cells with α dyes per unit cell is given by the Bloch function

$$\xi\Psi(q) = (1/\sqrt{N}) \sum_{ml\nu} \xi c_{ql}^{\nu} \phi_{\nu}(R_{ml}) e^{iqR_m}$$

where $\phi_{\nu}(R_{ml}) = \psi_o(R_{11}) \cdots \psi_{\nu}(R_{ml}) \cdots \psi_o(R_{N\alpha})$ is the configuration in which the molecule at R_{ml} is in the excited state ψ_{ν}, all others being in their ground states. The energy, $\xi E(q)$, and coefficients ξc_{ql}^{ν}, are determined from the equation

$$H_{tot}\, \xi\Psi(q) = \xi E(q)\, \xi\Psi(q)$$

TABLE 4. Molecular Transition Densities and Transition Energy

Atom	Pyridine Cyanine E = 2.6986 e.v.	Pyridine Carbocyanine E = 2.0391 e.v.	Pyridine Dicarbocyanine E = 1.6811 e.v.
1	0.0364	0.0310	-0.0254
2	0.0647	0.0594	-0.0553
3	0.0467	0.0550	-0.0526
4	0.0274	0.0262	-0.0236
5	0.0506	0.0313	-0.0258
6	0.0562	0.0474	-0.0475
7	0.0001	-0.0332	0.0208
8	-0.0574	-0.0004	0.0009
9	-0.0506	0.0331	0.0001
10	-0.0270	-0.0310	0.0002
11	-0.0480	-0.0472	-0.0201
12	-0.0627	-0.0550	0.0476
13	-0.0365	-0.0264	0.0231
14		-0.0310	0.0255
15		-0.0590	0.0546
16			0.0522
17			0.0253

TABLE 4 (continued)

Atom	Cyanine E = 2.1822 e.v.	Carbocyanine E = 1.7915 e.v.	Dicarbocyanine E = 1.2275 e.v.
1	-0.0419	-0.0364	0.0302
2	-0.0209	-0.0210	0.0181
3	-0.0090	-0.0116	0.0102
4	-0.0150	-0.0067	0.0095
5	-0.0265	-0.0270	0.0164
6	-0.0058	-0.0021	0.0025
7	-0.0269	-0.0236	0.0170
8	-0.0466	-0.0392	0.0345
9	-0.0005	-0.0288	0.0352
10	0.0149	-0.0481	0.0447
11	0.0210	-0.0243	0.0186
12	-0.0419	0.0003	-0.0182
13	-0.0309	0.0286	-0.0003
14	0.0468	0.0066	0.0184
15	0.0062	0.0210	-0.0354
16	0.0419	0.0389	-0.0094
17	0.0310	0.0024	-0.0182
18	0.0267	0.0366	-0.0343
19	0.0089	0.0241	-0.0025
20	0.0486	0.0270	-0.0301
21	0.0270	0.0115	-0.0186
22		0.0483	-0.0164
23		0.0236	-0.0102
24			-0.0447
25			-0.0170

TABLE 4 (continued)

	Phenanthroline Cyanine		Phenanthroline Carbocyanine	
Atom	E = 1.8522 e.v.	E = 2.2359 e.v.	E = 1.4773 e.v.	E = 1.9129 e.v.
1	-0.0018	-0.0119	-0.0014	0.0082
2	-0.0011	-0.0246	-0.0029	0.0201
3	-0.0019	-0.0108	-0.0012	0.0078
4	-0.0012	-0.0247	-0.0031	0.0201
5	-0.0020	-0.0112	-0.0013	0.0080
6	-0.0013	-0.0113	-0.0009	0.0079
7	-0.0023	-0.0191	-0.0020	0.0121
8	-0.0059	-0.0419	-0.0066	0.0302
9	0.0168	0.0208	0.0045	0.0217
10	-0.0493	0.0187	-0.0088	0.0467
11	0.0134	0.0120	-0.0036	0.0249
12	-0.0068	-0.0505	-0.0110	0.0018
13	-0.0050	-0.0397	0.0067	0.0227
14	-0.0110	0.0305	-0.0433	-0.0228
15	-0.0056	0.0112	0.0126	-0.0123
16	-0.0170	0.0264	-0.0088	-0.0433
17	0.0035	0.0263	-0.0054	-0.0085
18	0.0379	0.0093	-0.0111	-0.0276
19	0.0044	0.0050	0.0054	-0.0181
20	0.0089	0.0272	0.0389	-0.0060
21	0.0239	0.0114	0.0038	-0.0071
22	-0.0020	-0.0190	0.0136	-0.0395
23	-0.0051	-0.0415	0.0222	-0.0109
24	0.0183	0.0209	-0.0017	0.0120
25	-0.0567	0.0184	-0.0054	0.0301
26	0.0144	0.0120	0.0044	0.0209
27	-0.0062	-0.0509	-0.0079	0.0470
28	-0.0048	-0.0397	-0.0032	0.0251
29	-0.0128	0.0302	-0.0120	0.0018
30	-0.0072	0.0112	0.0070	0.0220
31	-0.0211	0.0262	-0.0487	-0.0224
32	0.0033	0.0265	0.0131	-0.0123
33	0.0419	0.0094	-0.0107	-0.0429
34	0.0048	0.0051	-0.0066	-0.0085
35	0.0102	0.0268	-0.0140	-0.0274
36	0.0265	0.0114	0.0054	-0.0180
37			0.0424	-0.0061
38			0.0038	-0.0072
39			0.0141	-0.0394
40			0.0241	-0.0109

where

$$H_{tot} = \sum_i H(R_i) + \sum_{i<j} V(R_i,R_j)$$

is the total Hamiltonian composed of the single dye Hamiltonians plus the interactions between the dyes. On multiplying through by $\phi_r^*(R_{st})$ and integrating over the electronic coordinates we obtain the secular equations for this CI calculation:

$$\xi c_{qt}^{r}\left(E_r - {}^{\xi}E(q)\right) + \sum_{m,l,\nu}{}' \; \xi c_{ql}^{\nu} \, M_{ml}^{r\nu t} \, e^{iqR_m} = 0$$

where E_r is the energy of a single dye in the r^{th} excited state,

$$M_{ml}^{r\nu t} = 2\int \phi_r^*(R_{st})V(r_i,r_j)\phi_\nu(R_{ml})d\tau$$

$$= 2\iint \rho_r(r_1,R_{st})V(r_1,r_2)\rho_\nu(r_2,R_{ml})dr_1dr_2$$

$\rho_r(r_1,R_{st})$ being the molecular transition density of state r for the molecule located at R_{st}. The interaction, $V(r_1,r_2)$, between charge densities on different molecules takes place in a region in which the electrons on the spine serve to screen such interactions. Thus the Thomas-Fermi screened interaction as calculated in the previous chapter is appropriate: $V(r_1,r_2) = e^2\exp(-\lambda r_{12})/r_{12}$. Diagonalizing the CI matrix gives the excitation energies ${}^{\xi}E(q)$ and coefficients ξc_{qt}^{r} for the exciton states as a function of wavenumber q and mode ξ.

Electrons in the spine interact via the screened Coulomb interaction, $V_o(q)$, and via the excitation of the dye molecules. The

scattering of an electron from state $|k\rangle$ to the state $|k-q\rangle$ with creation of an exciton of wavevector q has the following matrix element:

$$Q = \langle 1_q; k-q|V|0;k\rangle \quad . \tag{7}$$

Ignoring the decay of the exciton, we assume for simplicity that the state has a long lifetime. As a result, we may take the energy dependence to be a delta function at the exciton energy. In the calculation of this matrix element the tight-binding approximation is used for the electron state in the spine

$$|k\rangle = \phi_k(r) = (1/\sqrt{N}) \sum_j \phi(r - R_j) e^{ikR_j}$$

where ϕ is an atomic orbital of the metal atom. Thus (7) becomes

$$Q = (1/N)^{3/2} \int \sum_{j,k} \phi^*(r_1 - R_j)\phi(r_1 - R_k)\, e^{i\{kR_k - (k-q)R_j\}}$$

$$\times V(r_1, r_2) \sum_{m,l,\nu} \left[\xi_{c\,ql}^{\nu} \phi_\nu(R_{ml})\, e^{iqR_m} \right]^* \phi_o dr_1 dt_2 d\tau$$

If we assume zero differential overlap for the metal atom orbitals and orthogonality of the molecular orbitals on different molecules we have:

$$Q = (1/N)^{3/2} \iiint \sum |\phi(r_1 - R_j)|^2\, e^{iqR_j}\, V(r_1, r_2)$$

$$\times \sum_{m,l,\nu} \xi_{c\,ql}^{\nu *}\, \phi_\nu^*(R_{ml})\, e^{-iqR_{ml}}\, \phi_o(R_{ml})\, dr_1 dr_2 d\tau$$

Now

$$\rho_\nu(r_2, R_{ml}) = (1/\sqrt{2}) \int \psi_\nu^*(R_{ml}) \psi_o(R_{ml}) dr_3 dr_4 \quad .$$

So that

$$Q = \sqrt{2}/N^{3/2} \iint \sum_j |\phi(r_1 - R_j)|^2 V(r_1, r_2) \sum_{m,l,\nu} \xi c_{q1}^{\nu *} \rho_\nu(r_2, R_{ml}) \times e^{iq(R_j - R_m)} dr_1 dr_2 \quad .$$

And $\rho_\nu(r_2, R_{ml})$ can be written $\rho_\nu(r_2 - R_m - \bar{R}_l)$ where $\bar{R}_l$ is the site vector in the unit cell. Substituting

$$r = r_1 - R_j, \quad \text{and} \quad r' = r_2 - R_j ,$$

and noting that $V(r_1, r_2) \rightarrow V(r, r')$ we have

$$Q = \sqrt{2}/N^{3/2} \sum_{l,\nu} \iint \sum_{j,m} |\phi(r)|^2 V(r, r') \xi c_{q1}^{\nu *} \rho_\nu(r' + R_j - R_m - \bar{R}_l) e^{iq(R_j - R_m)} dr dr' .$$

Letting $R_t = R_m - R_j$ we get

$$Q = \sqrt{2}/N^{3/2} \sum_{l\nu} \iint \sum_{jt} |\phi(r)|^2 V(r, r') \xi c_{q1}^{\nu *} \rho_\nu(r', R_{tl}) e^{-iqR_t} dr dr' .$$

Since the integrand is independent of j for all N j-values, we have finally

$$Q = \sqrt{(2/N)} \iint \sum_{tl\nu} |\phi(r)|^2 V(r, r') \xi c_{q1}^{\nu *} \rho_\nu(r', R_{tl}) e^{-iqR_t} dr dr' .$$

The sum over unit cells, t, can be truncated after a small number of cells since the interaction of the charge density $|\phi(r)|^2$ with the transition density ρ_ν falls off as a dipole interaction with distance $|r - r'|$.

The interaction between electrons on the spine and the dye molecules will lead to electron scattering in first order. To second order the interaction results in an electron self-energy plus a coupling between spine electrons. Thus one electron polarizes the array of dye molecules while the other interacts with the polarization. In order for a superconducting phase to appear this coupling of electrons must result in an attractive interaction sufficiently large to overcome the direct Coulomb repulsion. Since this is a second order effect the square of the above matrix elements Q will be required.

The scattering matrix elements, exciton energies, etc., were calculated for a variety of the dyes shown in Figure 5. The dyes were placed symmetrically about a metal atom in a plane perpendicular to the spine with the nitrogen atom of the dye located 2.0 Å from the metal atom. See Figure 7. Larger dye-metal atom separations resulted in much weaker interactions. (See Chapter 5.) The spacing between metal atoms along the spine was 3.40 Å which is sufficiently large to accommodate parallel layers of dye molecules. The number of unit cells used in the calculation was 9, and the results were calculated for 10 values of q from 0 to π. Special calculations were performed which used longer chains or a greater number of q-values. This was not found to affect the results. (See Chapter 5.) In calculating the Coulomb repulsion between electrons on the spine, the Mataga expression $\gamma_{ii}/(r_{ij}+a)$ was used with $a = 2.80$ Å for the platinum atom size.

Table 5 gives the scattering matrix elements, $|Q|^2$, and the excitation energies, E_q, using 4 dye molecules per unit cell. The phenanthroline cyanine case is included in this table even though there

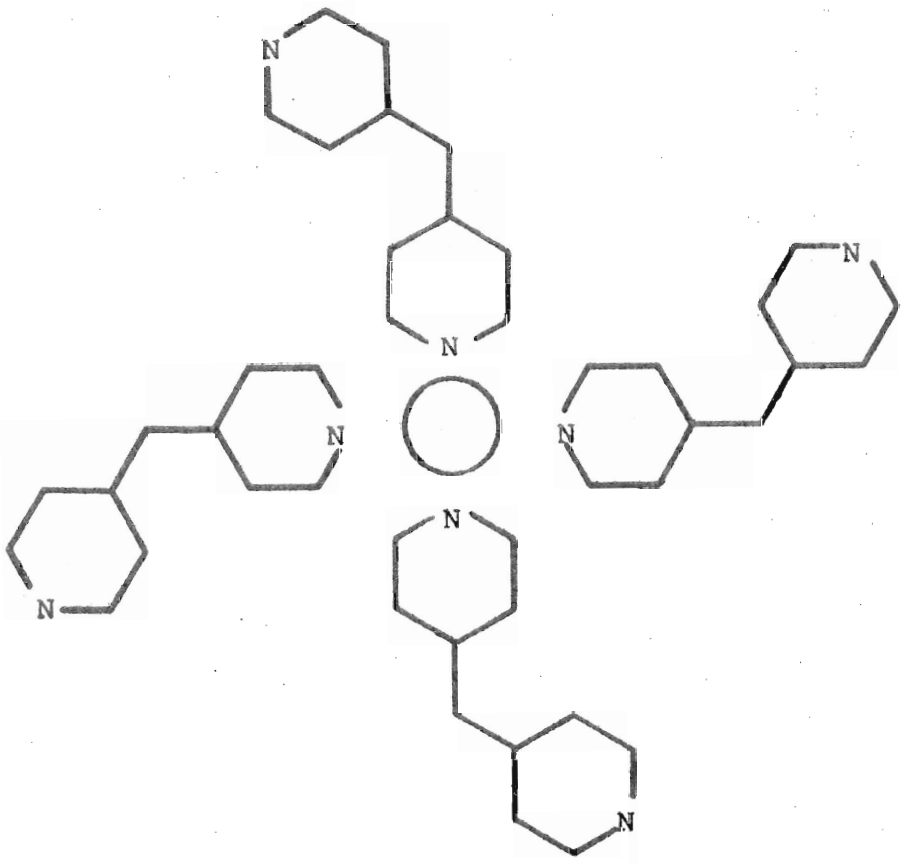

Figure 7 4-dye structure.

TABLE 5. 4-dye Array

Scattering Matrix Elements/Excitation Energies

4 dyes per unit cell Thomas-Fermi screening $\lambda = 0.14$ Å^{-1}

Dye Molecule q →	0.0	0.35	0.70	1.05	1.40	1.74	2.09	2.44	2.79	3.14
Pyridine	16.9113	14.1002	8.5764	4.4283	2.3493	1.3319	0.7393	0.4359	0.3395	0.3279
Cyanine	4.4426	4.2606	3.8232	3.3461	2.9643	2.6809	2.4629	2.3121	2.2370	2.2175
Pyridine	19.2204	15.6488	8.8996	4.2276	2.1430	1.2025	0.6427	0.3597	0.2857	0.2855
Carbocyanine	4.0406	3.8020	3.2452	2.6783	2.2714	1.9946	1.7805	1.6336	1.5707	1.5592
Pyridine	19.3219	15.4467	8.3356	3.7107	1.8281	1.0276	0.5326	0.2836	0.2303	0.2381
Dicarbocyanine	3.7344	3.4649	2.8493	2.2535	1.8615	1.6116	1.4118	1.2733	1.2228	1.2186
Phenanthroline	13.3756	10.9827	6.3879	3.1013	1.5670	0.8597	0.4530	0.2509	0.1940	0.1906
Cyanine	3.5696	3.4081	3.0252	2.6202	2.3111	2.0902	1.9203	1.8034	1.7434	1.7356

4 dyes per unit cell Thomas-Fermi screening $\lambda = 0.0$ Å^{-1}

Dye Molecule										
Pyridine	29.4369	23.0556	11.8379	5.1466	2.7101	1.6378	0.8265	0.4145	0.3619	0.4010
Cyanine	4.8598	4.5982	3.9926	3.3849	2.9529	2.6506	2.4045	2.2322	2.1602	2.1483
Pyridine	37.4567	28.2349	12.9008	4.8401	2.4764	1.5590	0.7255	0.3124	0.3039	0.3784
Carbocyanine	4.6816	4.3070	3.4700	2.7025	2.2411	1.9551	1.7024	1.5234	1.4725	1.4778
Pyridine	41.5883	30.3959	12.5827	4.1407	2.1072	1.4073	0.6067	0.2200	0.2442	0.3440
Dicarbocyanine	4.5564	4.0987	3.1021	2.2505	1.8118	1.5685	1.3204	1.1391	1.1108	1.1335
Phenanthroline	24.7443	18.9611	9.0973	3.6037	1.8199	1.0937	0.5115	0.2267	0.2070	0.2460
Cyanine	3.9522	3.7110	3.1616	2.6321	2.2815	2.0483	1.8532	1.7162	1.6663	1.6622

are actually only two molecules per unit cell. These molecules have essentially two dyes in each structure. This is verified by the large values for the scattering matrix elements. As in the subsequent cases the calculations were performed with and without Thomas-Fermi screening due to neighboring chains. The value for the screening length, 0.14 $\mathring{A}^{-1}$, is that appropriate to a density of chains and platinum oxidation state found in KCP-Cl.

The results given in Table 6 are for an arrangement of dyes in which two molecules are on opposite sides of the metal atom. This results in scattering matrix elements of half the strength of the 4-dye case while the excitation energies are shifted slightly lower.

In the final case 4-dye molecules were placed in alternate cells with the center of the nine cells occupied. This resulted in symmetric values of $|Q|^2$ and E_q about the value $q = \pi/2$ as shown in Table 7.

Finally one additional function of the dye molecules was investigated. The array of dyes acts as a dielectric background for the Coulomb interaction between electrons on the chain. This occurs through the higher excitations of the dyes and reduces the Coulomb interaction by a factor of about 2. The energies of these excitations are much larger than those of the excitations dealt with above and thus may be treated in the static limit.

In the RPA approximation the screened interaction $\tilde{V}_o(q)$ is given by

$$\tilde{V}_o(q) = V_o(q)/\left(1 - \Pi^o(q)V_o(q)\right)$$

where $\Pi^o(q)$ is the lowest-order proper polarization propagator. For

TABLE 6. 2-dye Array

Scattering Matrix Elements/Excitation Energies

2 dyes per unit cell Thomas-Fermi screening $\lambda = 0.14$ Å^{-1}

Dye Molecule q →	0.0	0.35	0.70	1.05	1.40	1.74	2.09	2.44	2.79	3.14
Pyridine	8.4551	7.0497	4.2880	2.2141	1.1746	0.6659	0.3696	0.2179	0.1607	0.1639
Cyanine	3.7845	3.6548	3.3419	2.9975	2.7167	2.5030	2.3353	2.2174	2.1570	2.1407
Pyridine	9.6099	7.8241	4.4497	2.1138	1.0715	0.6013	0.3214	0.1798	0.1429	0.1427
Carbocyanine	3.2498	3.0866	2.7044	2.3111	2.0218	1.8184	1.6580	1.5463	1.4960	1.4856
Pyridine	9.6608	7.7232	4.1678	1.8553	0.9140	0.5138	0.2663	0.1418	0.1151	0.1191
Dicarbocyanine	2.9179	2.7373	2.3226	1.9155	1.6390	1.4551	1.3059	1.2012	1.1598	1.1543

2 dyes per unit cell Thomas-Fermi screening $\lambda = 0.0$ Å^{-1}

Dye Molecule										
Pyridine	14.7173	11.5270	5.9186	2.5732	1.3550	0.8189	0.4132	0.2072	0.1809	0.2005
Cyanine	4.0563	3.8696	3.4366	2.9996	2.6841	2.4573	2.2691	2.1353	2.0772	2.0664
Pyridine	18.7276	14.1169	6.4502	2.4200	1.2382	0.7795	0.3627	0.1962	0.1519	0.1892
Carbocyanine	3.6561	3.3990	2.8238	2.2935	1.9685	1.7594	1.5716	1.4370	1.3951	1.3965
Pyridine	20.7955	15.1975	6.2912	2.0704	1.0536	0.7036	0.3633	0.1150	0.1221	0.1720
Dicarbocyanine	3.4329	3.1249	2.4550	1.8747	1.5686	1.3894	1.2065	1.0719	1.0457	1.0587

TABLE 7. Empty Cells Array

Scattering Matrix Elements/Excitation Energies

4 dyes per unit cell Thomas-Fermi screening $\lambda = 0.14\ \text{Å}^{-1}$

Dye molecules in alternate cells only

Dye Molecule q →	0.0	0.35	0.70	1.05	1.40	1.74	2.09	2.44	2.79	3.14
Pyridine	5.4872	4.7035	3.2187	2.1949	1.8027	1.8020	2.1918	3.2124	4.6972	5.4872
Cyanine	3.3300	3.2487	3.0674	2.9041	2.8221	2.8219	2.9035	3.0665	3.2480	3.3300
Pyridine	6.0477	5.0407	3.2083	2.0401	1.6372	1.6365	2.0368	3.2009	5.0327	6.0477
Carbocyanine	2.7999	2.6863	2.4392	2.2290	2.1325	2.1323	2.2283	2.4380	2.6853	2.7999
Pyridine	5.9625	4.8622	2.9225	1.7621	1.3976	1.3970	1.7591	2.9150	4.8535	5.9625
Dicarbocyanine	2.4765	2.3438	2.0611	1.8322	1.7360	1.7359	1.8315	2.0598	2.3427	2.4765

4 dyes per unit cell Thomas-Fermi screening $\lambda = 0.0\ \text{Å}^{-1}$

Dye molecules in alternate cells only

Dye Molecule										
Pyridine	9.1774	7.2991	4.1693	2.5219	2.1380	2.1375	2.5181	4.1577	7.2845	9.1774
Cyanine	3.5040	3.3792	3.1121	2.8942	2.8011	2.8009	2.8935	3.1109	3.3781	3.5040
Pyridine	11.3413	8.6003	4.3056	2.3255	1.9890	1.9889	2.3215	4.2967	8.5794	11.3412
Carbocyanine	3.0797	2.8897	2.4964	2.2019	2.0975	2.0973	2.2011	2.4947	2.8882	3.0797
Pyridine	12.3744	9.0240	4.0313	1.9766	1.7377	1.7379	1.9729	4.0148	8.9938	12.3743
Dicarbocyanine	2.8450	2.6048	2.1204	1.7849	1.6896	1.6895	1.7840	2.1183	2.6028	2.8450

the dye molecules we calculate $V^{(2)}(q)$, the second order term in the RPA expansion, from the expression

$$V^{(2)}(q) = \iiiint V_o(x,x_1)\Pi^o(x_1,x_2)V_o(x_2,x')e^{iq(x-x')}dxdx_1dx_2dx' \ .$$

$\Pi^o(x_1,x_2)$ is given by the mutual polarizability of a single dye unit, x_1 and x_2 being restricted to the same molecule. See Figure 8.

Figure 8 Infinite series for Coulomb interaction screened by higher excitations.

Then $\tilde{V}_o(q)$ is given by

$$\tilde{V}_o(q) = V_o(q)/\left(1 - V^{(2)}(q)/V_o(q)\right) \ .$$

Values for the screened interaction depend upon the dyes in the arrays. Table 8 presents values of $\tilde{V}_o(q)$ for the case of pyridine cyanine with 4 dyes per unit cell and $\lambda = 0.14\ \text{Å}^{-1}$. Values of $V_o(q)$ are presented for comparison.

TABLE 8. Coulomb Interaction along Spine

(Calculated using 9 unit cells)

q	No Screening	Thomas-Fermi Screening Only ($\lambda = 0.14$ Å^{-1})	Thomas-Fermi Plus Higher Excitation Screening (4 pyridine cyanine dyes) ($\lambda = 0.14$ Å^{-1})
0.0	16.7595	6.7432	2.5303
0.35	13.2219	6.1176	2.3052
0.70	6.4703	4.7605	1.8377
1.05	2.8737	3.6128	1.4994
1.40	3.3654	3.0351	1.4174
1.74	3.9712	2.7169	1.4233
2.09	2.6628	2.3804	1.3797
2.44	1.5635	2.1310	1.3470
2.79	2.2684	2.0931	1.3787
3.14	3.0384	2.1253	1.4078

IV. THEORETICAL DESCRIPTIONS OF SUPERCONDUCTIVITY

A. Phenomenological Theory

The theoretical description of superconductivity began with the phenomenological London equations[122] which sought to describe the electrodynamics of the superconducting state and especially to account for the Meissner effect.[2] An elaboration of these equations was made by Ginsburg and Landau.[123] Whereas the London equations treated all electrons as belonging to the superconducting phase, the Ginsburg-Landau equations dealt with the intermediate state which consisted of both superconducting and normal regions, the order parameter, $\psi(r)$, characterizing the degree of superconductivity at each point in the material. The essential correctness of the Ginsburg-Landau equations has been confirmed by detailed study of the microscopic theory (BCS) and have found wide application in the electrodynamics of superconductors near the transition temperature.[124]

B. Microscopic Theory

The first microscopic theory to account for the various experimental observations of superconductors, as mentioned in the introductory chapter, is the well-known theory of Bardeen, Cooper, and Schrieffer.[6] Two fundamental breakthroughs which led to the development of the BCS theory were first, the theoretical prediction by Frohlich[125] and experimental observation by several workers[4,5] of the isotope effect, and second, the discovery by Cooper[126] that two

electrons excited above a Fermi sea and interacting via an arbitrarily weak attractive interaction form a bound pair thus making the entire Fermi sea unstable to the formation of such pairs. The BCS approach is highly intuitive. The isotope effect indicated that the lattice played a fundamental role. It was known at the time that the perturbation of the electron states by the phonons when carried to second order led to a self-energy correction for an electron through the diagonal elements and to electron-electron interaction via phonon exchange through the off-diagonal elements. The second order interaction in the notation of second quantization is

$$H'' = \sum_{q} \sum_{\vec{k}\vec{k}'} \frac{|M_q|^2 \omega_q}{(\epsilon_k - \epsilon_{k-q})^2 - \omega_q^2} \; c^{\dagger}_{k'+q} c_{k'} c^{\dagger}_{k-q} c_k \qquad (8)$$

where ϵ_k is the energy of the electron state $\vec{k}$ measured from the Fermi surface, $c^{\dagger}_k$ and c_k are the creation and annihilation operators for the state $\vec{k}$, respectively, and ω_q is the frequency of a longitudinal phonon of wavevector $\vec{q}$. Figure 9 shows the graphical representation of this interaction. BCS noted that for $|\epsilon_{k\pm q} - \epsilon_k| < \omega_q$ the interaction was attractive. However, due to the Fermi statistics obeyed by the electrons, the field operators acting on the ground state wave function, e.g., $c^{\dagger}_{k'+q} c_{k'} c^{\dagger}_{k-q} c_k \Phi_o$, could result in either positive or negative values depending on the particular occupation of states which preceded the field operators. This is analogous to the difference in sign between the direct and exchange terms in a Hartree-Fock treatment of a molecular wave function that results on permuting two states in a Slater determinant.

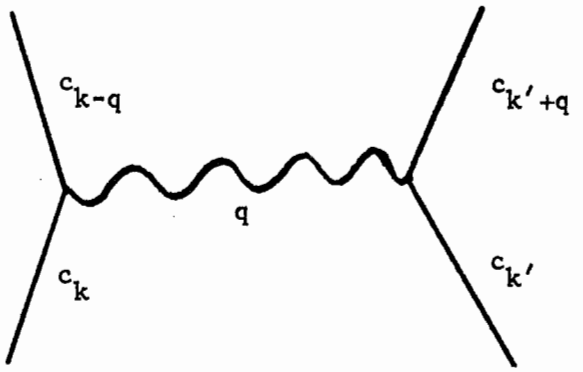

Figure 9 Phonon exchange

BCS circumvented this alternation in sign of the matrix elements by imposing the restriction that only wave functions in which occupancy of electron states occurred in pairs would be considered in constructing the ground state. The choice of pairs, viz., pairs of opposite spin and momentum, was based on the following: 1) interaction between opposite spin electrons was stronger due to the lack of the exchange term, and 2) using pairs of opposite momentum gave the largest number of states available for interaction within an energy range ω_c from the Fermi surface in the absence of magnetic fields. With these restrictions the BCS reduced Hamiltonian encompassed only a small part of the total Hamiltonian. However, as seen a posteriori, it contained just that part which gives rise to the superconducting state. This reduced Hamiltonian can be written

$$H_{red} = \sum_k \epsilon_k (c_k^\dagger c_k + c_{-k}^\dagger c_{-k}) - \sum_{kk'} V_{kk'} c_{k'}^\dagger c_{-k'}^\dagger c_{-k} c_k$$

which operates only within the pair sub-space.

The trial wave function was constructed by placing electrons in pair states with probability of occupancy given by h_k . Thus

$$\Psi = \prod_k \left[(1 - h_k)^{1/2} + h_k \, c^{\dagger}_{-k\downarrow} c^{\dagger}_{k\uparrow} \right] \Phi_o$$

where Φ_o is the vacuum. The variational method was then applied to determine the function h_k which would give the lowest energy for this type of wave function. The energy of the occupied states is given by

$$W_{KE} = 2 \sum \epsilon_k h_k$$

where the 2 accounts for spin up and spin down electrons. The interaction term is

$$W_I = -\sum V_{kk'} \left| h_k (1 - h_k) h_{k'} (1 - h_{k'}) \right|^{1/2} .$$

Minimization of the total energy, $W_o = W_{KE} + W_I$, leads to the equation

$$\frac{[h_k (1 - h_k)]^{1/2}}{1 - 2h_k} = \frac{\sum V_{kk'} [h_{k'} (1 - h_{k'})]^{1/2}}{2\epsilon_k} . \qquad (9)$$

With the definition

$$\Delta_k \equiv \sum_{k'} V_{kk'} [h_{k'} (1 - h_{k'})]^{1/2}$$

we have the result

$$h_k = 1/2 \left[1 - \frac{\epsilon_k}{(\epsilon_k^2 + \Delta_k^2)^{1/2}} \right]$$

Noting that

$$[h_k(1-h_k)]^{1/2} = \frac{\Delta_k}{2(\epsilon_k^2+\Delta_k^2)^{1/2}} \tag{10}$$

and substituting (10) into (9), we obtain the BCS condition determining the energy gap:

$$\Delta_k = \sum_{k'} V_{kk'} \frac{\Delta_{k'}}{2(\epsilon_{k'}^2+\Delta_{k'}^2)^{1/2}} \tag{11}$$

It is this gap function and the transition temperature related to it that we wish to determine for our linear chain - dye systems.

BCS found an approximate solution to the above gap equation by assuming $V_{kk'}$ to be a separable potential with a cutoff:

$$V_{kk'} = \begin{cases} V & |\epsilon_k|, |\epsilon_{k'}| < \omega_c \\ 0 & \text{otherwise,} \end{cases}$$

giving

$$\Delta_o = 2\hbar\omega_c e^{-1/\mathcal{N}(0)V} \tag{12}$$

in the weak-coupling limit. $\mathcal{N}(0)$ is the density of states at the Fermi surface.

The same calculation can be carried out for finite temperatures giving an equation similar to (11), but including the probability, $(1-2f_{k'})$, that states $\vec{k}',-\vec{k}'$ to which $\vec{k},-\vec{k}$ are scattered, are unoccupied:

$$\frac{[h_k(1-h_k)]^{1/2}}{1-2h_k} = \sum_{k'} V_{kk'}[h_{k'}(1-h_{k'})]^{1/2}(1-2f_{k'}) \quad .$$

Minimization of the free energy with respect to f_k gives

$$f_k = \frac{1}{e^{\beta E_k} + 1}$$

where

$$E_k = (\epsilon_k^2 + \Delta_k^2)^{1/2} \quad .$$

This leads to the integral equation

$$\Delta_k = \sum_{k'} \frac{V_{kk'}\Delta_{k'}}{2(\epsilon_{k'}^2 + \Delta_{k'}^2)^{1/2}} \tanh\left((\beta/2)[\epsilon_{k'}^2 + \Delta_{k'}^2]^{1/2}\right) \qquad (13)$$

$$\beta = 1/kT$$

which determines the transition temperature; at $T = T_c$, $\Delta_k = 0$. Thus

$$kT_c = 1.14\hbar\omega_c e^{-1/\mathcal{N}(0)V} \qquad (14)$$

in the weak-coupling limit. Combining (12) and (14) we find

$$2\Delta_o(0)/kT_c = 3.50 \quad , \qquad (15)$$

which is predicted to be the same for all superconductors based on the law of corresponding states. We will use this relationship to estimate T_c from the calculated gap function at $T = 0^oK$.

The simple form for the BCS potential combines all the factors producing an attractive interaction at the Fermi surface into one effective potential well whose depth, V , and width, $2\omega_c$, then characterize the system. While this method works quite well for the so-called "weak-coupling" superconductors, it completely ignores

the details of the interaction which leads to Cooper pair formation. An investigation of these details is necessary for the strong-coupling superconductors because the electron states involved in pair formation can no longer be treated as simple Landau quasiparticles since their decay rate becomes comparable with their energy.[127] In addition, superconductivity has the inherent difficulty of involving a retarded interaction. Coupling of the exciton (or phonon) field with the electrons may result in overscreening or underscreening for frequency dependent charge distributions. Indeed, overscreening of the Coulomb repulsion between electrons is the basic reason for the attractive interaction which results in Cooper pair formation.[128] The Hamiltonian scheme requires that two-body potentials be instantaneous, thus a retarded potential would have to be simulated by a velocity dependent potential.

C. Compensation of Dangerous Diagrams

Soon after the BCS treatment a new approach was developed by Bogoliubov which applied a canonical transformation to the Frohlich Hamiltonian. This transformation had previously been developed for Bose-Einstein systems.[129] The new method, which allowed for explicit inclusion of the coupling of the electron and phonon fields, is known as the Method of Compensation of Dangerous Diagrams.[130] This method will be developed below to derive the integral equations for the gap function and to show that different interpretations of the determining condition lead to different gap equations.[131-133]

The Bogoliubov compensation of dangerous diagrams approach begins with the Frohlich Hamiltonian that describes the coupled Fermi and Bose fields. In this development we will use phonons for the Bose field. The Hamiltonian can be written as the sum of the ion Hamiltonian:

$$H_{ion} = \sum_{l} P_l^2/2M_l + V(x_l) \quad ,$$

the electron Hamiltonian:

$$H_{el} = \sum_{i} p_i^2/2m + \sum_{i<j} \frac{e^2}{|r_i - r_j|} \quad ,$$

and the interaction term:

$$H_{int} = \sum_{il} U(r_i, x_l) \quad .$$

In the notation of second quantization this becomes

$$H = H_o + H_{int} = \sum_{k\sigma} \epsilon_k c^{\dagger}_{k\sigma} c_{k\sigma} + \sum_{q} \omega_q b^{\dagger}_q b_q + \sum_{\substack{kk'\sigma \\ q=k'-k}} M_q c^{\dagger}_{k\sigma} c_{k'\sigma} (b^{\dagger}_q + b_{-q}) \quad .$$

It is the second order perturbation term of H_{int} that leads to the attractive interaction as noted above. While the BCS method eliminates the phonon field and deals only with an electron field with an effective interaction due to H_{int}, the Bogoloubov approach deals with both fields. In dealing with the phonon field the basic motivation is to transform the electron field operators c_k and $c^{\dagger}_k$ in such a manner that the effect of H_{int} on the ground state disappears to low order in the interaction.

The general form of the Bogoliubov transformation is given by:

$$\alpha_k^\dagger = u_k c_{k\uparrow}^\dagger - v_k c_{-k\downarrow} \qquad \alpha_k = u_k c_{k\uparrow} - v_k c_{-k\downarrow}^\dagger$$

$$\beta_{-k} = u_k c_{-k\downarrow} + v_k c_{k\uparrow}^\dagger \qquad \beta_{-k}^\dagger = u_k c_{-k\downarrow}^\dagger + v_k c_{k\uparrow}$$

where $u_k^2 + v_k^2 = 1$ is required to retain the anti-commutation properties of the operators making the transformation canonical:

$$[\alpha_k, \alpha_{k'}^\dagger]_+ = \delta_{kk'} \qquad [\alpha_k, \alpha_{k'}]_+ = [\alpha_k^\dagger, \alpha_{k'}^\dagger]_+ = 0$$

$$[\beta_k, \beta_{k'}^\dagger]_+ = \delta_{kk'} \qquad [\beta_k, \beta_{k'}]_+ = [\beta_k^\dagger, \beta_{k'}^\dagger]_+ = 0 \quad .$$

The inverse transformation is easily found to be:

$$c_{k\uparrow}^\dagger = u_k \alpha_k^\dagger + v_k \beta_{-k} \qquad c_{k\uparrow} = u_k \alpha_k + v_k \beta_{-k}^\dagger$$

$$c_{-k\downarrow} = u_k \beta_{-k} - v_k \alpha_k^\dagger \qquad c_{-k\downarrow}^\dagger = u_k \beta_{-k}^\dagger - v_k \alpha_k \quad .$$

This transformation thus anticipates the pairing of time-reversed electron states. With these definitions the Frohlich Hamiltonian can be written, (see Appendix):

$$H = H_o + H_1^\alpha + H_2^\alpha + H_1^\beta + H_R + U \quad ,$$

where

$$H_o = \sum_k E_k (\alpha_k^\dagger \alpha_k + \beta_{-k}^\dagger \beta_{-k}) + \sum_q \omega_q b_q^\dagger b_q$$

$$H_1^\alpha = \sum_{\substack{kk' \\ q=k'-k\neq 0}} M_q [(u_k v_{k'} + u_{k'} v_k)(\alpha_k^\dagger \beta_{-k'}^\dagger + \beta_{-k} \alpha_{k'})(b_q^\dagger + b_{-q})]$$

$$H_1^{\beta} = \sum_k 2\epsilon_k u_k v_k (\alpha_k^{\dagger}\beta_{-k}^{\dagger} + \beta_{-k}\alpha_k)$$

$$H_R = \sum_k (\epsilon_k(u_k^2 - v_k^2) - E_k)(\alpha_k^{\dagger}\alpha_k + \beta_{-k}^{\dagger}\beta_{-k})$$

$$U = \sum_k 2\epsilon_k v_k^2 = \text{constant}$$

$$H_2^{\alpha} = \sum_{\substack{kk' \\ q=k'-k\neq 0}} M_q[(u_k u_{k'} - v_k v_{k'})(\alpha_k^{\dagger}\alpha_{k'} + \beta_{-k'}^{\dagger}\beta_{-k})(b_q^{\dagger} + b_{-q})] \quad .$$

The first step in the method of compensation of dangerous diagrams is to note that it is the matrix elements of H_1^{β} which give rise to the dangerous terms. These matrix elements have energy denominators of the form

$$\{\epsilon(k_1) + \epsilon(k_2) + \ldots + \epsilon(k_n)\}$$

which lead to singularities as each $\epsilon_k \to 0$, i.e., at the Fermi surface. In the normal state, terms such as these are not dealt with because in that case the number of particles is fixed.

Bogoliubov chose to compensate for these terms by requiring that they cancel with certain other terms arising from the other perturbations. It is the ambiguity of choice of compensating terms which leads to the several possible results for the gap equation. We consider first the case treated by Bogoliubov. Figure 10 shows in diagram form the compensation condition. We compensate for the creation of the pair of quasiparticles by the combined application of H_1^{α} and H_2^{α}. In each of the diagrams the starting point is the vacuum state $|0\rangle$, and the final state $|F\rangle$ has two quasiparticles

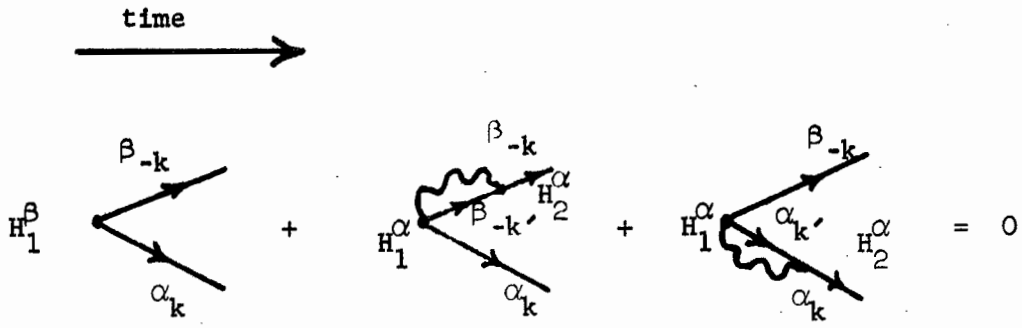

Figure 10 Compensation condition for creation of pairs.

and no phonons, $|F\rangle = |1_{\alpha_k}, 1_{\beta_{-k}}; 0\rangle$. The two possible intermediate states generated by H_1^α are given by the two diagrams on the right. In terms of matrix elements we have:

$$\langle F|H_1^\beta|0\rangle + \sum_I \frac{\langle F|H_2^\alpha|I\rangle\langle I|H_1^\alpha|0\rangle}{E_0 - E_I} = 0 \quad .$$

On substituting the expressions for H_1^β, H_1^α, and H_2^α and noting that $E_0 = U$, $E_I = \epsilon_k(u_k^2 - v_k^2) + \epsilon_{k'}(u_{k'}^2 - v_{k'}^2) + \omega_q + U$, the above expression becomes, (see Appendix),

$$2\epsilon_k u_k v_k - 2\sum_{k'} |M_q|^2 \frac{(u_{k'}u_k - v_{k'}v_k)(u_{k'}v_k + v_{k'}u_k)}{\epsilon_k(u_k^2 - v_k^2) + \epsilon_{k'}(u_{k'}^2 - v_{k'}^2) + \omega_q} = 0 \quad . (16)$$

If we neglect the renormalization of H_R and set $E_k = \epsilon_k(u_k^2 - v_k^2)$, then (16) becomes

$$\left\{\epsilon_k - \sum_{k'} \frac{|M_q|^2(u_{k'}^2 - v_{k'}^2)}{E_{k'} + E_k + \omega_q}\right\} u_k v_k - (u_k^2 - v_k^2) \sum_{k'} |M_q|^2 \frac{u_{k'}v_{k'}}{E_{k'} + E_k + \omega_q} = 0 \quad .$$

Finally, we define ξ_k by the leftmost term above, and write u_k and

v_k in terms of the gap function using the definition

$$u_k^2 = (1/2)\left(1 + \frac{\xi_k}{\sqrt{\xi_k^2 + \Delta_k^2}}\right); \quad v_k^2 = (1/2)\left(1 - \frac{\xi_k}{\sqrt{\xi_k^2 + \Delta_k^2}}\right) .$$

We find the equation for the gap function:

$$\Delta_k = \sum_{k'} \frac{\Delta_{k'}}{\sqrt{\xi_{k'}^2 + \Delta_{k'}^2}} \frac{|M_q|^2}{E_{k'} + E_k + \omega_q} .$$

Comparison with (11) shows two differences of this result with the BCS result:

$$\epsilon_k \text{ is replaced by } \xi_k = \epsilon_k - \sum_{k'} \frac{|M_q|^2 (u_{k'}^2 - v_{k'}^2)}{E_{k'} + E_k + \omega_q}$$

and

$$V_{kk'} \text{ is replaced by } \frac{|M_q|^2}{E_{k'} + E_k + \omega_q} .$$

The ground state shows qualitatively the same properties in both cases, i.e., an energy gap in the excitation spectrum of minimum magnitude Δ_o.

Suppose that we investigate the destruction of pairs rather than their creation in the dangerous diagrams method. That is, we use the compensation condition expressed in Figure 11. The analysis proceeds as in the previous case except that the energy denominator, $E_O - E_I$, now becomes

$$E_O - E_I = \left\{ 2\epsilon_k (u_k^2 - v_k^2) + U \right\} - \left\{ \epsilon_k (u_k^2 - v_k^2) + \epsilon_{k'} (u_{k'}^2 - v_{k'}^2) + \omega_q + U \right\}$$

$$= \epsilon_k (u_k^2 - v_k^2) - \epsilon_{k'} (u_{k'}^2 - v_{k'}^2) - \omega_q ,$$

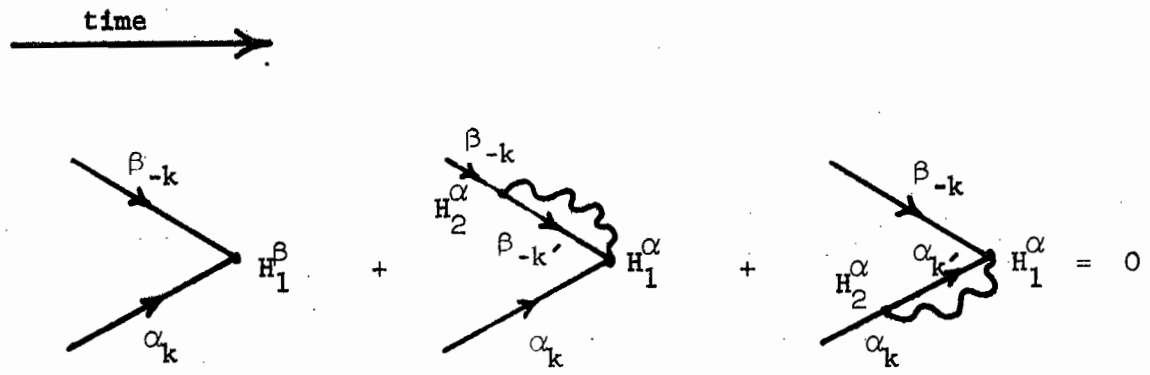

Figure 11 Compensation condition for destruction of pairs.

which leads to the gap equation

$$\Delta_k = \sum_{k'} \frac{\Delta_{k'}}{\sqrt{\xi_{k'}^2 + \Delta_{k'}^2}} \frac{|M_q|^2}{E_{k'} - E_k + \omega_q} \quad .$$

As a final adaptation of the method of compensation of dangerous diagrams we now allow for the renormalization of the quasiparticle energy through the term H_R . ξ_k and Δ_k will be chosen in such a manner that the corrections to the quasiparticle energy $E_k = \sqrt{\xi_k^2 + \Delta_k^2}$ in H_o will cancel with the second order terms from H_1^α and H_2^α . This is shown in diagram form in Figure 12.

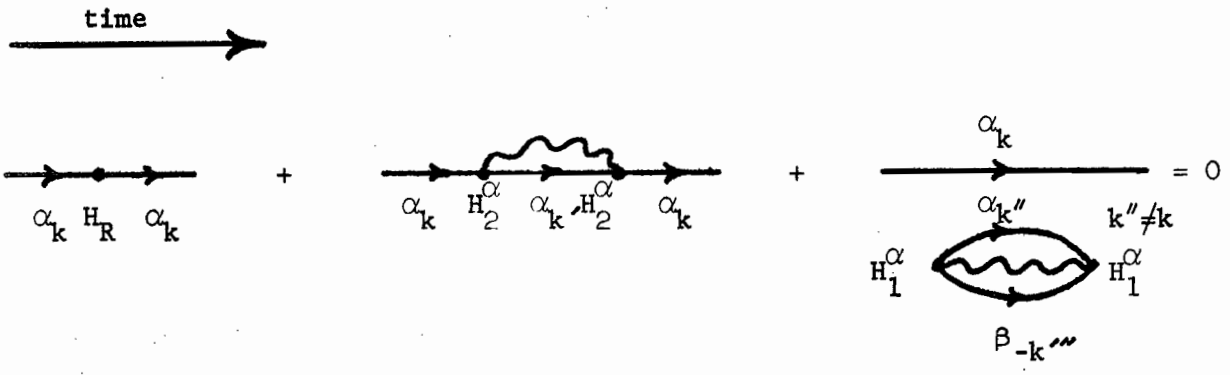

Figure 12 Compensation condition using renormalization.

As a result of this renormalization, the denominator for a process generated by H_1^β is no longer singular as the energy approaches the Fermi energy. We note that the presence of the α_k quasiparticle in the rightmost diagram of Figure 12 prevents the vacuum polarization process with $k'' = k$. In developing the expressions for these diagrams we choose the initial and final states to contain one quasiparticle, α_k. The same result would be obtained for β_{-k}. Then

$$|F\rangle = \alpha_k^\dagger |0\rangle$$

where $|0\rangle$ is the vacuum state for the quasiparticle operators. Expressed in terms of matrix elements the compensation condition is:

$$\langle F|H_R|F\rangle + \sum_I \left\{ \frac{\langle F|H_2^\alpha|I\rangle\langle I|H_2^\alpha|F\rangle}{E_F - E_I^{EX}} \quad \frac{\langle F|H_1^\alpha|I\rangle\langle I|H_1^\alpha|F\rangle}{E_F - E_I^{VP}} \right\} = 0 .$$

Substituting for the operators H_R, H_2^α, and H_1^α, the matrix elements may be expanded as in the above cases (see Appendix). We find for the second order process, energy terms E_F, E_I^{EX}, and E_I^{VP} given by

$$E_F = \epsilon_k(u_k^2 - v_k^2) + U$$

$$E_I^{EX} = \epsilon_{k'}(u_{k'}^2 - v_{k'}^2) + \omega_q + U$$

$$E_I^{VP} = \epsilon_k(u_k^2 - v_k^2) + \epsilon_{k''}(u_{k''}^2 - v_{k''}^2) + \epsilon_{k'''}(u_{k'''}^2 - v_{k'''}^2) + \omega_q + U$$

As shown in the Appendix, the compensation condition reduces to:

$$\epsilon_k(u_k^2 - v_k^2) - E_k - \sum_{\substack{k' \\ q=k-k'}} |M_q|^2 \left[\frac{(u_{k'}u_k - v_{k'}v_k)^2}{E_{k'} - E_k + \omega_q} - \frac{(u_{k'}v_k + u_k v_{k'})^2}{E_{k'} + E_k + \omega_q} \right] = 0.$$

Now with the definition of the renormalization factor

$$\xi_k = \epsilon_k/\gamma_k , \qquad \gamma_k = 1 + \sum_{k'} \frac{|M_q|^2}{(\omega_q + E_{k'})^2 - E_k^2} ,$$

we have

$$\Delta_k = (1/2\gamma_k) \sum_{k'} |M_q|^2 \frac{\Delta_{k'}}{\sqrt{\xi_{k'}^2 + \Delta_{k'}^2}} \left\{ \frac{1}{E_{k'} - E_k + \omega_q} + \frac{1}{E_{k'} + E_k + \omega_q} \right\} ,$$

thus including both the resonant and nonresonant denominators which occurred separately in the previous treatments. We see, therefore, that all the different interpretations of the method of compensation of dangerous diagrams eliminate the singular energy denominators for processes described by H_1^{β} , but lead to different expressions for the gap equation.

A further significant development carried out by Bogoliubov was the inclusion of the instantaneous Coulomb repulsion in the Hamiltonian.[134] It was found that the Coulomb repulsion lowers the transition temperature to a smaller extent than would be anticipated on the basis of the BCS theory. Thus for a Coulomb pseudopotential of strength V_C the BCS theory gives

$$\Delta = 2\hbar\omega_c e^{-1/\mathcal{N}(0)(V-V_C)}$$

whereas Bogoliubov found

$$\Delta = 2\hbar\omega_c \exp\left\{-1/\mathcal{N}(0)\left[V - \frac{V_C}{1 + V_C \ln(E_f/\bar{\omega})}\right]\right\} .$$

This result was confirmed with the development of the Green's function technique which also gave a natural definition to the cutoff frequency $\bar{\omega}$ in the Coulomb pseudopotential.[135] The Green's function technique

has the advantage that it may easily be extended beyond the second order of perturbation theory. This allows us to deal with strong-coupling superconductors which occur in the case of the excitonic mechanism as well as for many phonon superconductors.

D. Green's Function Method — Gor'kov

Initial development of the Green's function method was carried out by Gor'kov.[136] It had been known for some time that a perturbation expansion of the electron-phonon Hamiltonian did not lead to superconductivity to any order in the expansion even though formally the expansion parameter (or coupling constant) was small. This is due to the strong scattering between states near the Fermi surface and was confirmed in the BCS gap equation by the appearance of the coupling constant in the form $e^{-1/g}$ which has an essential singularity as $g \to 0$. We have reviewed thus far two methods for resolving this dilemma. BCS used a variational approach within the space which allows for the pairing of electrons. Bogoliubov compensates to low order in perturbation theory for the dangerous terms leading to the divergent scattering. The Green's function technique of Gor'kov follows along the first of these two by explicitly taking into account the formation of Cooper pairs. This is a feature common to the subsequent Green's function treatments.

Gor'kov develops the simplest case with a model Hamiltonian describing only the Fermions which interact via an instantaneous four Fermion interaction:

$$H = \int \left\{ - (\psi^\dagger \nabla^2 / 2m\psi) + (g/2)(\psi^\dagger(\psi^\dagger\psi)\psi) \right\} dx$$

If we were to treat only the kinetic energy term and possibly a one-electron potential in zeroth order, we would obtain zeroth order Green's functions for the particles in plane wave states

$$G_o^N(p,\omega) = \frac{1}{\omega - \epsilon_p + i\omega\delta} .$$

However, this does not allow for the pairing interaction to be taken into account and does not lead to a superconducting ground state. Rather than dealing with this in a perturbation approach, the total Hamiltonian is used to describe the ground state. In the equations of motion for the field operators there then arise terms such as $(\psi^\dagger\psi)\psi(x)$, which subsequently occur in the equation for the Green's function as the time-ordered product

$$\langle T(\psi_\alpha(x_1)\psi_\beta(x_2)\psi_\gamma^\dagger(x_3)\psi_\delta^\dagger(x_4))\rangle .$$

If this term is approximated by combining creation and destruction operators, the resulting expression,

$$\langle T(\psi_\alpha\psi_\delta^\dagger)\rangle\langle T(\psi_\beta\psi_\gamma^\dagger)\rangle - \langle T(\psi_\alpha\psi_\gamma^\dagger)\rangle\langle T(\psi_\beta\psi_\delta^\dagger)\rangle ,$$

gives rise to the direct and exchange terms of the Hartree-Fock approximation. Gor'kov showed that one may account for the creation and destruction of pairs of particles by including the additional term

$$\langle N|T(\psi_\alpha\psi_\beta)|N+2\rangle\langle N+2|T(\psi_\gamma^\dagger\psi_\delta^\dagger)|N\rangle .$$

The change in particle number by ±2 on creation or destruction of a pair is shown explicitly. Thus we are again dealing with a system having a variable number of particles as in the BCS and Bogoliubov cases.

Both results are in agreement with the BCS theory. The lifetimes for these states, determined by the imaginary part of the Green's function, were not calculated.

While the Gor'kov paper is important in that it was the first to treat the superconducting problem using the Green's function technique, it is based on a simplified four-Fermion interaction thus neglecting phonon field (or exciton, as in the present study). Because of this simplicity, the true Green's function could be determined for this model system.

E. Green's Function Method – Eliashberg

Inclusion of the phonon field using the Green's function approach was first carried out by Eliashberg.[137] The interaction between the two fields was treated according to the full interaction Hamiltonian (unsimplified), and on account of this, the true Green's function could not be determined directly, but rather approximated by summing an infinite perturbation series according to the Feynman-Dyson method. We should note, however, that it is not the fact that a certain class of Feynman diagrams are summed to all orders that gives rise to the superconducting ground state solution. Rather one starts at the outset with a bare Green's function, $G_o(p,\omega)$, which already describes, along with $F_o^{\dagger}(p,\omega)$, the superconducting ground state. Thus we are not contradicting the assertion that the superconducting ground state cannot be achieved by perturbation theory to any order. We are improving upon a zeroth order superconducting ground state. We now have the apparatus necessary to describe the details of individual superconducting

materials through the phonon's Green's function $D_o(q,\omega)$.

Several accounts of the Eliashberg method have been published.[138] The original paper introduced unwieldy 4-component vectors $\psi = (\psi_{1/2}, \psi_{-1/2}, \psi^{\dagger}_{-1/2}, \psi^{\dagger}_{1/2})$ in order to treat the pair formation. Contemporary work by Nambu[139] on the gauge invariance introduced the widely used spinor notation in which the new field operators are two-component operators that pair time reversed states:

$$\Psi_k = \begin{pmatrix} c_{k\uparrow} \\ c^{\dagger}_{-k\downarrow} \end{pmatrix}, \text{ and its Hermitian adjoint: } \Psi^{\dagger}_k = \begin{pmatrix} c^{\dagger}_{k\uparrow} \\ c_{-k\downarrow} \end{pmatrix}.$$

The simplicity of the Feynman diagram technique is preserved by using the Ψ_k operators. The result is a 2 x 2 matrix equation which treats the normal and pair Green's functions equally. We shall not require the spinor notation in the detailed treatment of the method by Kirzhnits, et. al., and shall continue to use the separate functions, $G(p,\omega)$ and $F^{\dagger}(p,\omega)$, for the single particle and pair propagators, respectively.

Eliashberg's approach is along the following lines. We begin with the Hamiltonian for the coupled electron-phonon system

$$H = H_o + H_{int}$$

$$H_o = \int \psi^{\dagger}_{\sigma}(x)[H_{el}(x) - \mu]\psi_{\sigma}(x)dx + H_{ph}$$

$$H_{int} = \int \psi^{\dagger}_{\sigma}(x)\psi_{\sigma}(x)\phi(x)dx$$

$$\psi_{\sigma}(x) = \Omega^{-1/2} \sum_k a_k e^{ik\cdot x}$$

$$\phi(x) = \Omega^{-1/2} \sum_{q<q_m} \alpha_q (b_q + b^{\dagger}_{-q}) e^{iq\cdot x}$$

$$\alpha^2_q = \lambda_o \pi^2 s_q / k_o$$

where $H_{el}(x)$ is the one-electron Hamiltonian and H_{ph} is the non-interacting phonon Hamiltonian. The chemical potential is included in H_o as a Lagrange multiplier — we are dealing again with a system of variable number of particles.

The Hamiltonian for the non-interacting electrons, H_{el}, is diagonal in the ψ-representation, and the Green's function applicable to the normal state is given by

$$G_o^N(p,\omega) = \frac{1}{\omega - \epsilon_p + i\omega\delta} ,$$

as noted in connection with Gor'kov's treatment. To develop the non-interacting Green's function for the superconducting state, $G_o(p,\omega)$, Eliashberg included a certain portion of the electron-phonon interaction in a redefined zeroth-order Hamiltonian, $\tilde{H}_o = \tilde{H}_{el} + H_{ph}$, by carrying out a unitary transformation from the operators $\psi_{k\uparrow}, \psi_{k\downarrow}$ to new operators χ_o and χ_1: $U_{\alpha\beta}\psi_\alpha = \chi_\beta$. Bogoliubov, as seen above, had shown that such a transformation would yield the superconducting ground state provided 1) the χ_o, χ_1 operators satisfied the anti-commutation relations for Fermi operators, and 2) that certain "dangerous" terms were eliminated from the Hamiltonian to low order. Essentially the same requirements were applied by Eliashberg, although the second requirement was given more clearly by requiring that $\tilde{H}_{el}$ be diagonal in the χ-representation. The first of these requirements allows Wick's theorem to be applied to time ordered products of ψ operators even though the ground state is not their vacuum state as it is for the χ operators. The second requirement allows us to calculate the zeroth order Green's function,

$G_o(p,\omega) = -i\langle T\chi\chi^\dagger\rangle$, from its equation of motion just as simply as we found $G^N_o(p,\omega)$. On the other hand, we may continue to use the normal state operators ψ by applying the inverse transformation to the zeroth-order Hamiltonian:

$$\chi^*\tilde{H}_{el}\chi = \psi^* U^{-1}\tilde{H}_{el}U\psi \ .$$

As a result the new zeroth-order Hamiltonian $U^{-1}\tilde{H}_{el}U$ is no longer diagonal in the ψ-representation, and the equations of motion for ψ and $\psi^\dagger$ are coupled giving, as in the Gor'kov treatment, single particle and pair propagators, $G_o(p,\omega)$ and $F^\dagger_o(p,\omega)$.

While the non-interacting propagators are easily evaluated, the full propagators, $G(p,\omega)$ and $F^\dagger(p,\omega)$, depend upon the full Hamiltonian and must be approximated. The Feynman-Dyson perturbation series allows this approximation to be carried to infinite order for a certain class of diagrams.

One first determines the equation of motion for $G(xt,x't')$, or for $F^\dagger(xt,x't')$, from the expression for the time derivative, say for example,

$$i\frac{\partial G}{\partial t}{\uparrow\uparrow}(xt,x't') = \delta(t-t')\delta(x-x') + \left\langle T\frac{\partial\psi}{\partial t}{\uparrow}(xt)\psi{\uparrow}(x't')\right\rangle \ ,$$

by substituting for the time derivative of the field operator:

$$i\frac{\partial\psi}{\partial t}{\uparrow} = [\psi{\uparrow},\tilde{H}_{el}] \ .$$

The self-energy in the resulting equation for $G{\uparrow\uparrow}(xt,x't')$ is given

in terms of the vertex function,

$$\Gamma(xt,x't') \equiv \langle T\phi(xt)\psi(xt)\psi^{\dagger}(x't')\rangle \quad ,$$

which arises from the coupling of the electron and phonon fields in H_{int}. The expression for $G_{\uparrow\uparrow}(xt,x't')$ becomes

$$\left[i\frac{\partial}{\partial t} - H^{(0)}(x) + \mu\right] G_{\uparrow\uparrow}(xt,x't') - \delta(t-t')\delta(x-x')$$

$$= \int d\tau dy \left\{\Sigma_1(xt,y\tau)G_{\uparrow\uparrow}(y\tau,x't') + \Sigma_2(xt,y\tau)F^{\dagger}_{\downarrow\uparrow}(y\tau,x't')\right\}$$

$$= -i\,\langle T\phi(xt)\psi(xt)\psi^{\dagger}(x't')\rangle \quad .$$

The total vertex function is shown in diagram form in Figure 13. The

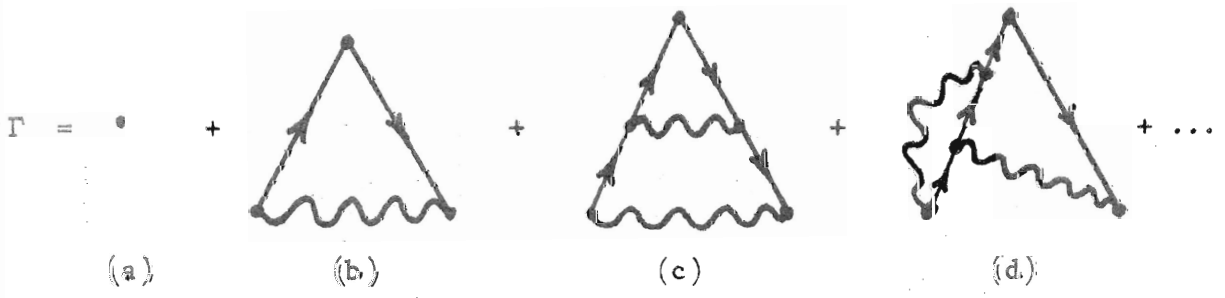

Figure 13 Total vertex function.

Feynman-Dyson series for the self-energy may be obtained by using the series for the vertex function along with the full propagators, $G(xt,x't')$ and $D(xt,x't')$, giving the expression:

$$\sum(xt,x't') = \int dy d\tau D(xt,y\tau)\, G(xt,y\tau)\, \Gamma(y\tau,x't') \quad .$$

This is shown in Figure 14. By using the full propagators Dyson's Equation gives the sum of the contributions of each order to the

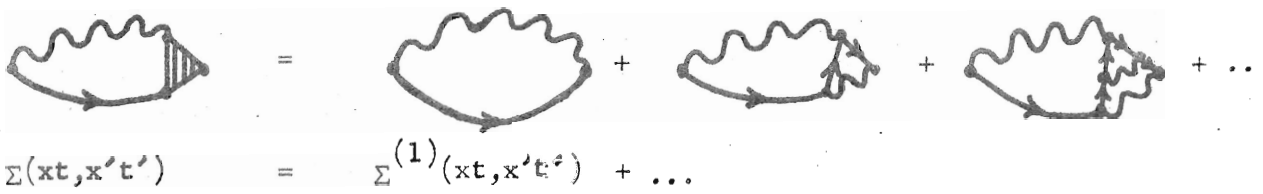

Figure 14 Feynman-Dyson series for the proper self-energy.

self-energy. In order to solve the two equations for $G(p,\omega)$ and $\Sigma(p,\omega)$, the Fourier transforms for a translationally invariant system, several approximations are introduced. First, Eliashberg asserts that the total vertex function may be approximated by the simple vertex $\Gamma^{(1)}$ (see diagram (a) in Figure 13). This had been shown to be possible for the normal state by Migdal.[140] Second, the phonon propagator is assumed to be the same in the superconducting state as in the normal state. Thus the phonon propagator determined by Migdal may be used in this case also. With these two approximations we have two simultaneous equations for the functions $G(p,\omega)$ and $\Sigma(p,\omega)$. Because of the coupling of ψ and $\psi^{\dagger}$ the matrix expressions for Σ and G consist of two parts, one involving Σ_1, the self-energy for single particles, while the second involves Σ_2, the self-energy for pairs. Dyson's equation is then the pair of equations:

$$\Sigma_1(p,\omega) = \frac{i}{(2\pi)^4} \int G(k,\omega') \, D(p-k,\omega-\omega') d^3k d\omega'$$

$$\Sigma_2(p,\omega) = -\frac{i}{(2\pi)^4} \int F^{\dagger}(k,\omega') \, D(p-k,\omega-\omega') d^3k d\omega' .$$

We shall see that the second of these leads to the starting point for the Kirzhnits' method which follows.

Substituting the Fourier transforms of the expressions for G (or $F^{\dagger}$) into the above expressions gives the self-energies. Σ_1 amounts to a renormalization of the energy of the electron states while Σ_2 determines the gap in the excitation energies as well as their damping rate. On solving the resulting equations, Eliashberg determines the gap function, $C(\omega)$, to be

$$C(\omega) = \frac{\mathrm{Re}\Sigma_2(\omega)}{(1-f(\omega)/\omega)} = \frac{1}{4\pi^2 k_o}\frac{1}{1+\lambda}\int_0^{q_1} q\,\alpha_q^2\,\frac{\omega_q(0)}{\omega_q}\,dq$$

$$\times \int_0^{\infty} \frac{C(\omega_1(\xi))d\xi}{\sqrt{\xi^2+\Delta^2}}\left(\frac{1}{\omega_1(\xi)-\omega+\omega_q}+\frac{1}{\omega_1(\xi)+\omega+\omega_q}\right).$$

where

$$\Delta = \sqrt{\xi^2(k_o)+C^2(k_o)} \quad .$$

The details of the phonon spectrum are accounted for by the function $\alpha_q^2\frac{\omega_q(0)}{\omega_q}$. Eliashberg noted the difference between the above gap equation and that of Bogoliubov, a difference which only occurs for large ω, the region in which the diagrams are no longer "dangerous".

Because the Eliashberg method sums certain terms in the perturbation series to all orders rather than only to second order as in the Bogoliubov method, it is expected to give better agreement with experiment. Such agreement, found in the work of Scalapino, et. al.,[141] and McMillan, et al.,[142] on the tunneling results in superconductors, supports the strong-coupled theory. The Eliashberg formalism has also

been employed by Morel and Anderson[135] who used an Einstein phonon spectrum and included the Coulomb repulsion. They found good order-of-magnitude agreement for calculated transition temperatures although their results for the isotope effect conflicted with experiment for certain metals.

Swihart[143] compared results for the energy gap using three different kernels in the gap equation: 1) the Bardeen-Pines potential[144] (see Eq. (8)), 2) the Bogoliubov potential, and 3) the Eliashberg potential. He found that all three resulted in a gap function at the Debye energy which agreed with the anomalous tunneling behavior of Pb if the Coulomb interaction was included. However, only the behavior of the gap function calculated from the Eliashberg potential conformed to data on the critical field for Hg and Pb. Such data depend strongly on the form of the gap at the Fermi surface.

The Eliashberg method has also been employed for estimating transition temperatures of strong-coupled superconducting metals and alloys by McMillan.[26] Finally it should be mentioned that this method has been applied to the excitonic mechanism for superconductivity by Allender, Bray, and Bardeen[28] for two-dimensional metal-semiconductor systems.

F. Dielectric Response Method

Recently another Green's function method has been developed which incorporates the infinite summation in orders of perturbation theory using the Feynman-Dyson method, but which results in a simplified kernel in the energy gap integral equation through the use of

the spectral weight function and by setting the temperature of the system to the as-yet-to-be-determined superconducting transition temperature. This is the method of Kirzhnits, Maksinov, and Khomskii.[29] We shall derive the Kirzhnits gap equation in detail and show how it is modified for our one-dimensional system.

The method of Kirzhnits, et. al., takes the approach common to the Eliashberg method in that we begin with Green's functions which already describe the "non-interacting" superconducting state. That is, the only interactions included in zeroth order are the interactions which result in Cooper pair formation. Thus we begin as in the Eliashberg method with a single particle propagator, $G_o(p,\omega)$, and an anomalous propagator, $F_o^\dagger(p,\omega)$. In the Eliashberg equations we improved upon the zeroth order Green's functions by summing a perturbation series for the self-energies of the single particle and the pair propagators. We noted that the first leads to a renormalization of the excitation energy while the second leads to the gap in the energy spectrum. The Kirzhnits approach ignores this renormalization and deals only with the anomalous propagator. A justification for this will be given below.

The self-consistent equation for the true anomalous propagator, $F^\dagger(p,\omega)$, is based on the first-order term in the perturbation expansion using Wick's theorem. A sum over diagrams is then obtained by replacing the non-interacting propagator, $F_o^\dagger(p,\omega)$, by $F^\dagger(p,\omega)$. For the zero-temperature expression we have

$$F^\dagger(p,\omega) = \frac{+i}{(2\pi)^4} G_o(p,\omega)G_o(-p,-\omega)\Gamma^{(1)} \iint d^3k d\omega' V(p-k,\omega-\omega')F^\dagger(k,\omega') \times \Gamma(p-k,\omega-\omega') . \quad (17)$$

The Feynman diagram for this equation is shown in Figure 15 and differs

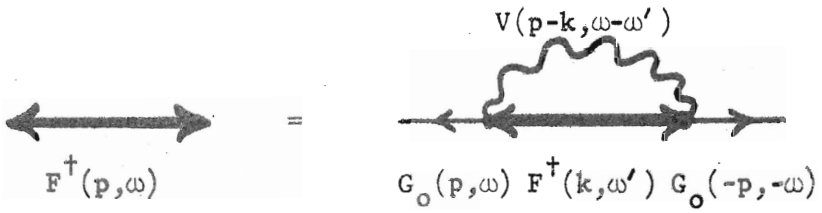

Figure 15 Feynman diagram for anomalous propagator equation.

from that for $\Sigma(p,\omega)$ (see Figure 14) by the addition of the single particle propagators $G_o(p,\omega)$ and $G_o(-p,-\omega)$. We introduce immediately the two assumptions used by Eliashberg. First, the propagator for the effective interaction, $V(q,\omega)$, is assumed to be the same in the superconducting state as in the normal state. Second, the total vertex function is replaced by the simple vertex, $\Gamma^{(1)}$, which may be included in the expression for $V(q,\omega)$. In light of this second assumption we have neglected diagrams such as that of Figure 16 which requires a vertex of greater complexity.

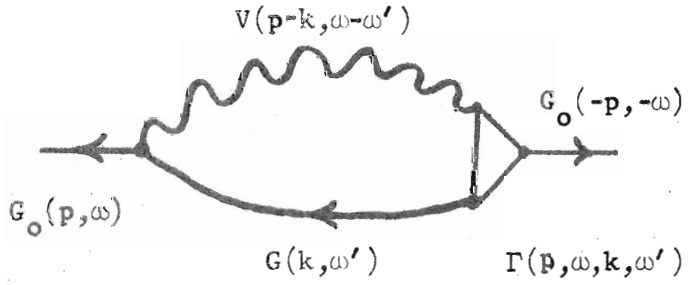

Figure 16 Higher order term for anomalous propagator.

In a second paper on the Green's function method in superconductivity, Eliashberg computed the temperature Green's functions $\mathcal{G}(p,i\omega_n)$ and $\mathcal{F}^{\dagger}(p,i\omega_n)$; this was a simple extension of the original work. In the Kirzhnits method, however, the use of the finite temperature formalism is an essential feature, and in particular, Kirzhnits begins by setting the temperature equal to the critical temperature. This results in a considerable simplification. As the critical temperature is approached the anomalous self-energy tends to zero so that the single particle Green's function for the superconducting state may be replaced by its normal state counterpart:

$$\mathcal{G}(p,i\omega_n) = \frac{z_p}{i\omega_n - \xi_p}$$

where $\xi_p = (p^2/2m) - \epsilon_F$. The renormalization factor z_p can be determined by computing the self-consistent single particle propagator. As noted above, we ignore this renormalization setting $z_p = 1$. This is consistent with the weak-coupling approximation.[29]

The second essentially new feature of the Kirzhnits method is the use of the Lehmann or spectral representation[145] for the effective interaction and for the anomalous propagator. The representation for the effective interaction,

$$V(q,\omega) = V_o(q)/\epsilon(q,\omega) \quad , \tag{18}$$

derives from that of the charge-to-charge response function which

satisfies the causality principle:

$$\frac{1}{\epsilon(q,\omega)} = 1 + \int_0^\infty \mathrm{Im}\left[\frac{1}{\epsilon(q,\omega)}\right]\left(\frac{1}{E+\omega-i\delta} + \frac{1}{E-\omega+i\delta}\right) dE \quad .$$

We define $\rho(q,E) = -(1/\pi)\ \mathrm{Im}(1/\epsilon(q,E))$, giving the following finite temperature spectral representation for the effective interaction

$$V(q,i\omega_n) = V_o(q)\left[1 - \int_0^\infty \frac{\rho(q,E)\ dE^2}{\omega_n^2 + E^2}\right] \quad , \qquad (19)$$

where $V_o(q)$ is the bare Coulomb interaction. It has been noted by several authors that the spectral density function for the dielectric response function is related to the form factor for electron scattering in a metal:[146]

$$\rho(q,E) = V_o(q)[S(q,E) - S(q,-E)] \quad .$$

Similarly, the anomalous propagator has the spectral representation:

$$\mathscr{F}^\dagger(p,i\omega_n) = \int_{-\infty}^\infty \frac{f(p,x)dx}{i\omega_n - x} \quad .$$

We may write the finite temperature form of (17) at $T = T_c$, viz.,

$$\mathscr{F}^\dagger(p,i\omega_n) = -\mathscr{G}(p,i\omega_n)\mathscr{G}(-p,-i\omega_n)T_c \sum_m \int \frac{d^3k}{(2\pi)^3} V(p-k,i\omega_n - i\omega_m) \times \mathscr{F}^\dagger(k,i\omega_m) \quad ,$$

in the following manner using these spectral representations:

$$\int_{-\infty}^\infty \frac{f(p,x)}{i\omega_n - x}\, dx = \frac{1}{(i\omega_n)^2 - \xi_p^2} T_c \sum_m \int \frac{d^3k}{(2\pi)^3} V_o(p-k) \int_{-\infty}^\infty \frac{dy f(k,y)}{i\omega_m - y} \times \left[1 - \int_0^\infty \rho(p-k,E)\left\{\frac{1}{E+i\omega_n - i\omega_m} + \frac{1}{E-i\omega_n + i\omega_m}\right\} dE\right] \quad . \qquad (20)$$

The gap function is given in terms of the wave-vector dependent part of the spectral representation:

$$\phi(p) = 2|\xi_p| \int_0^\infty f(p,x)\, dx \quad . \tag{21}$$

We derive the integral equation for the gap function by first simplifying (20).

We first apply the standard procedure for frequency sums in the finite temperature scheme by using the relation

$$T_c \sum_{n=-\infty}^{\infty} g(i\omega_n) = -\frac{1}{2\pi i} \int_C \frac{g(\omega)d\omega}{e^{\beta_c \omega} + 1}$$

where $\beta_c = 1/kT_c$ and the contour C is shown in Figure 17.

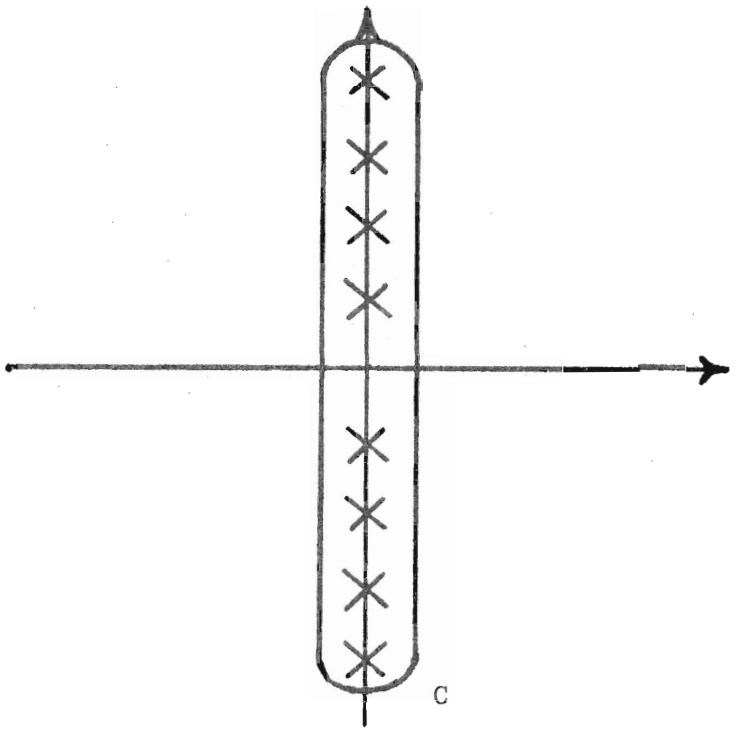

Figure 17 Contour for frequency sums.

The function $1/(e^{\beta_c \omega} + 1)$ provides the first order poles at each $i\omega_n$. In the present case we have

$$T_c \sum_{m=-\infty}^{\infty} \left[\frac{1}{i\omega_m - y}\right]\left[1 - \int_0^{\infty} \rho(q,E)\left\{\frac{1}{E + i\omega_n - i\omega_m} + \frac{1}{E - i\omega_n + i\omega_m}\right\} dE\right]$$

$$= -\frac{1}{2\pi i}\int_C \frac{d\omega}{e^{\beta_c \omega} + 1}\,\frac{1}{\omega - y}\left[1 - \int_0^{\infty} \rho(q,E)\left\{\frac{1}{E+i\omega_n - \omega} + \frac{1}{E - i\omega_n + \omega}\right\} dE\right]$$

where $q = p - k$. The first term,

$$-(1/2\pi i)\int_C \frac{d\omega}{e^{\beta_c \omega} + 1}\,\frac{1}{\omega - y}\ ,$$

is evaluated by deforming the contour to that shown in Figure 18(a). Picking up the contribution from the pole at $\omega = y$, which is circled clockwise, gives

$$\mathrm{Res}\left[\frac{1}{e^{\beta_c \omega} + 1}\right]_{\omega = y} = \frac{1}{e^{\beta_c y} + 1}$$

$$= \frac{2(1/2)e^{-\beta_c y/2} + (1/2)e^{\beta_c y/2} - (1/2)e^{\beta_c y/2}}{e^{\beta_c y/2} + e^{-\beta_c y/2}}$$

$$= (1/2)[1 - \tanh(\beta_c y/2)]\ .$$

The second and third terms,

$$-(1/2\pi i)\int_C \frac{d\omega}{e^{\beta_c\omega}+1}\,\frac{1}{\omega-y}\left\{\frac{1}{\omega-E-i\omega_n}-\frac{1}{\omega+E-i\omega_n}\right\}\quad,$$

are evaluated with the deformed contour of Figures 18(b) and (c).

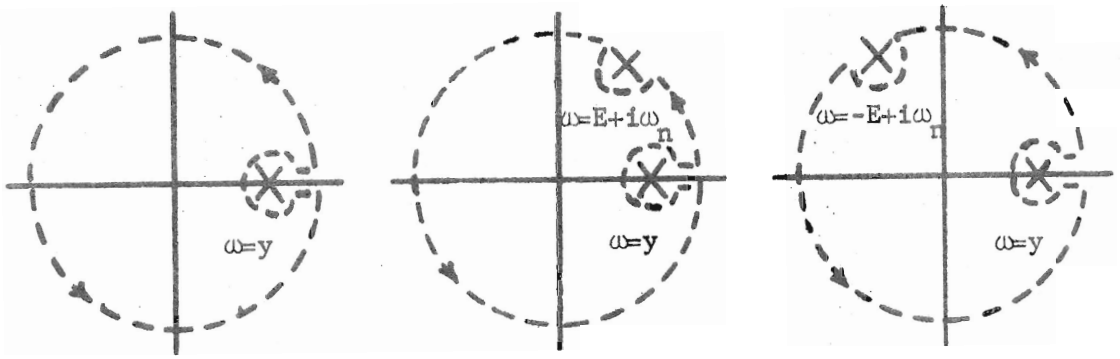

(a) (b) (c)

Figure 18 Deformed contours for frequency sums

Picking up the contributions from both poles gives

$$\mathrm{Res}\left[\frac{1}{e^{\beta_c\omega}+1}\cdot\frac{\pm 1}{\omega-i\omega_n\mp E}\right]_{\omega=y}+\mathrm{Res}\left[\frac{1}{e^{\beta_c\omega}+1}\,\frac{\pm 1}{\omega-y}\right]_{\omega=\pm E+i\omega_n}\quad,$$

where the upper (lower) sign refers to the second (third) term. Thus we have

$$\frac{1}{e^{\beta_c y}+1}\left\{\frac{1}{y-i\omega_n-E}-\frac{1}{y-i\omega_n+E}\right\}+\frac{1}{e^{\beta_c(E+i\omega_n)}+1}\,\frac{1}{E+i\omega_n-y}$$

$$-\frac{1}{e^{\beta_c(-E+i\omega_n)}+1}\,\frac{1}{-E+i\omega_n-y}\quad.$$

The correct analytic continuation is obtained by setting $e^{i\beta_c \omega_n} = -1$, giving

$$\left\{ \frac{1}{e^{\beta_c y}+1} + \frac{1}{e^{-\beta_c E}-1} \right\} \frac{1}{i\omega_n - y - E} + \left\{ \frac{-1}{e^{\beta_c y}+1} + \frac{-1}{e^{\beta_c E}-1} \right\} \frac{1}{i\omega_n - y + E} \quad .$$

We arrange the terms in braces as follows:

$$\frac{1}{e^{\beta_c y}+1} + \frac{1}{e^{-\beta_c E}-1} = \frac{2(1/2)e^{-\beta_c y/2}}{e^{\beta_c y/2} + e^{-\beta_c y/2}} + \frac{2(1/2)e^{\beta_c E/2}}{e^{-\beta_c E/2} - e^{\beta_c E/2}} \quad . \quad (22)$$

Adding and subtracting

$$\frac{(1/2)e^{\beta_c y/2}}{e^{\beta_c y/2} + e^{-\beta_c y/2}} + \frac{(1/2)e^{-\beta_c E/2}}{e^{-\beta_c E/2} - e^{\beta_c E/2}} \quad ,$$

(22) becomes

$$-(1/2)\frac{e^{\beta_c y/2} - e^{-\beta_c y/2}}{e^{\beta_c y/2} + e^{-\beta_c y/2}} - (1/2)\frac{e^{\beta_c E/2} + e^{-\beta_c E/2}}{e^{\beta_c E/2} - e^{-\beta_c E/2}}$$

$$= -(1/2)[\coth(\beta_c E/2) + \tanh(\beta_c y/2)] \quad .$$

Similarly,

$$\frac{-1}{e^{\beta_c y}+1} + \frac{-1}{e^{-\beta_c E}+1} = -(1/2)[\coth(\beta_c E/2) - \tanh(\beta_c y/2)] \quad .$$

Collecting this together, (20) becomes

$$\int_{-\infty}^{\infty} \frac{f(p,x)dx}{i\omega_n - x} = \frac{1}{(i\omega_n)^2 - \xi_p^2} \int \frac{d^3k}{(2\pi)^3} V_o(q) \int_{-\infty}^{\infty} dy f(k,y)$$

$$\times \left\{ (1/2)[1 - \tanh(\beta_c y/2)] - (1/2) \int_0^{\infty} \rho(q,E) \right. \qquad (23)$$

$$\left. \times \left[\frac{\coth(\beta_c E/2) + \tanh(\beta_c y/2)}{i\omega_n - y - E} + \frac{\coth(\beta_c E/2) - \tanh(\beta_c y/2)}{i\omega_n - y + E} \right] dE \right\}$$

Having noted above that $\Sigma_2(k,\omega)$ and $F^{\dagger}(k,\omega)$, which is derived from it, are even functions of ω, we find

$$\mathscr{F}^{\dagger}(k,i\omega_m) = \int_{-\infty}^{\infty} \frac{f(k,y)dy}{i\omega_m - y}$$

$$\mathscr{F}^{\dagger}(k,-i\omega_m) = \int_{-\infty}^{\infty} \frac{f(k,y)dy}{-i\omega_m - y} \qquad (24)$$

$$= \int_{-\infty}^{\infty} \frac{-f(k,-y)dy}{i\omega_m - y} \qquad (y \rightarrow -y) \ .$$

Then $f(k,y) = -f(k,-y)$ is an odd function of y so that in (23)

$$\int_{-\infty}^{\infty} dy f(k,y)(1/2)[1-\tanh(\beta_c y/2)] = -\int_0^{\infty} dy f(k,y)\tanh(\beta_c y/2) \ .$$

Similarly,

$$-(1/2)\int_0^\infty \rho(q,E)dE \int_{-\infty}^{\infty} dy f(k,y) \left[\frac{\coth(\beta_c E/2)+\tanh(\beta_c y/2)}{i\omega_n - y - E} + \frac{\coth(\beta_c E/2)-\tanh(\beta_c y/2)}{i\omega_n - y + E} \right]$$

$$= -(1/2)\int_0^\infty \rho(q,E)dE \int_0^\infty dy f(k,y) \times \left\{ [\coth(\beta_c E/2)-\tanh(\beta_c y/2)] \left[\frac{1}{i\omega_n - y + E} - \frac{1}{i\omega_n + y - E} \right] \right.$$

$$\left. [\coth(\beta_c E/2)+\tanh(\beta_c y/2)] \left[\frac{1}{i\omega_n - y - E} - \frac{1}{i\omega_n + y + E} \right] \right\} .$$

An expression similar to that in braces in the equation above appears in Eliashberg's treatment of the finite temperature case.[147] Eliashberg claims that the expression in braces simplifies to

$$2\tanh(\beta_c y/2) \left[\frac{1}{i\omega_n - y - E} - \frac{1}{i\omega_n + y + E} \right]$$

with error of order $(T_c/\omega_o)^2$ where $\omega_o = 2sp_o$, s being the speed of sound and p_o the Fermi momentum. This approximation has been used by Allender, et. al.,[28] and may be seen in the following manner.[148] We note first that the $\coth(\beta_c E/2)$ terms are non-singular in T_c. The $\tanh(\beta_c y/2)$ terms can be arranged as follows:

$$\tanh(\beta_c y/2) \left[\frac{1}{i\omega_n - y - E} - \frac{1}{i\omega_n + y + E} - \frac{1}{i\omega_n - y + E} + \frac{1}{i\omega_n + y - E} \right] .$$

This follows from (24) since

$$\frac{1}{x \pm i\delta} = P\frac{1}{x} \mp \pi i\delta(x) \; . \qquad (26)$$

Thus we have

$$f(p,x) = -(1/2\pi i)\int \frac{d^3k}{(2\pi)^3} V_o(q) \int_0^\infty dy f(k,y)\tanh(\beta_c y/2) \left[\left\{ \frac{1}{(x-i\delta)^2 - \xi_p^2} - \frac{1}{((x+i\delta)^2 - \xi_p^2} \right\} \right.$$

$$+ \int_0^\infty \rho(q,E)dE \left(\frac{1}{(x-i\delta)^2 - \xi_p^2} \left\{ \frac{1}{x-i\delta-y-E} - \frac{1}{x-i\delta+y+E} \right\} \right.$$

$$\left. \left. - \frac{1}{(x+i\delta)^2 - \xi_p^2} \left\{ \frac{1}{x+i\delta-y-E} - \frac{1}{x+i\delta+y+E} \right\} \right) \right] \; . \qquad (27)$$

Although Kirzhnits, et. al. omit the details of their derivation, it appears that at this point (26) is applied to the above expression to develop the kernel, $K(x,y,p,k)$, for the integral equation. We shall briefly show the steps involved in this development. However, we take a different approach in arriving at the gap equation and shall show this following the digression.

In the Kirzhnits method we apply (26) and write

$$\frac{1}{2\pi i}\left[\frac{1}{(x-i\delta)^2 - \xi_p^2} - \frac{1}{(x+i\delta)^2 - \xi_p^2} \right] = \frac{1}{2\pi i}\left[\frac{1}{x^2 - \xi_p^2 - \mathrm{sgn}(x)i\delta} - \frac{1}{x^2 - \xi_p^2 + \mathrm{sgn}(x)i\delta} \right]$$

$$= \mathrm{sgn}(x)\delta(x^2 - \xi_p^2)$$

$$= (1/2|\xi_p|)\mathrm{sgn}(x)[\delta(x-|\xi_p|)+\delta(x+|\xi_p|)]$$

(28)

Adding and subtracting

$$\tanh(\beta_c y/2)\left[\frac{1}{i\omega_n - y - E} - \frac{1}{i\omega_n + y + E}\right] ,$$

gives

$$2\tanh(\beta_c y/2)\left[\frac{1}{i\omega_n - y - E} - \frac{1}{i\omega_n + y + E}\right]$$
$$+ \tanh(\beta_c y/2)\left[\left\{\frac{1}{i\omega_n + y - E} - \frac{1}{i\omega_n - y - E}\right\} + \left\{\frac{1}{i\omega_n + y + E} - \frac{1}{i\omega_n - y + E}\right\}\right] .$$

Since the variable y in the second line is restricted to values near zero, the contribution of these terms vanishes in the lowest order approximation in y. Thus (23) becomes

$$\mathscr{F}^{\dagger}(p, i\omega_n) = \int_{-\infty}^{\infty} \frac{f(p,x)dx}{i\omega_n - x}$$

$$= \frac{-1}{(i\omega_n)^2 - \xi_p^2} \int \frac{d^3k}{(2\pi)^3} V_o(q) \int_0^{\infty} dy f(k,y) \tanh(\beta_c y/2)$$
$$\times \left[1 + \int_0^{\infty} \rho(q,E')dE' \left\{\frac{1}{i\omega_n - y - E'} - \frac{1}{i\omega_n + y + E'}\right\}\right]$$

We may now develop from the above equation an expression for the weight function, $f(p,x)$, which can be used in (21) to determine the gap function. The weight function can be determined from the discontinuity of the propagator across the real axis:

$$f(p,x) = (1/2\pi i)[\mathscr{F}^{\dagger}(p, x - i\delta) - \mathscr{F}^{\dagger}(p, x + i\delta)] . \qquad (25)$$

where we have used the identity:[149]

$$\delta(g(x)) = \sum_n |g'(x_n)|^{-1}\delta(x-x_n) \qquad \text{where} \quad g(x_n) = 0 \ .$$

Similarly,

$$\frac{1}{2\pi i}\left[\frac{1}{(x-i\delta)^2-\xi_p^2}\,\frac{1}{x-A-i\delta} - \frac{1}{(x+i\delta)^2-\xi_p^2}\,\frac{1}{x-A+i\delta}\right] = \frac{P}{x^2-\xi_p^2}\,\delta(x-A) + \frac{P}{x-A}\,\frac{1}{2|\xi_p|}\,\delta(x-|\xi_p|) \ .$$

Thus

$$\frac{1}{2\pi i}\left[\frac{1}{(x-i\delta)^2-\xi_p^2}\left\{\frac{1}{x-i\delta-y-E} - \frac{1}{x-i\delta+y+E}\right\} - \frac{1}{(x+i\delta)^2-\xi_p^2}\left\{\frac{1}{x+i\delta-y-E} - \frac{1}{x+i\delta+y+E}\right\}\right]$$

$$= \frac{P}{x^2-\xi_p^2}\left\{\delta(x-y-E)-\delta(x+y+E)\right\} + \left\{\frac{P}{x-y-E} - \frac{P}{x+y+E}\right\}\frac{1}{2|\xi_p|}\,\delta(x-|\xi_p|) \ .$$

Combining this with (28) and noting that the gap function is given by the integral of $f(p,x)$ for positive values of x only, we have

$$f(p,x) = -\int\frac{d^3k}{(2\pi)^3}\int_0^\infty dy f(k,y)\tanh(\beta_c y/2)K(x,y,p,k)$$

where

$$K(x,y,p,k) = V_o(q)\left[\frac{1}{2|\xi_p|}\,\delta(x-|\xi_p|) + \int_0^\infty dE\rho(q,E)\right.$$

$$\left.\times\left\{\frac{\delta(x-|\xi_p|)}{2|\xi_p|}\left(\frac{P}{x-y-E} - \frac{P}{x+y+E}\right) + \frac{\delta(x-y-E)}{x^2-\xi_p^2}\right\}\right.$$

$$= V_o(q)\,\frac{\delta(x-|\xi_p|)}{2|\xi_p|}\left\{1 - \int_0^\infty dE\rho(q,E)\left\{\frac{P}{E+y+x} + \frac{P}{E+y-x}\right\}\right\}$$

$$\left. + P\,\frac{\rho(q,x-y)\theta(x-y)}{x^2-\xi_p^2}\right] \ ,$$

which is Eq. (8) in the paper by Kirzhnits, et. al.[29]

At this point an integration may be performed with respect to x as indicated in (21) giving the gap equation. Instead we return now to our approach and proceed from (27) by integrating immediately with respect to x along the contour shown in Figure 19. The contribution to the integral along the positive imaginary axis vanishes as $\delta \to 0$. For the first term we have

$$\frac{1}{2\pi i}\int_C dx\left[\frac{1}{(x-i\delta)^2-\xi_p^2}-\frac{1}{(x+i\delta)^2-\xi_p^2}\right] = \frac{1}{2\pi i}\int_C \frac{dx}{(x-\xi_p-i\delta)(x+\xi_p-i\delta)} \quad ;$$

in the second term the poles are not enclosed by the contour. There are two possible cases. These are shown in Figures 19(a) and (b). For $\xi_p > 0$ we have

$$\mathrm{Res}\left[\frac{1}{x+\xi_p-i\delta}\right]_{x=\xi_p+i\delta} = 1/2\xi_p \ .$$

For $\xi < 0$ we have

$$\mathrm{Res}\left[\frac{1}{x-\xi_p-i\delta}\right]_{x=-\xi_p+i\delta} = -1/2\xi_p \ .$$

Thus the first term gives $1/2|\xi_p|$. In the second term we have

$$\frac{1}{2\pi i}\int_C dx\left[\frac{1}{(x-i\delta)^2-\xi_p^2}\left\{\frac{1}{x-i\delta-y-E}-\frac{1}{x-i\delta+y+E}\right\}\right.$$
$$\left.-\frac{1}{(x+i\delta)^2-\xi_p^2}\left\{\frac{1}{x+i\delta-y-E}-\frac{1}{x+i\delta+y+E}\right\}\right] \ .$$

Again in the second term the poles are not enclosed by the contour. Figures 19(c) and (d) show the two cases to be considered.

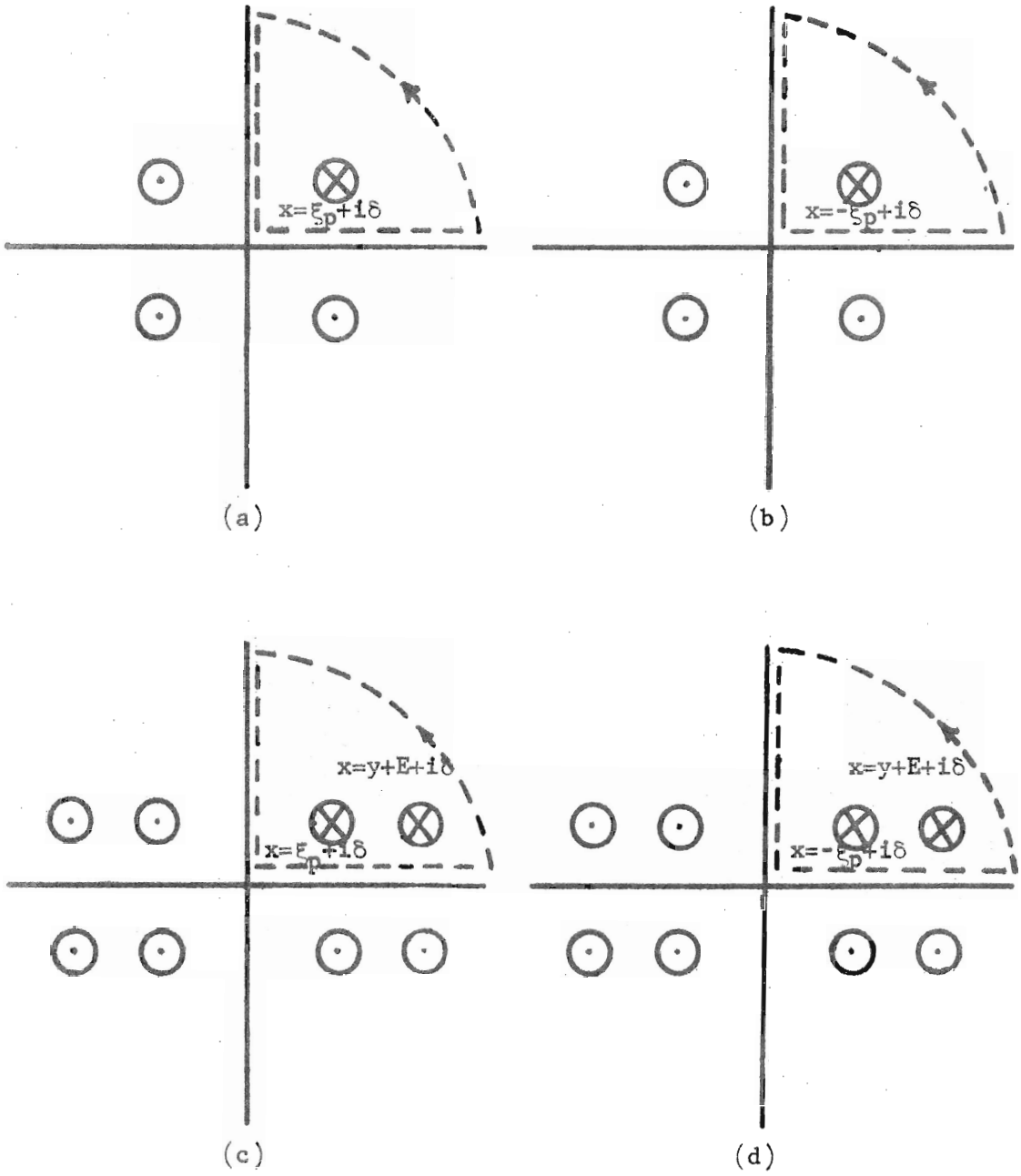

Figure 19 Poles enclosed by contour in x-integration.

Then from the definition of the gap function we have

$$\phi(p) = -\int \frac{d^3k}{(2\pi)^3} \int_0^\infty dy f(k,y) \tanh(\beta_c y/2) V_o(q) \left[1 - 2\int_0^\infty \frac{\rho(q,E)dE}{|\xi_p| + y + E} \right] . \quad (29)$$

We now wish to show explicitly the gap function $\phi(k)$ under the integral.

Kirzhnits notes that from the explicit expression for the pair propagator in terms of the anomalous self-energy, the spectral weight function may be written in the general form as

$$f(p,x) = \mathrm{Re}\left[\frac{1}{\pi i} \frac{\Delta(p,x)}{(x-i\delta)^2 - \xi_p^2} \right] = \frac{\mathrm{Re}\Delta(p,x)}{2|\xi_p|} \delta(x - |\xi_p|) + \frac{1}{\pi} \mathrm{Im}\Delta(p,x) \frac{P}{x^2 - \xi_p^2} .$$

This follows from (26) and the fact that $T = T_c$. From this we can see that the Kirzhnits gap function gives only the real part of the gap. In addition, the spectral weight function has a delta function singularity at each $|\xi_p|$. Thus the major contribution in the integral with respect to y will occur at $y = |\xi_k|$. Replacing y by $|\xi_k|$ throughout (29) neglects the difference term:

$$-\int \frac{d^3k}{(2\pi)^3} V_o(q) \int_0^\infty dy f(k,y) \left\{ \tanh(\beta_c y/2) \left[1 - 2\int_0^\infty \frac{\rho(q,E)dE}{E + y + |\xi_p|} \right] \right.$$
$$\left. - \tanh(\beta_c |\xi_k|/2) \left[1 - 2\int_0^\infty \frac{\rho(q,E)dE}{E + |\xi_k| + |\xi_p|} \right] \right\} ,$$

which is regular in T_c. Kirzhnits claims that "this term leads only to a numerical factor of the order of unity in the pre-exponential factor in the expression for T_c."[29] Thus, the final form for the

Kirzhnits gap equation in three dimensions is

$$\phi(p) = -\int \frac{d^3k}{(2\pi)^3} V_o(q) \frac{\phi(k)}{2|\xi_k|} \tanh(\beta_c|\xi_k|/2) \left[1 - 2\int_0^\infty \frac{\rho(q,E)dE}{E+|\xi_k|+|\xi_p|}\right] .$$

We may note that the equation has the same form as the finite temperature BCS equation at $T = T_c$ if we define the effective interaction by

$$U(p,k) = V_o(q)\left[1 - 2\int_0^\infty \frac{\rho(q,E)\, dE}{E+|\xi_k|+|\xi_p|}\right] ,$$

giving

$$\phi(p) = -\int \frac{d^3k}{(2\pi)^3} U(p,k) \frac{\phi(k)}{2|\xi_k|} \tanh(\beta_c|\xi_k|/2) . \qquad (30)$$

Although $U(p,k)$ is similar to the effective interaction for electron scattering [see Eqs. (18) and (19)] in that both involve the bare interaction $V_o(q)$ and the scattering matrix elements, $|Q|^2 = V_o(q)\rho(q,E)$, (see Chapter III), they differ in the form of the energy integral. Ginsburg has pointed out that this difference is "associated with the fact that superconductivity does not reduce to the scattering of two electrons on each other with the exchange of phonons."[150] We have noted this above in connection with the inability to describe the superconducting state in a power series expansion in the (small) electron-phonon coupling constant.

The temperature dependence in (30) occurs in the hyperbolic tangent function. The same functional dependence on temperature is found by Eliashberg in the finite temperature case, and by BCS, cf. (11) and (13). Eliashberg remarks: "Thanks to this, the usual relation between T_c and $\Delta(T=0)$ is preserved (Eq. (15))."[147] We take

advantage of this in the numerical computational procedure thus eliminating the computation of $|\xi_k|^{-1} \tanh(\beta_c|\xi_k|/2) \to \beta_c/2$ in the limit as $|\xi_k|$ approaches the Fermi surface. Equation (30) becomes

$$\phi(p) = -\int \frac{d^3k}{(2\pi)^3} \frac{U(p,k)\,\phi(k)}{2\sqrt{(\xi_k^2 + \phi_k^2)}} \quad .$$

In the development of the gap equation it is generally assumed that the material is isotropic or that one is dealing with a "dirty" superconductor.[151] This allows the integration over k-space to be replaced by an immediate integration over the angular variables plus an integration over the energy:

$$\int \frac{d^3k}{(2\pi)^3} \to \int N(\xi)d\xi \quad .$$

In the present treatment of one-dimensional conducting systems, such a simplification is not applicable. However, in the present case, only the variation of $\phi(p)$ with respect to p_z is important, so that in this case also we are left with an integration over one variable:

$$\phi(p) = -(2\pi)^{-1} \int_{-\pi}^{\pi} dk \frac{U(p,k)\,\phi(k)}{2\sqrt{(\xi_k^2 + \phi_k^2)}} \quad . \qquad (31)$$

In the metal-atom-dye arrangements we will be considering, there is a reflection plane of symmetry normal to the z-axis. Thus we have $\xi_k = \xi_{-k}$ and $U(p,k) = U(-p,-k)$ giving $\phi(p) = \phi(-p)$, so that we may write (31) as

$$\phi(p) = -(4\pi)^{-1} \int_0^{\pi} dk \frac{\phi(k)}{\sqrt{(\xi_k^2 + \phi_k^2)}} \{U(p,k) + U(p,-k)\} \quad . \qquad (32)$$

The methods for calculating the quantities which enter the one-dimensional form for the effective potential, viz. the Coulomb interaction, either screened by higher excitations, $\tilde{V}_o(q)$, or unscreened $V_o(q)$, the scattering matrix element, $|Q|^2$, and the excitation energy, E_q , are given in Chapter III. As noted there, the matrix elements for the spectral density, have a delta-function dependence on the energy:

$$\rho(p-k,E) = \rho(p-k)\,\delta(E - E_q) \quad .$$

Using this we may write the final form for the gap equation as used for numerical calculation:

$$\phi(p) = -(4\pi)^{-1} \int_0^{\pi} \frac{dk\phi(k)}{\sqrt{(\xi_k^2 + \phi_k^2)}} \left\{ V_o(p-k) - \frac{2|Q(p-k)|^2}{E_{p-k} + |\xi_p| + |\xi_k|} + V_o(p+k) - \frac{2|Q(p+k)|^2}{E_{p+k} + |\xi_p| + |\xi_k|} \right\} . \quad (33)$$

V. RESULTS AND CONCLUSIONS

A. Numerical Method

Numerical computation of the gap equation based on several of the descriptions given in Chapter IV have been carried out. Swihart used the Bardeen-Pines potential in the BCS equation (13). to determine the temperature dependence of the energy gap, the ratio of the energy gap to the critical temperature, and several other parameters in the weak-coupling case.[152] At the same time Culler, et. al. found numerical solutions for the gap equation using the Eliashberg equation.[153] Results of these calculations differed in form for $\Delta(\omega)$ near the Fermi level. This has been discussed subsequently by Swihart.[143] More recent numerical calculations using the Eliashberg equation have also been reported.[26,154,155] Numerical calculations using the Kirzhnits equation have not been previously published.

In the present method we assume that if a solution to the integral equation (32) exists it may be found by an iteration procedure:

$$\phi_{i+1}(p) = -\frac{1}{4\pi}\int_0^{\pi} \frac{dk}{\sqrt{\left(\xi^2(k)+\phi_i^2(k)\right)}}\,\phi_i(k)[U(p,k)+U(p,-k)] \quad (34)$$

Although the kernel of the integral is non-singular, a large contribution occurs for values of k in the region near k_F where $\xi(k)$ vanishes. We treat the region within $\pm k_o$ of k_F separately by dividing the interval $[0,\pi]$ into two regions: $\Re_1 \equiv [k_F-k_o, k_F+k_o]$ and $\Re_2 \equiv [0,k_F-k_o]\cup[k_F+k_o,\pi]$. Thus we have the inhomogeneous

equation for $p \in \mathcal{R}_2$:

$$\phi_{i+1}(p) = f(p) - \frac{1}{4\pi}\int_{\mathcal{R}_2} \frac{dk}{\sqrt{\left(\xi^2(k) + \phi_i^2(k)\right)}}\, \phi_i(k)[U(p,k) + U(p,-k)] \quad (35)$$

where

$$f(p) \equiv -\frac{1}{4\pi}\int_{\mathcal{R}_1} \frac{dk}{\sqrt{\left(\xi^2(k) + \phi_i^2(k)\right)}}\, \phi_i(k)[U(p,k) + U(p,-k)] \quad .$$

Repeated iteration of (35) gives a converged solution in $\mathcal{R}_2$ that is used in a subsequent iteration in $\mathcal{R}_1$. In this manner iterations in the sensitive region, $\mathcal{R}_1$, are based on converged solutions in $\mathcal{R}_2$. This procedure was used by Swihart[152] who also used the Tolmachev "quasi-linearization" method.[134] Initial studies showed the latter method to be unnecessary to achieve convergence for the Kirzhnits equation.

The procedure of iterating in $\mathcal{R}_2$ to convergence before each iteration in $\mathcal{R}_1$ was continued until the function was found to have converged in $\mathcal{R}_1$ also. This was followed by a final series of iterations in which new values of $\phi_{i+1}(p)$ were calculated for both regions. The criterion for final convergence was

$$(1/N) \sum_j |\phi_{i+1}(p_j) - \phi_i(p_j)| < \mathrm{MAX}(\phi_{i+1}(p_j)) \times 10^{-4} \quad . \quad (36)$$

The integration was carried out by using Simpson's Rule. In the region near the Fermi level, however, this method was found to be inadequate because of the denominator: $E(k) = \sqrt{\xi^2(k) + \phi_i^2(k)}$. In a small

region within $\pm\delta$ of k_F Simpson's Rule was replaced by an analytic integration in the following manner. The grid of points in $\mathcal{R}_1$ was chosen such that

$$N_2 - N_1 = 4N - 2 \quad , \tag{37}$$

where N_1 is the number of points from zero to $k_F - k_o$ and N_2 is the number of points from zero to $k_F + k_o$. See Figure 20. In this manner a point, N_o , fell at the Fermi level with weight 4 in the Simpson's Rule method. The analytic correction is then given by

$$-\frac{1}{4\pi}\int_{k_F-\delta}^{k_F+\delta}\frac{dk}{\sqrt{\left(\xi^2(k)+\phi_i^2(k)\right)}}\phi_i(k)[U(p,k)+U(p,-k)] - \frac{\delta}{3}[K(N_o-1) + 4K(N_o) + K(N_o+1)]$$

where $K(I)$ is the value of the integrand at I, and δ is the distance between points in $\mathcal{R}_1$. The analytic integral may be approximated by setting $k = k_F$ in the slowly varying functions of k , giving

$$-\frac{1}{2\pi}\phi_i(k_F)[U(p,k_F)+U(p,-k_F)]\int_0^{\pi}\frac{dk}{\sqrt{\left(\xi^2(k)+\phi_i^2(k_F)\right)}} \quad . \tag{38}$$

Following the results of Abarbanel[96] for a platinum chain system, we use a cosine band shape with band width E_o :

$$\xi(k) = (E_o/2)\left(\cos(k_F) - \cos(k)\right) \quad .$$

For k near the Fermi level we have

$$\xi(k) \approx (E_o/2)(k - k_F)\sin(k_F) \quad .$$

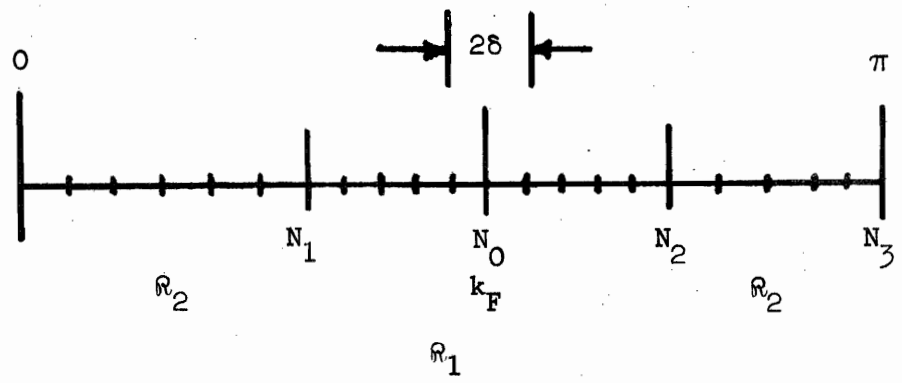

Figure 20. Grid for numerical integration.

From this approximation the analytic contribution at the Fermi level, (38) becomes

$$-\frac{1}{\pi}\,\phi_i(k_F)[U(p,k_F)+U(p,-k_F)]\,\frac{1}{E_o\sin(k_F)}\,\ell n\left|\frac{E_o\sin(k_F)/2+\sqrt{(E_o\sin(k_F)/2)^2+\phi_i^2(k_F)}}{\phi_i(k_F)}\right|$$

In general the grid consisted of $N_1 = 20$ points in the first section of R_2, $N_2 - N_1 = 30$ points in R_1, and $N_3 - N_2 = 10$ additional points in the second section of R_2. Grids with as few as 40 points with various distributions in R_1 and R_2 subject to restriction (37) gave the same transition temperature to within 2%.*

Initial trial solutions, $\phi_o(I)$, were chosen to be constant. The uniqueness of the converged gap function was examined by using values of the constant both larger and smaller than the resulting

*A minimum of 10 points in each region was also imposed.

gap at the Fermi level. It was found that the solutions coincided and the transition temperatures agreed to better than 0.1% using the convergence criterion (36).

B. Parameters

Parameters for the standard model system for comparison of transition temperatures and for investigation of uniqueness and stability are given in Table 9. The parameters fall into two categories. In the first category are those parameters that determine the effective interaction between electrons on the spine through the dielectric response function (18). The results for the standard model and for the other systems have been given in Tables 5 – 7 for the scattering matrix elements and the excitation energies as a function of the wave vector. In addition, the Coulomb interaction along the spine is given in Table 8 for the bare interaction, the Thomas-Fermi screened interaction, and for the particular case of Thomas-Fermi screening as well as screening by the higher excitations of four pyridine cyanine molecules per unit cell as given in the standard model system.

The band width and Fermi level parameters in the second category are treated as independent of those in the first category for the purpose of determining the effect of their variation on the transition temperature. Certain parameters are related, however. The Thomas-Fermi screening length is weakly dependent on the density of states at the Fermi level. The organometallic compound $K_2Pt(CN)_4Cl_{0.32}\cdot 2.6H_2O$ has served as the reference for most of the spine-related parameters. The Thomas-Fermi screening length used in the calculation, 0.14 Å^{-1},

TABLE 9 Parameters for Standard Model System

Parameters for calculation of effective interaction	
Dye molecule	Pyridine Cyanine
Number of dyes per unit cell	4
Number of unit cells	9
Number of q values	10
Platinum - nitrogen distance (in plane)	2.0 Å
Platinum - platinum distance (along chain)	3.4 Å
Platinum atom size	2.8 Å
Thomas-Fermi screening length	0.14 $Å^{-1}$
Screening from higher excitations	yes
Parameters for calculation of transition temperature	
Band width	3.0 e.v.
Fermi level (k_F/π)	5/6

is the one appropriate to this compound as determined in Chapter II. This introduces some inconsistency since the lattice constants of KCP-Cl are too small to accommodate the large dye molecules which we envision in the unit cell. The enlarged structure would have some unknown, smaller value for the screening length. The transition temperatures were calculated without Thomas-Fermi screening in order to make the appropriate comparison.

The band width is directly related to the platinum-platinum distance along the spine. The band structures determined by Abarbanel were for the compound $PtCl^{=}$ at a variety of trial platinum-platinum separations.[96] At a separation of 2.8 Å the band width was found to be 2.5 e.v., but at 3.25 Å it was found to be 1.2 e.v. The exact band width for KCP-Cl is unknown although as noted in Chapter II it should be of the order of that for $PtCl^{=}$ at 2.89 Å. Calculations have been made using the two band width values, 3.0 and 2.5 e.v., for each of the ligand systems. These values thus represent the largest band widths to be expected. It may be noted from Table 9 that the platinum-platinum distance for the standard model system suggests that a smaller value of the band width should be used. The separation used in the calculation, 3.4 Å, was chosen to allow for the Van der Waals contact distance between parallel layers of cyanine dyes. As seen in the next section, however, the transition temperature is relatively insensitive to the band width over this range of Pt-Pt separation. A conservative estimate can then be obtained using these larger band widths.

One other standard parameter bears explaining, namely, the Fermi level. The value 5/6 is that appropriate again to the model compound for the spine and reflects the partial oxidation of these compounds. Because of this unfilled band these compounds show metallic behavior.

C. Results and Discussion

In Table 10 we have selected eight cases giving a representative variation of the parameters for the model system and list the calculated transition temperatures. Figures 21(a) - (h) show the form of the kernel (33) (the term in braces) for each of these cases. The equipotential lines are plotted using the following color scheme: red=+4.0, red-orange=+3.0, orange=+2.0, yellow=+1.0, white=0.0, green=-1.0, blue-green=-2.0, blue=-3.0, pink=-4.0 all in electron volts. The attractive regions, a function of electron states p and k, can easily be seen. Several observations may be made. High transition temperatures result when the attractive interaction occurs for a large range of electron states and correspondingly for a deep potential. Neglect of Thomas-Fermi screening, Case #5, results in a high transition temperature even though the attractive region is significantly smaller than in the standard model and thus shows the importance of the depth of the attractive potential. The sharply reduced effective interaction in this particular case of empty alternate cells, Case #7, results in no attractive region along the diagonal, $p = k$, and gives no solution to the gap equation.

TABLE 10 Transition Temperatures for Variations of the Standard Model System

Case	Variation	Transition Temperature (^{o}K)
#1	All standard parameters	3060
#2	No screening by higher excitations	13
#3	Band width = 2.5 e.v.	3249
#4	Fermi level = 4/5	2863
#5	Thomas-Fermi screening neglected	2517
#6	2 molecules per unit cell	6
#7	Alternate cells empty	----
#8	Phenanthroline cyanine molecule	3021

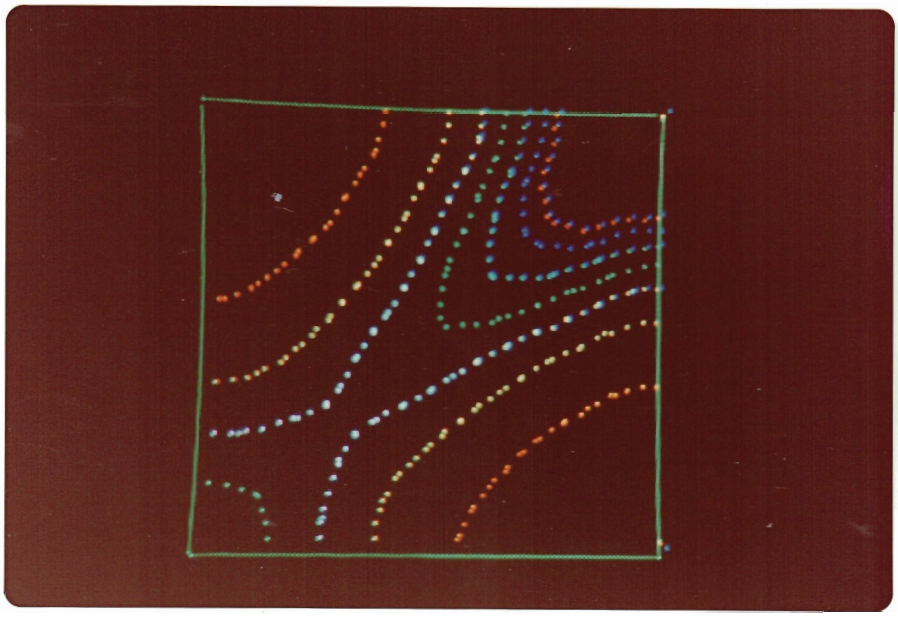

(a)

Figure 21 Kernel of integral in the gap equation

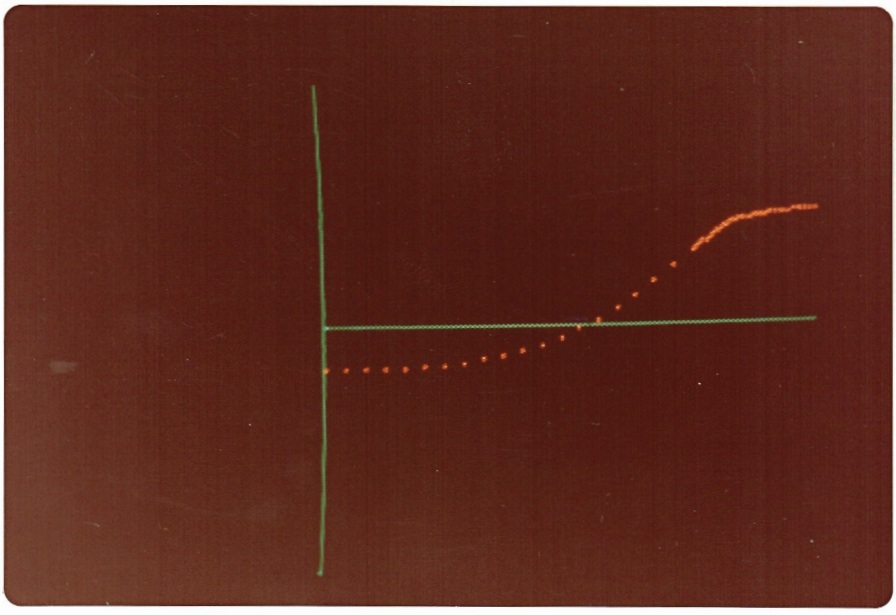

$\Delta(k_F) = 0.46$ e.v.

Figure 22(a) Gap function

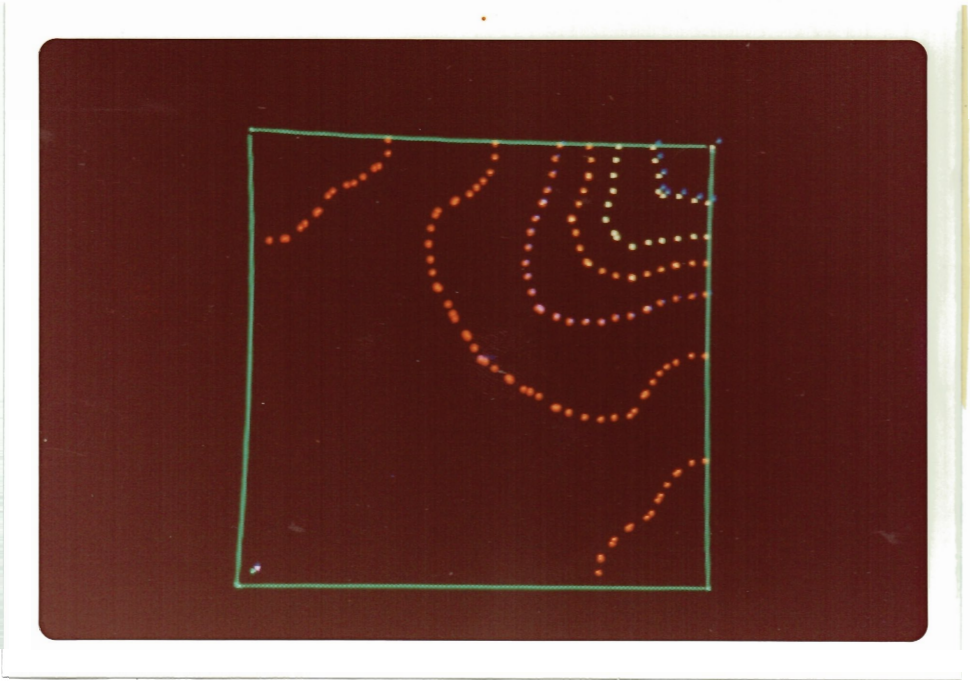

Figure 21 (b)

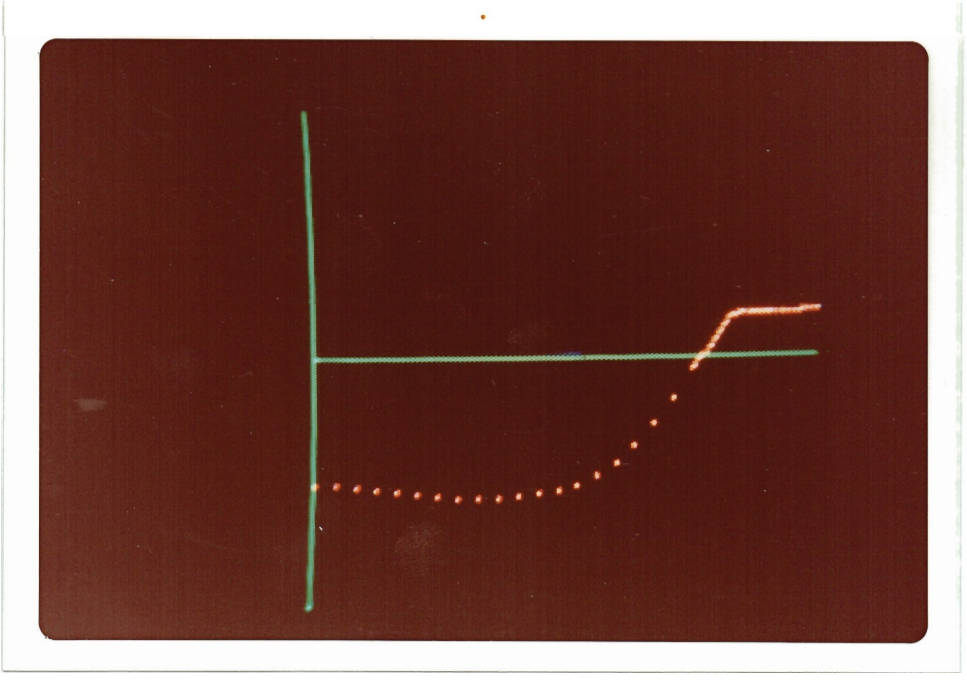

$\Delta(k_F) = 0.14 \times 10^{-2}$ e.v.

Figure 22 (b)

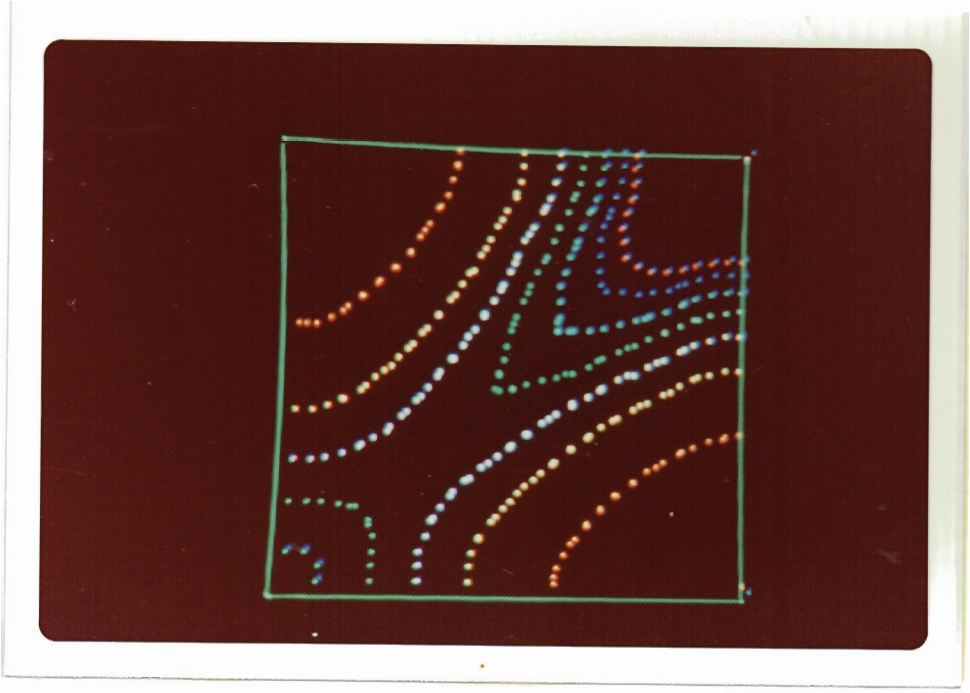

Figure 21 (c)

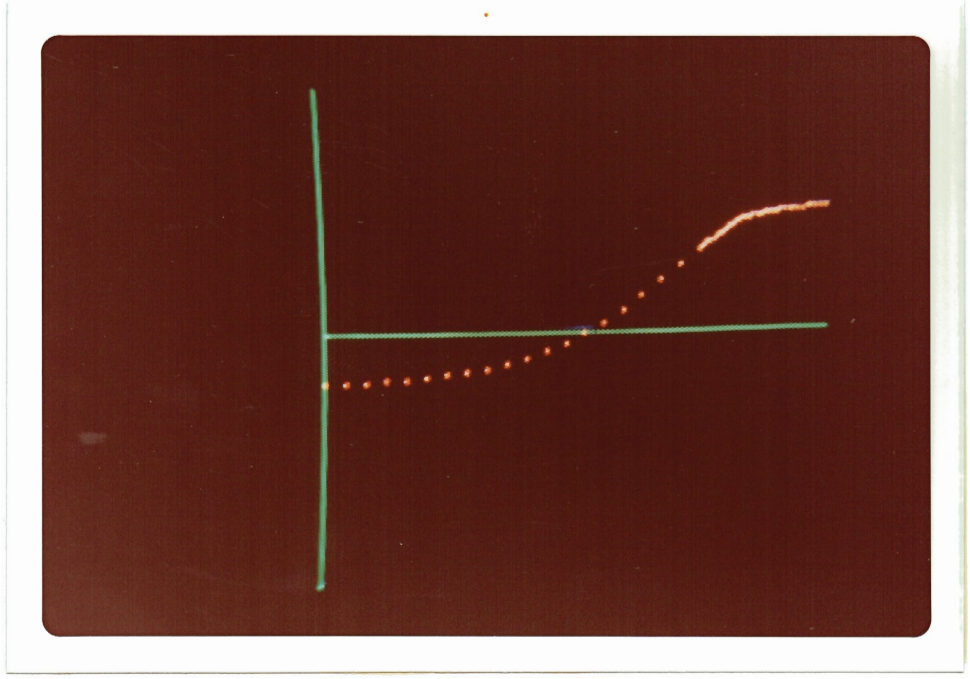

$\Delta(k_F) = 0.49$ e.v.

Figure 22 (c)

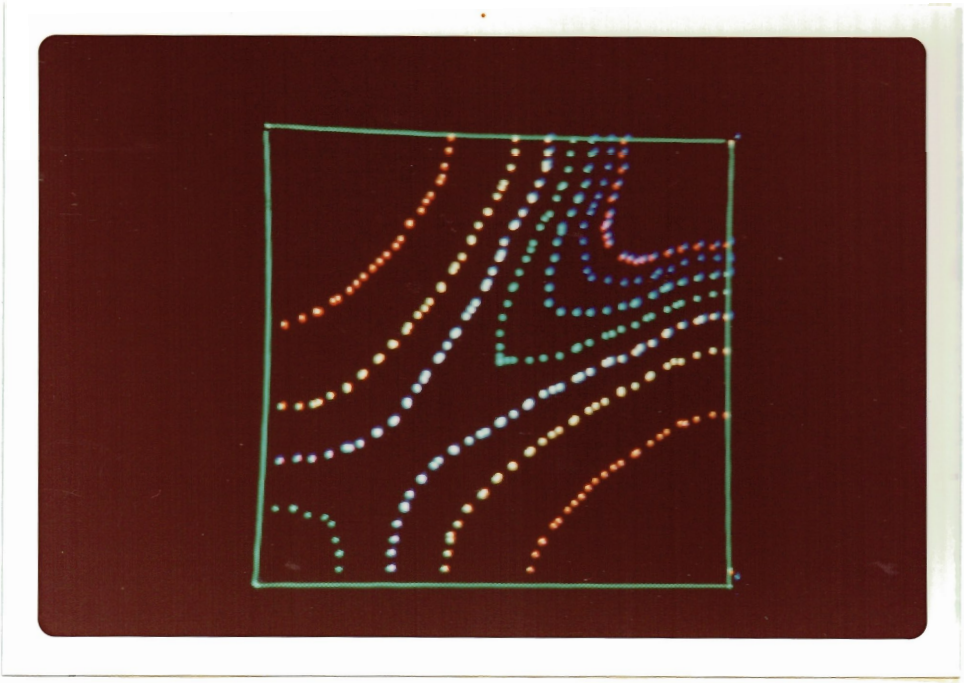

Figure 21 (d)

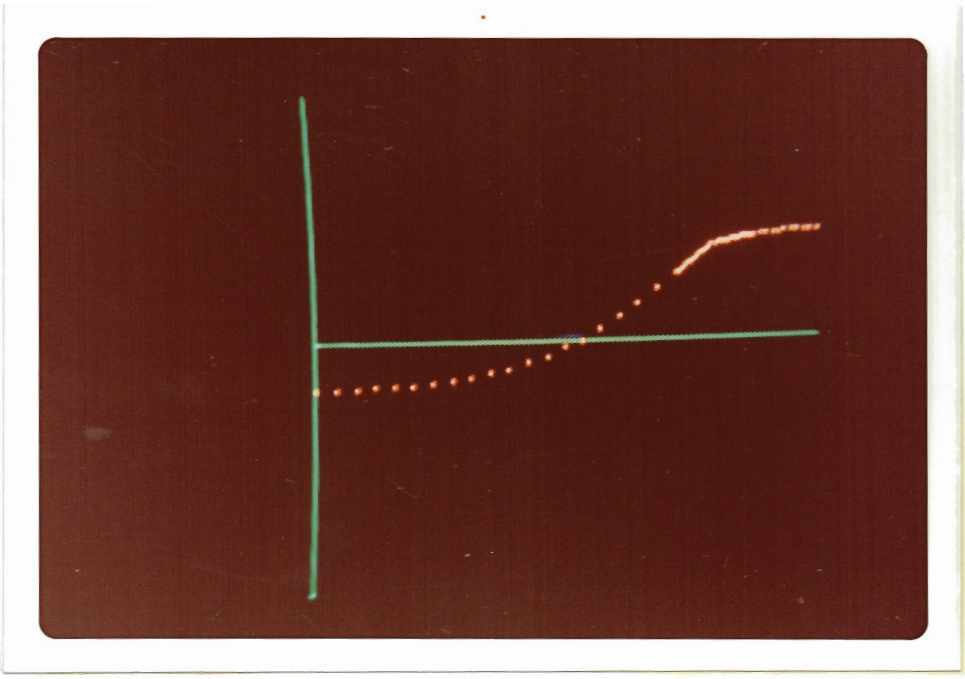

$\Delta(k_F) = 0.43$ e.v.

Figure 22 (d)

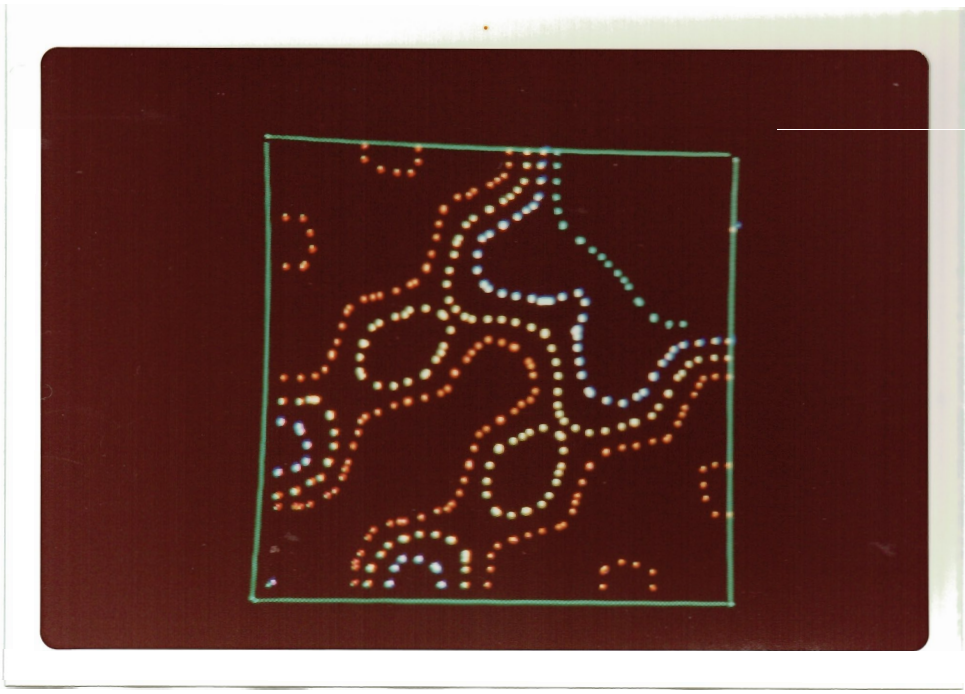

Figure 21 (e)

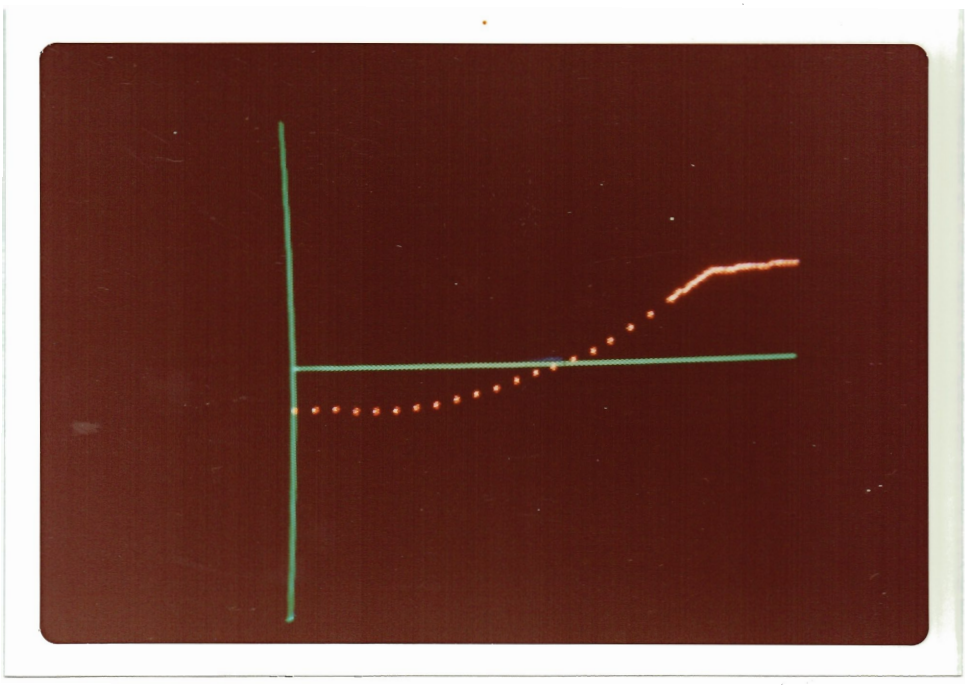

$\Delta(k_F) = 0.38$ a.v.

Figure 22 (e)

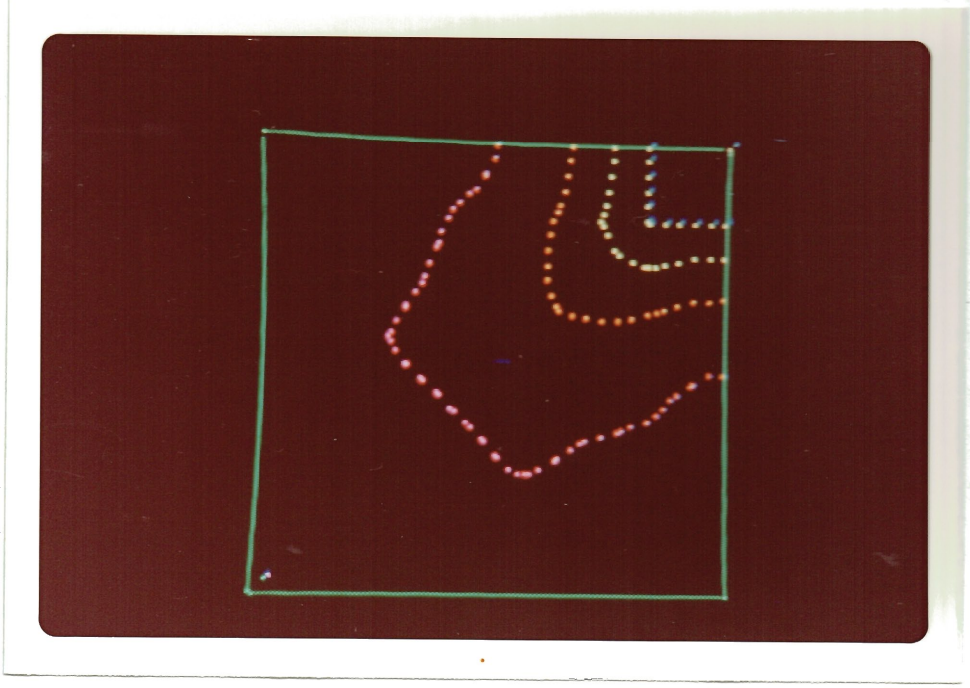

Figure 21 (f)

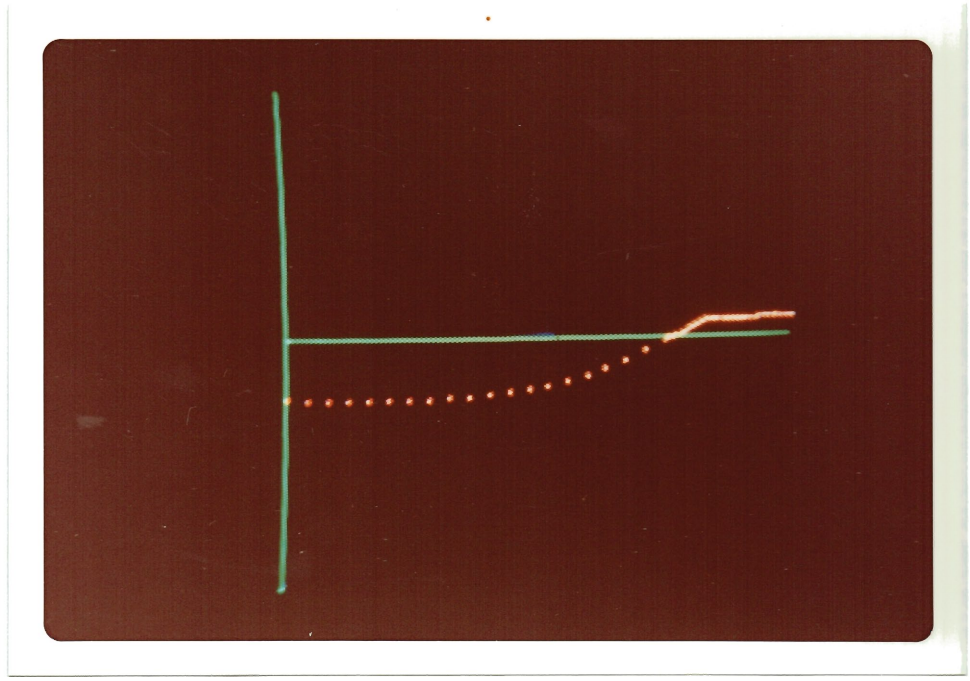

$\Delta(k_F) = 0.83 \times 10^{-3}$ e.v.

Figure 22 (f)

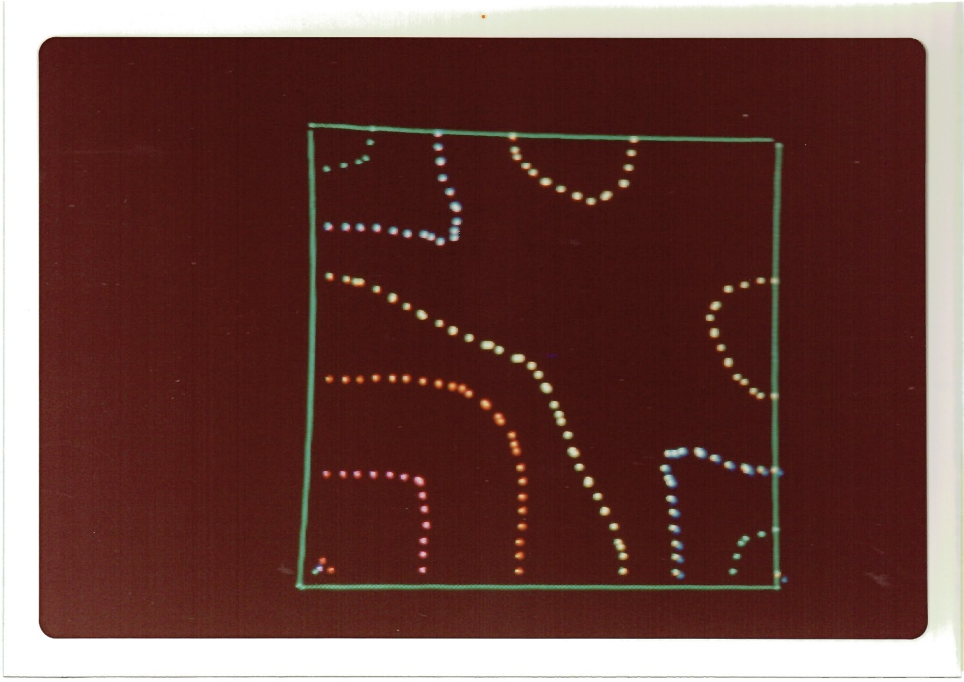

Figure 21 (g)

No solution

Figure 22 (g)

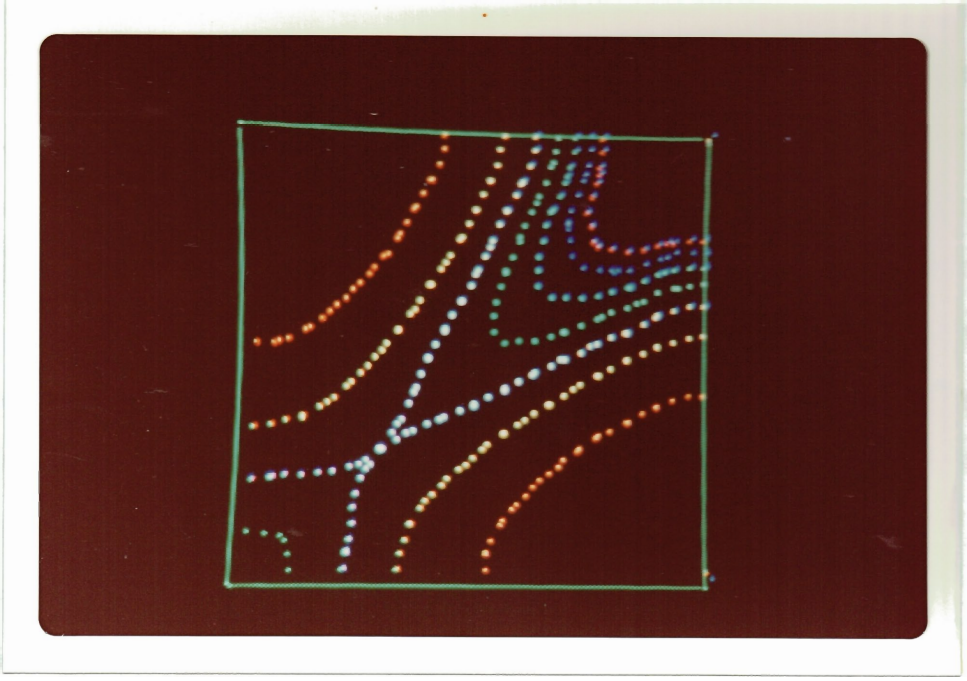

Figure 21 (h)

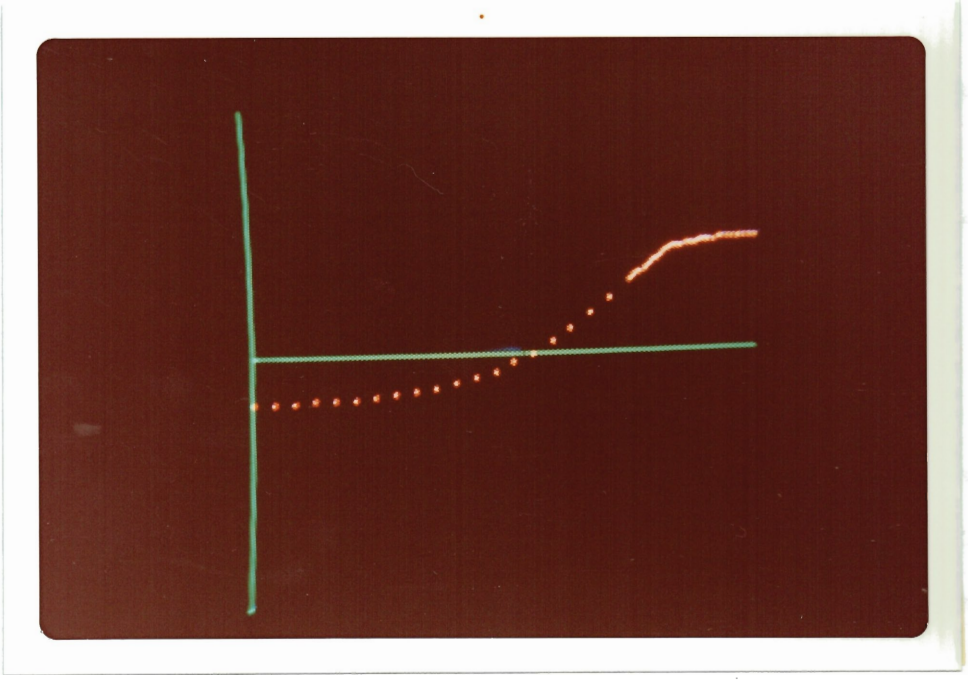

$\Delta(k_F)$ = 0.46 e.v.

Figure 22 (h)

We have plotted the corresponding gap function for each of these cases, except Case #7, in Figures 22(a) – (h). Each figure shows the calculated value of the gap function at the Fermi surface.

Table 11 shows the transition temperatures calculated for the arrays with 4 dyes per unit cell. Variation with band width, Fermi level, screening from higher excitations, and Thomas-Fermi screening is shown. The inclusion of screening from the higher excitations of the π-electron system is found to be of primary importance in obtaining high transition temperatures. The standard reference model has a transition temperature of $3060^{\circ}K$; neglecting this screening gives a Coulomb potential that dominates the attractive interaction for nearly all values of p and k and results in a transition temperature so close to zero that one might not expect to find a superconducting state.

Thomas-Fermi screening is found to have only a moderate effect on the transition temperature. Thus larger lattices required to accommodate the dyes would not rule out superconductivity caused by the lack of screening by neighboring chains. The close proximity of the dye molecules to the chain compared with the interchain distance results in the screening from higher excitations of the π-electron system being more important than interchain Thomas-Fermi screening. Thomas-Fermi screening has the positive effect of reducing the direct interaction between electrons on the spine. It also has the negative effect of reducing the overall interaction of the spine electrons with the dipole induced on the dye molecule. Thus inclusion of Thomas-Fermi screening generally results in a slight increase in T_c, but in several cases the balance of these two effects results in a

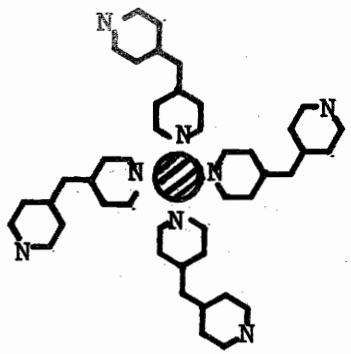

Pyridine Cynanine (A)

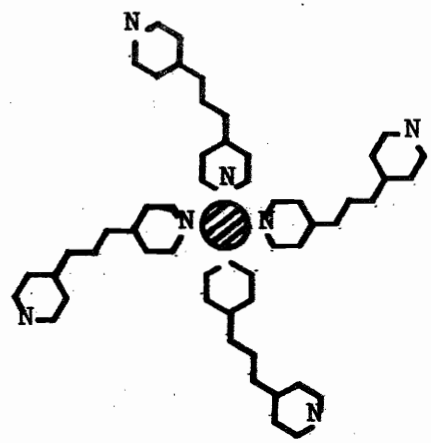

Pyridine Carbocyanine (B)

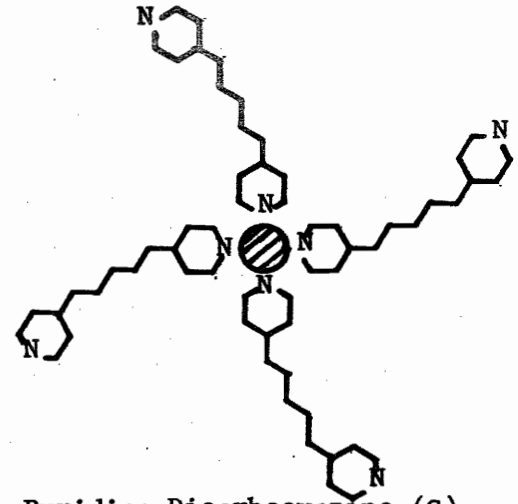

Pyridine Dicarbocyanine (C)

	Fermi Level	Band Width	$\lambda = 0.0$ Å^{-1} A T_c (^oK)	$\lambda = 0.0$ Å^{-1} B T_c	$\lambda = 0.0$ Å^{-1} C T_c	$\lambda = 0.14$ Å^{-1} A T_c	$\lambda = 0.14$ Å^{-1} B T_c	$\lambda = 0.14$ Å^{-1} C T_c
	5/6	3.0 e.v.	0	0	816	13	1028	1534
v_o	5/6	2.5	0	0	1033	57	1259	1765
	4/5	3.0	0	0	364	0	541	1057
	5/6	3.0	2517	4915	6117	3060	4270	4839
$\tilde{v}_o$	5/6	2.5	2765	5213	6441	3249	4494	5084
	4/5	3.0	2319	4682	5897	2863	4063	4611

TABLE 11. Transition Temperatures for Arrays with Four Dyes per Unit Cell

decrease in the transition temperature. The accuracy of these calculations from first principles, it should be noted, is insufficient to support conclusions for these mixed trends in the Thomas-Fermi screening based on, for example, chain length of the dye.

The length of the chain in the various cyanine dye molecules does correlate with the transition temperature if other factors are fixed. The longer chain length results in a larger transition dipole and a smaller transition energy. Both these results favor a stronger effective interaction with the spine electrons.

As noted in Chapter III in the case of two phenanthroline cyanine dye molecules per unit cell, we expect results similar to the case of four pyridine cyanine dyes. No solutions were found for the models that neglected screening from the higher excitations. With the inclusion of this screening, the transition temperatures were found to be essentially the same as those for pyridine cyanine. Although the scattering matrix elements are smaller for the phenanthroline than for the pyridine cyanine, this is compensated by a smaller energy for the excited state as well as increased π-electron screening from the extra ring structure close to the metal atom chain. See Figure 23. The transition temperatures were found to be $3021^{o}K$ and $3311^{o}K$, with and without Thomas-Fermi screening, respectively. In both cases standard values for the band width and Fermi level were used.

In Table 12 we present the calculated transition temperature for the arrays that contain 2 dye molecules per unit cell. An attractive interaction is found only under optimum conditions.

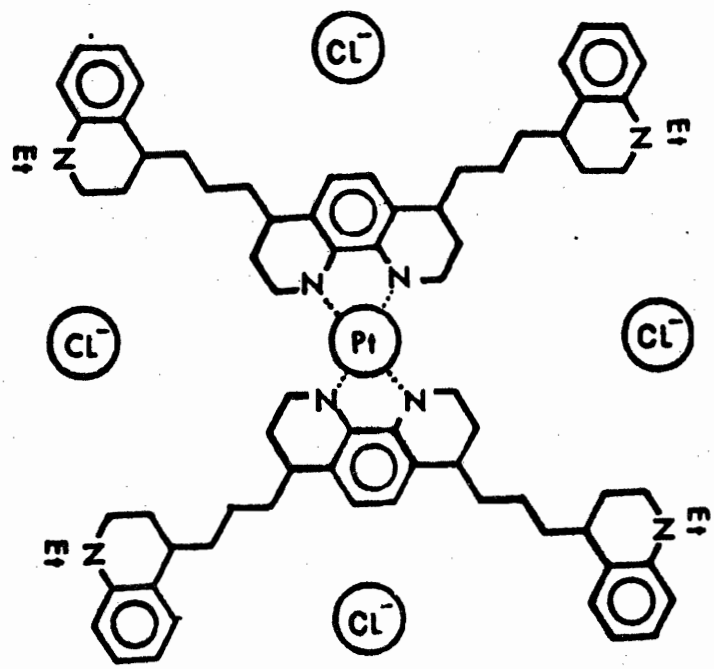

Figure 23 Unit cell with two phenanthroline cyanine dyes.

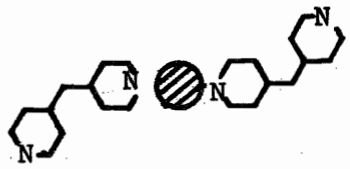

Pyridine Cyanine (A)

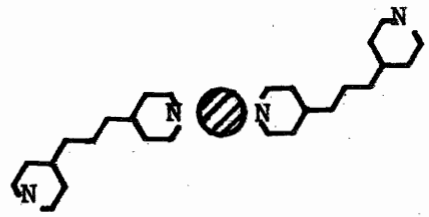

Pyridine Carbocyanine (B)

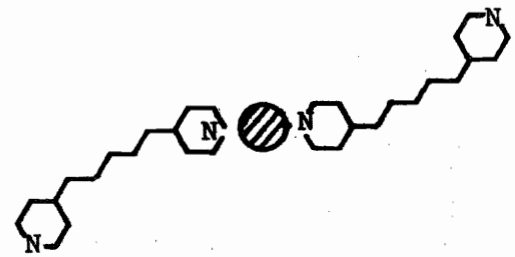

Pyridine Dicarbocyanine (C)

	Fermi Level	Band Width	$\lambda = 0.0$ Å^{-1} A T_c (°K)	$\lambda = 0.0$ Å^{-1} B T_c	$\lambda = 0.0$ Å^{-1} C T_c	$\lambda = 0.14$ Å^{-1} A T_c	$\lambda = 0.14$ Å^{-1} B T_c	$\lambda = 0.14$ Å^{-1} C T_c
	5/6	3.0 e.v.	0	0	0	0	0	0
v_o	5/6	2.5	-	-	-	-	-	-
	4/5	3.0	-	-	-	-	-	-
	5/6	3.0	0	0	104	6	562	1054
$\tilde{v}_o$	5/6	2.5	-	-	-	-	-	-
	4/5	3.0	-	-	-	-	-	-

TABLE 12 Transition Temperatures for Arrays with Two Dyes per Unit Cell

In the cases primarily considered, we envision each cell being occupied by two or more dye molecules. For this reason we calculated the effective interaction caused by the dyes using a platinum-platinum distance of 3.4 Å. On considering the case in which we attach dyes in alternate cells only, we found no solutions except in the cases of pyridine carbocyanine (17°K) and dicarbocyanine (155°K), parameters for the reference system being used in both cases. It may be possible to choose ligands for the empty cells that require less space along the spine axis. Such ligands would not be expected to contribute to the attractive interaction, but would allow the platinum-platinum distance to be reduced and thus make the overall model more consistent with the known reference spine compound, KCP-Cl.

One of the synthetic requirements assumed thus far is the ability to complex the dye to the metal atom thereby bringing the excitonic medium into intimate contact with the conducting spine. In the calculation of the effective interaction, we have assumed that the exchange contribution of the spine electrons with those in the molecular orbitals of the dyes is small compared with the direct interaction. For the carbon spine this can be arranged by having the dyes lie in the plane perpendicular to the spine thereby making the spine π orbital orthogonal to the π orbital of the nearby nitrogen atom. In the case of the transition metal atom chain, the radial extent of the d_{z^2} conduction band is small compared with the other d orbitals on the metal, giving little overlap with the dye molecular orbitals. Neglect of exchange is then consistent with the Zero-Differential-Overlap approximation used in calculating the molecular orbitals.

We have modeled systems in which the dye molecules are removed from the metal atom and find that the interaction falls off rapidly with the platinum-nitrogen distance. At 3.0 Å separation finite transition temperatures were found for pyridine carbocyanine (526°K with Thomas-Fermi screening; 77°K without) and for pyridine dicarbocyanine (1015°K with Thomas-Fermi screening; 770°K without). No solutions were found if screening due to higher excitations was neglected. This places a great emphasis on the necessity to synthesize compounds having the dye molecules complexed directly to the metal atom. Ligand structures such as shown in Figure 2 position the dye molecule too far from the conducting spine and cannot be expected to give an attractive interaction with the dye molecules we have considered.

The effect of variation of the band width and Fermi level may be determined from Table 11. Variation of the band width over the full range from 1.0 e.v. to 3.0 e.v. has been done and the results are presented in Table 13 for the standard system.

TABLE 13 Variation of Transition Temperature with Band Width

Band width (e.v.):	1.0	1.5	2.0	2.5	3.0
T_c	4033°K	3698°K	3456°K	3249°K	3060°K

Calculated transition temperatures thus appear to be relatively insensitive to the band width in the region of interest.

Checks were made to determine if the 9 unit cells and 10 q values in the standard model system were sufficient to give transition temperatures which were independent of the number of unit cells and q values.

Representative results are shown in Table 14 using 10 q values with various numbers of unit cells with four pyridine dicarbocyanine molecules per unit cell. Results using 20 q values and 17 unit cells are shown in parentheses in Table 14. As can be seen from the table, use of the small number of unit cells and q values may account for a variation in T_c of the order of 20%.

TABLE 14 Variation of Transition Temperature with Number of Unit Cells and q Values

Number of unit cells:		9	11	13	15	17	
T_c $(\lambda = 0.0)$	v_o	816°K	811°K	886°K	928°K	942°K	(886°K)
	$\tilde{v}_o$	6117°K	6083°K	6030°K	5998°K	5993°K	(5862°K)

We may comment now on several of the objections raised against the possibility of high temperature excitonic superconductivity as noted in Chapter I. Perhaps the most apparent conclusion is that structures with metal atom chains complexed with certain dye molecules can give rise to a large attractive interaction between spine electrons. Lack of Thomas-Fermi screening on the level found in metals does not result in Coulomb domination of the excitonic interaction as Kuper suggested.[23]

The possibility of a Peierls instability still remains one of competing mechanisms. The transition temperatures of the order of 10^3 °K obtained in the present calculations are expected to be larger than characteristic temperatures for a Peierls transition. Such a competition may occur in Nb_3Sn and similar compounds (known as A-15 compounds) that have a linear chain structure.[156] A theoretical

treatment of these mechanisms has been carried out by Gutfreund, et. al.,[157] who conclude that in principle either mechanism may dominate. Calculation of the Peierls transition temperature along the lines given by Gutfreund, et. al. could be carried out, but comparison of order of magnitude results for T_p with current ones for T_c would not likely support a definitive conclusion.

Among the objections noted in the first chapter, the most elusive seems to be that of the general stability of the lattice for negative values of the static dielectric function. Cohen and Anderson[27] and Allender, Bray, and Bardeen[28] have claimed that the strength of the electron-exciton coupling is not limited by this requirement — inclusion of Umklapp processes being the necessary feature to remove the limitation. Pines and Nozieres[158] have discussed this problem using a jellium model for which the lattice structure is neglected, thus Umklapp processes are not relevant. They find that negative values for the static dielectric function would be accompanied by density waves in the jellium background. A simple calculation by using (19) and the values for the Coulomb interaction, scattering matrix elements, and transition energy for the standard reference system, for example, gives a value $\mathrm{Re}(1/\epsilon(q=0,\omega=0)) = -2$. Thus this question of lattice stability is significant, but as yet it is not known if Umklapp processes and other lattice features would allow for a stable lattice under these conditions. Perhaps this comment by Ginsburg should be noted:[159] "One should keep in mind that even [$V(q,\omega) = V_o(q)/\epsilon(q,\omega)$ (18)] is not always applicable since it does

not take into account the anisotropy and inhomogeniety of the crystal (generally, the dielectric permeability $\epsilon_{ij}(\omega,\vec{q})$ is a tensor), and, more important, in an inhomogeneous system (crystal), this tensor describes the electromagnetic properties of the medium only for waves with wavelength $\lambda \gg a$."

From the results of our present calculations, or estimations since they rely on parameters taken in some cases from systems that model only a portion, (for example, the spine), of the total system, we may reasonably conclude that excitonic superconductivity can be expected from structures that conform to the basic requirements of the Little model. Of primary importance is the close proximity (complexation appears to be the only possibility) of the excitonic system to the spine. Also important is the use of dye molecules with a large transition dipole for a low-lying excited state and which provide for dielectric screening in the region near the spine.

The particular dye molecules we have used in the models have not yet been complexed to the metal atoms. If this is possible, three problem areas remain to be solved by ingeneous synthesis. First, the metal-atom - ligand system must stack in chains. Without this, no delocalization of the electrons on the metal atoms can take place. Second, the spacing between metal atoms along the chain must be sufficiently small for banding to occur. And, finally, a partial oxidation of the spine must be achievable without destroying the ligand system. Thus far, partial oxidation of platinum chain systems has been carried out for a few ligand systems.[160] These are formidable synthetic challenges.

APPENDIX

APPLICATION OF THE BOGOLIUBOV TRANSFORMATION TO THE FROHLICH HAMILTONIAN

The Frohlich Hamiltonian for the coupled electron-phonon system is given by

$$H = \sum_{k\sigma} \epsilon_k c^\dagger_{k\sigma} c_{k\sigma} + \sum_q \omega_q b^\dagger_q b_q + \sum'_{k,k',\sigma} M_q \, c^\dagger_{k\sigma} \, c_{k'\sigma} \, (b^\dagger_q + b_{-q})$$

where $q = k' - k$, the prime on the summation sign indicates the $k = k'$ term is omitted, and ϵ_k is the unrenormalized electron state energy with $\epsilon_k = \epsilon_{-k}$ for an isotropic system. The Bogoliubov transformation takes the general form

$$\alpha^\dagger_k = u_k c^\dagger_{k\uparrow} - v_k c_{-k\downarrow} \qquad \alpha_k = u_k c_{k\uparrow} - v_k c^\dagger_{-k\downarrow}$$

$$\beta_{-k} = u_k c_{-k\downarrow} + v_k c^\dagger_{k\uparrow} \qquad \beta^\dagger_{-k} = u_k c^\dagger_{-k\downarrow} + v_k c_{k\uparrow}$$

and $u_k^2 + v_k^2 = 1$ is imposed to preserve the anti-commutation properties for the quasiparticle operators:

$$[\alpha_k, \alpha^\dagger_{k'}]_+ = \delta_{kk'} \qquad [\alpha_k, \alpha_{k'}]_+ = [\alpha^\dagger_k, \alpha^\dagger_{k'}]_+ = 0$$

$$[\beta_k, \beta^\dagger_{k'}]_+ = \delta_{kk'} \qquad [\beta_k, \beta_{k'}]_+ = [\beta^\dagger_k, \beta^\dagger_{k'}]_+ = 0 \; .$$

Combinations of α and β operators anti-commute. The inverse

transformation is given by:

$$c^{\dagger}_{k\uparrow} = u_k\alpha^{\dagger}_k + v_k\beta_{-k} \qquad c_{k\uparrow} = u_k\alpha_k + v_k\beta^{\dagger}_{-k}$$

$$c_{-k\downarrow} = u_k\beta_{-k} - v_k\alpha^{\dagger}_k \qquad c^{\dagger}_{-k\downarrow} = u_k\beta^{\dagger}_{-k} - v_k\alpha_k \ .$$

The general product of a creation and destruction operator for spin-up electrons transforms as:

$$c^{\dagger}_{k\uparrow}c_{k'\uparrow} = (u_k\alpha^{\dagger}_k + v_k\beta_{-k})(u_{k'}\alpha_{k'} + v_{k'}\beta^{\dagger}_{-k'})$$

$$= u_ku_{k'}\alpha^{\dagger}_k\alpha_{k'} + v_ku_{k'}\beta_{-k}\alpha_{k'} + u_kv_{k'}\alpha^{\dagger}_k\beta^{\dagger}_{-k'} + v_kv_{k'}\beta_{-k}\beta^{\dagger}_{-k'}$$

and for spin-down electrons:

$$c^{\dagger}_{-k\downarrow}c_{-k'\downarrow} = (u_k\beta^{\dagger}_{-k} - v_k\alpha_k)(u_{k'}\beta_{-k'} - v_{k'}\alpha^{\dagger}_{k'})$$

$$= u_ku_{k'}\beta^{\dagger}_{-k}\beta_{-k'} - v_ku_{k'}\alpha_k\beta_{-k'} - u_kv_{k'}\beta^{\dagger}_{-k}\alpha^{\dagger}_{k'} + v_kv_{k'}\alpha_k\alpha^{\dagger}_{k'} \ .$$

Thus the terms of the Frohlich Hamiltonian become

$$\sum_{k\sigma} \epsilon_k c^{\dagger}_{k\sigma}c_{k\sigma} = \sum_k \epsilon_k\left\{c^{\dagger}_{k\uparrow}c_{k\uparrow} + c^{\dagger}_{-k\downarrow}c_{-k\downarrow}\right\}$$

$$= \sum_k \epsilon_k\left\{u_k^2\alpha^{\dagger}_k\alpha_k + u_kv_k(\alpha^{\dagger}_k\beta^{\dagger}_{-k} + \beta_{-k}\alpha_k) + v_k^2\beta_{-k}\beta^{\dagger}_{-k}\right.$$

$$\left. + u_k^2\beta^{\dagger}_{-k}\beta_{-k} - u_kv_k(\beta^{\dagger}_{-k}\alpha^{\dagger}_k + \alpha_k\beta_{-k}) + v_k^2\alpha_k\alpha^{\dagger}_k\right\}$$

$$= \sum_k \epsilon_k\left\{(u_k^2 - v_k^2)(\alpha^{\dagger}_k\alpha_k + \beta^{\dagger}_{-k}\beta_{-k}) + 2u_kv_k(\alpha^{\dagger}_k\beta^{\dagger}_{-k} + \beta_{-k}\alpha_k) + 2v_k^2\right\}$$

and

$$\sum_{k,k'\sigma}{}' M_q c^\dagger_{k\sigma} c_{k'\sigma} (b^\dagger_q + b_{-q})$$

$$= \sum_{k,k',\sigma}{}' M_q (c^\dagger_{k\uparrow} c_{k'\uparrow} + c^\dagger_{-k'\downarrow} c_{-k\downarrow})(b^\dagger_q + b_{-q})$$

$$= \sum_{k,k'}{}' M_q (b^\dagger_q + b_{-q}) \Big\{ u_k u_{k'} \alpha^\dagger_k \alpha_{k'} + v_k u_{k'} \beta_{-k} \alpha_{k'} + u_k v_{k'} \alpha^\dagger_k \beta^\dagger_{-k'} + v_k v_{k'} \beta_{-k} \beta^\dagger_{-k'}$$

$$+ u_k u_{k'} \beta^\dagger_{-k'} \beta_{-k} - u_k v_{k'} \alpha_{k'} \beta_{-k}$$

$$- u_{k'} v_k \beta^\dagger_{-k} \alpha^\dagger_{k'} + v_k v_{k'} \alpha_{k'} \alpha^\dagger_k \Big\}$$

$$= \sum_{k,k'}{}' M_q \Big\{ (u_k v_{k'} + u_{k'} v_k)(\alpha^\dagger_k \beta^\dagger_{-k'} + \beta_{-k} \alpha_{k'})(b^\dagger_q + b_{-q})$$

$$+ (u_k u_{k'} - v_k v_{k'})(\alpha^\dagger_k \alpha_{k'} + \beta^\dagger_{-k'} \beta_{-k})(b^\dagger_q + b_{-q}) \Big\} \quad .$$

Collecting, we may write this as

$$H = H_0 + H_1^\alpha + H_2^\alpha + H_1^\beta + H_R + U$$

where

$$H_0 \equiv \sum_k E_k (\alpha^\dagger_k \alpha_k + \beta^\dagger_{-k} \beta_{-k}) + \sum_q \omega_q \, b^\dagger_q \, b_q$$

$$H_1^\alpha \equiv \sum_{k,k'}{}' M_q \Big\{ (u_k v_{k'} + u_{k'} v_k)(\alpha^\dagger_k \beta^\dagger_{-k'} + \beta_{-k} \, \alpha_{k'})(b^\dagger_q + b_{-q}) \Big\}$$

$$H_2^\alpha \equiv \sum_{k,k'}{}' M_q \Big\{ (u_k u_{k'} - v_k v_{k'})(\alpha^\dagger_k \alpha_{k'} + \beta^\dagger_{-k'} \beta_{-k})(b^\dagger_q + b_{-q}) \Big\}$$

$$H_1^\beta \equiv \sum_k 2\epsilon_k u_k v_k (\alpha_k^\dagger \beta_{-k}^\dagger + \beta_{-k} \alpha_k)$$

$$H_R \equiv \sum_k \left(\epsilon_k (u_k^2 - v_k^2) - E_k \right) (\alpha_k^\dagger \alpha_k + \beta_{-k}^\dagger \beta_{-k})$$

$$U \equiv \sum_k 2\epsilon_k v_k^2 = \text{constant} .$$

Compensation of dangerous diagrams for the creation of a pair of quasiparticles gives the condition

$$\langle F | H_1^\beta | 0 \rangle + \sum_I \frac{\langle F | H_2^\alpha | I \rangle \langle I | H_1^\alpha | 0 \rangle}{E_0 - E_I} = 0$$

where $|0\rangle$ is the vacuum state with energy U, $|I\rangle$ the intermediate state generated by H_1^α, and the final state $|F\rangle$ has a pair of quasiparticles, α_k and β_{-k} (see Figure 10). The energy of the intermediate state is given by

$$\langle I | H | I \rangle = \langle I | \sum_{k''} \epsilon_{k''} (u_{k''}^2 - v_{k''}^2)(\alpha_{k''}^\dagger \alpha_{k''} + \beta_{-k''}^\dagger \beta_{-k''}) + \sum_q \omega_q b_q^\dagger b_q + U | I \rangle .$$

This gives the same energy for $|I\rangle = |1_{\alpha_k}, 1_{\beta_{-k}}; 1_{\omega_q}\rangle$ and $|I\rangle = |1_{\alpha_{k'}}, 1_{\beta_{-k}}; 1_{\omega_q}\rangle$, namely:

$$E_I = \epsilon_k (u_k^2 - v_k^2) + \epsilon_{k'} (u_{k'}^2 - v_{k'}^2) + \omega_q + U .$$

The energy denominator is then $-\{\epsilon_k (u_k^2 - v_k^2) + \epsilon_{k'} (u_{k'}^2 - v_{k'}^2) + \omega_q\}$.

For the matrix elements we have

$$\langle F|H_1^{\beta}|0\rangle = \langle 1_{\alpha_k}, 1_{\beta_{-k}}| \sum_{k''} 2\epsilon_{k''} u_{k''} v_{k''} (\alpha^{\dagger}_{k''}\beta^{\dagger}_{-k''} + \beta_{-k''}\alpha_{k''})|0\rangle$$

$$= 2\epsilon_{k''} u_{k''} v_{k''} \quad \delta_{k,k''} \quad ,$$

$$\langle I|H_1^{\alpha}|0\rangle = \langle 1_{\alpha_k}, 1_{\beta_{-k'}}; 1_{\omega_q}| \sum_{k''k'''}{}' M_q \Big\{ (u_{k''} v_{k'''} + u_{k'''} v_{k''}) \times (\alpha^{\dagger}_{k''}\beta^{\dagger}_{-k'''} + \beta_{-k''}\alpha_{k'''})(b^{\dagger}_q + b_{-q}) \Big\} |0\rangle$$

$$= M_q (u_{k''} v_{k'''} + u_{k'''} v_{k''}) \ \delta_{k'',k} \delta_{k''',k'} \quad ,$$

$$\langle F|H_2^{\alpha}|I\rangle = \langle 1_{\alpha_k}, 1_{\beta_{-k}}| \sum_{k'',k'''}{}' M_q \Big\{ (u_{k''} u_{k'''} - v_{k''} v_{k'''})(\alpha^{\dagger}_{k''}\alpha_{k'''} + \beta^{\dagger}_{-k'''}\beta_{-k''}) \times (b^{\dagger}_q + b_{-q}) \Big\} |1_{\alpha_k}, 1_{\beta_{-k'}}; 1_{\omega_q}\rangle$$

$$= M_q (u_{k''} u_{k'''} - v_{k''} v_{k'''}) \ \delta_{k'',k'} \delta_{k''',k} \quad .$$

Similarly

$$\langle 1_{\alpha_k}, 1_{\beta_{-k}}|H_2^{\alpha}|1_{\alpha_{k'}}, 1_{\beta_{-k}}; 1_{\omega_q}\rangle \langle 1_{\alpha_{k'}}, 1_{\beta_{-k'}}; 1_{\omega_q}|H_1^{\alpha}|0\rangle$$

$$= \Big\{ M_q (u_{k''} u_{k'''} - v_{k''} v_{k'''}) \delta_{k'',k} \delta_{k''',k'} \Big\} \Big\{ M_q (u_{k''} v_{k'''} + u_{k'''} v_{k''}) \delta_{k'',k'} \delta_{k''',k} \Big\} \quad .$$

Thus both intermediates give the same value and the compensation

condition becomes

$$2\epsilon_k u_k v_k - 2 \sum_{k'}' \frac{|M_q|^2 (u_{k'} u_k - v_{k'} v_k)(u_{k'} v_k + u_k v_{k'})}{\epsilon_k (u_k^2 - v_k^2) + \epsilon_{k'} (u_{k'}^2 - v_{k'}^2) + \omega_q} = 0 \quad .$$

Rearranging the terms gives

$$\epsilon_k u_k v_k - \sum_{k'}' \frac{|M_q|^2 \{ (u_{k'}^2 - v_{k'}^2) u_k v_k + (u_k^2 - v_k^2) u_{k'} v_{k'} \}}{\epsilon_k (u_k^2 - v_k^2) + \epsilon_{k'} (u_{k'}^2 - v_{k'}^2) + \omega_q} = 0 \quad .$$

We denote $\epsilon_k (u_k^2 - v_k^2)$ by E_k and define the renormalized quasi-particle energy by

$$\xi_k \equiv \epsilon_k - \sum_{k'}' \frac{|M_q| (u_{k'}^2 - v_{k'}^2)}{E_k + E_{k'} + \omega_q} \quad .$$

Defining the gap function by

$$u_k^2 = (1/2) \left(1 + \frac{\xi_k}{\sqrt{\xi_k^2 + \Delta_k^2}} \right) \quad , \quad \text{then} \quad v_k^2 = (1/2) \left(1 - \frac{\xi_k}{\sqrt{\xi_k^2 + \Delta_k^2}} \right)$$

and

$$u_k v_k = (1/2) \left\{ \left(1 + \frac{\xi_k}{\sqrt{\xi_k^2 + \Delta_k^2}} \right) \left(1 - \frac{\xi_k}{\sqrt{\xi_k^2 + \Delta_k^2}} \right) \right\}^{1/2}$$

$$= (1/2) \left\{ 1 - \frac{\xi_k^2}{\xi_k^2 + \Delta_k^2} \right\}^{1/2}$$

$$= (1/2) \frac{\Delta_k}{\sqrt{\xi_k^2 + \Delta_k^2}} \quad .$$

The compensation condition becomes

$$0 = \xi_k u_k v_k - (u_k^2 - v_k^2) \sum_{k'}{}' \frac{|M_q| u_{k'} v_{k'}}{E_k + E_{k'} + \omega_q}$$

$$= (1/2) \frac{\xi_k \Delta_k}{\sqrt{\xi_k^2 + \Delta_k^2}} - (1/2) \frac{\xi_k}{\sqrt{\xi_k^2 + \Delta_k^2}} \sum_{k'}{}' \frac{\Delta_{k'}}{\sqrt{\xi_{k'}^2 + \Delta_{k'}^2}} \frac{|M_q|^2}{E_k + E_{k'} + \omega_q} ,$$

giving the gap equation

$$\Delta_k = \sum_{k'} \frac{\Delta_{k'}}{\sqrt{\xi_{k'}^2 + \Delta_{k'}^2}} \frac{|M_q|^2}{E_k + E_{k'} + \omega_q} .$$

Compensation of dangerous diagrams using the renormalization term H_R gives the condition

$$\langle F|H_R|F\rangle + \sum_I \frac{\langle F|H_2^\alpha|I\rangle\langle I|H_2^\alpha|F\rangle}{E_F - E_I^{EX}} + \frac{\langle F|H_1^\alpha|I\rangle\langle I|H_1^\alpha|F\rangle}{E_F - E_I^{VP}} = 0 ,$$

where the initial and final states are $|F\rangle = |1_{\alpha_k}\rangle$. Diagrams for these terms are given in Figure 12. The energies of the initial state, intermediate exchange state, and intermediate vacuum polarization state are

$$E_F = \langle 1_{\alpha_k}|H|1_{\alpha_k}\rangle = \langle 1_{\alpha_k}| \sum_{k''} \epsilon_{k''}(u_{k''}^2 - v_{k''}^2)\alpha_{k''}^\dagger \alpha_{k''} + U |1_{\alpha_k}\rangle$$

$$= \epsilon_k(u_k^2 - v_k^2) + U$$

$$E_I^{EX} = \langle 1_{\alpha_{k'}}; 1_{\omega_q}| \sum_{k''} \epsilon_{k''}(u_{k''}^2 - v_{k''}^2)\alpha_{k''}^\dagger \alpha_{k''} + \sum_q \omega_q b_q^\dagger b_q + U |1_{\alpha_{k'}}; 1_{\omega_q}\rangle$$

$$= \epsilon_{k'}(u_{k'}^2 - v_{k'}^2) + \omega_q + U$$

$$E_I^{VP} = \langle 1_{\alpha_k}, 1_{\alpha_{k''}}, 1_{\beta_{-k'''}}; 1_{\omega_q} | \sum_{k'} \epsilon_{k'}(u_{k'}^2 - v_{k'}^2)(\alpha_{k'}^\dagger \alpha_{k'} + \beta_{-k'}^\dagger \beta_{-k'}) + \sum_q \omega_q b_q^\dagger b_q + U | 1_{\alpha_k}, 1_{\alpha_{k''}}, 1_{\beta_{-k'''}}; 1_{\omega_q} \rangle$$

$$= \epsilon_k(u_k^2 - v_k^2) + \epsilon_{k''}(u_{k''}^2 - v_{k''}^2) + \epsilon_{k'''}(u_{k'''}^2 - v_{k'''}^2) + \omega_q + U \quad .$$

For the matrix elements we have

$$\langle F | H_R | F \rangle = \langle 1_{\alpha_k} | \sum_{k'} \left(\epsilon_{k'}(u_{k'}^2 - v_{k'}^2) - E_{k'} \right) (\alpha_{k'}^\dagger \alpha_{k'} + \beta_{-k'}^\dagger \beta_{-k'}) | 1_{\alpha_k} \rangle$$

$$= \left\{ \epsilon_{k'}(u_{k'}^2 - v_{k'}^2) - E_{k'} \right\} \delta_{k',k} \quad ,$$

$$\langle I | H_2^\alpha | F \rangle = \langle 1_{\alpha_{k'}}; 1_{\omega_q} | \sum_{k'',k'''}{}' M_q \Big\{ (u_{k''} u_{k'''} - v_{k''} v_{k'''})(\alpha_{k''}^\dagger \alpha_{k'''} + \beta_{-k'''}^\dagger \beta_{-k''}) \times (b_q^\dagger + b_{-q}) | 1_{\alpha_k} \rangle$$

$$= M_q(u_{k''} u_{k'''} - v_{k''} v_{k'''}) \, \delta_{k',k''} \delta_{k,k'''}$$

and

$$\langle I | H_1^\alpha | F \rangle = \langle 1_{\alpha_k}, 1_{\alpha_{k''}}, 1_{\beta_{-k'''}}; 1_{\omega_q} | \sum_{k',k'''}{}' M_q(u_{k'} v_{k'''} + u_{k'''} v_{k'}) \times (\alpha_{k'}^\dagger \beta_{-k'''}^\dagger + \beta_{-k'} \alpha_{k'''})(b_q^\dagger + b_{-q}) | 1_{\alpha_k} \rangle$$

$$= M_q(u_{k'} v_{k'''} + u_{k'''} v_{k'}) \, \delta_{k',k''} \delta_{k''',k'''} \quad .$$

Collecting this together with the energy denominators gives the compensation condition

$$\epsilon_k(u_k^2 - v_k^2) - E_k + \sum_{k'}{}' \frac{|M_q|^2(u_{k'}u_k - v_{k'}v_k)^2}{\epsilon_k(u_k^2 - v_k^2) - \epsilon_{k'}(u_{k'}^2 - v_{k'}^2) - \omega_q}$$

$$+ \sum_{\substack{k'',k''' \\ k''\neq k \\ k'''\neq k''}} \frac{|M_q|^2(u_{k''}v_{k'''} + u_{k'''}v_{k''})}{-\epsilon_{k''}(u_{k''}^2 - v_{k''}^2) - \epsilon_{k'''}(u_{k'''}^2 - v_{k'''}^2) - \omega_q} = 0 .$$

The last term can be made independent of k by adding and subtracting from the equation

$$\sum_{k'''\neq k} \frac{|M_q|^2(u_k v_{k'''} + u_{k'''}v_k)}{-\epsilon_k(u_k^2 - v_k^2) - \epsilon_{k'''}(u_{k'''}^2 - v_{k'''}^2) - \omega_q} .$$

This gives

$$\epsilon_k(u_k^2 - v_k^2) - E_k - \sum_{k'}{}' \frac{|M_q|^2(u_{k'}u_k - v_{k'}v_k)^2}{E_{k'} - E_k + \omega_q} + \sum_{k'}{}' \frac{|M_q|^2(u_k v_{k'} + u_{k'}v_k)}{E_{k'} + E_k + \omega_q} = 0$$

where we have let $k''' \to k'$ in the final term and dropped the constant term. Renormalization makes a negligible contribution in the energy denominators, therefore we have used E_k and $E_{k'}$.

Using the previous definitions for the gap Δ_k in terms of u_k and v_k we find

$$(u_{k'}u_k - v_k v_{k'})^2 = \frac{1}{2}\left\{1 + \frac{\xi_k\xi_{k'} - \Delta_k\Delta_{k'}}{\sqrt{(\xi_k^2 + \Delta_k^2)(\xi_{k'}^2 + \Delta_{k'}^2)}}\right\}$$

and

$$(u_{k'}v_k + u_k v_{k'})^2 = \frac{1}{2}\left\{1 - \frac{\xi_k\xi_{k'} - \Delta_k\Delta_{k'}}{\sqrt{(\xi_k^2+\Delta_k^2)(\xi_{k'}^2+\Delta_{k'}^2)}}\right\} .$$

Using these in the compensation condition gives

$$\epsilon_k(u_k^2 - v_k^2) - E_k - \frac{1}{2}\sum_{k'}' |M_q|^2 \left\{\left[1 + \frac{\xi_k\xi_{k'} - \Delta_k\Delta_{k'}}{\sqrt{(\xi_k^2+\Delta_k^2)(\xi_{k'}^2+\Delta_{k'}^2)}}\right]\frac{1}{E_{k'} - E_k + \omega_q}\right.$$

$$\left. - \left[1 - \frac{\xi_k\xi_{k'} - \Delta_k\Delta_{k'}}{\sqrt{(\xi_k^2+\Delta_k^2)(\xi_{k'}^2+\Delta_{k'}^2)}}\right]\frac{1}{E_{k'} + E_k + \omega_q}\right\} = 0 .$$

Making use of the symmetry about the Fermi surface, terms odd in $\xi_{k'}$ vanish in the sum giving

$$\epsilon_k(u_k^2 - v_k^2) - E_k - \frac{1}{2}\sum_{k'}' |M_q|^2 \left\{\frac{1}{E_{k'} - E_k + \omega_q} - \frac{1}{E_{k'} + E_k + \omega_q}\right\}$$

$$+ \frac{1}{2}\frac{\Delta_k}{\sqrt{\xi_k^2+\Delta_k^2}}\sum_{k'}' |M_q|^2 \frac{\Delta_{k'}}{\sqrt{\xi_{k'}^2+\Delta_{k'}^2}}\left\{\frac{1}{E_{k'} - E_k + \omega_q} + \frac{1}{E_{k'} + E_k + \omega_q}\right\} = 0 .$$

We are led to make the definition of the renormalization factor γ_k by

$$\xi_k \equiv \epsilon_k/\gamma_k \quad \text{where} \quad \gamma_k \equiv 1 + \sum_{k'}' \frac{|M_q|^2}{(\omega_q + E_{k'})^2 - E_k^2} .$$

Thus we have

$$\epsilon_k \frac{\xi_k}{\sqrt{\xi_k^2+\Delta_k^2}} - E_k - \frac{1}{2}\sum_{k}' \frac{2|M_q|^2 E_k}{(E_{k'} + \omega_q)^2 - E_k^2} + \frac{1}{2}\frac{\Delta_k}{\sqrt{\xi_k^2+\Delta_k^2}}\sum_{k'}' |M_q|^2 \frac{\Delta_{k'}}{\sqrt{\xi_{k'}^2+\Delta_{k'}^2}}$$

$$\times\left\{\frac{1}{E_{k'} - E_k + \omega_q} + \frac{1}{E_{k'} + E_k + \omega_q}\right\} = 0 .$$

Multiplying through by $\sqrt{\xi_k^2 + \Delta_k^2}$ and setting $E_k = \sqrt{\xi_k^2 + \Delta_k^2}$ gives

$$\epsilon_k \xi_k - (\xi_k^2 + \Delta_k^2)\gamma_k + \frac{\Delta_k}{2} \sum_{k'}' |M_q|^2 \frac{\Delta_{k'}}{\sqrt{\xi_{k'}^2 + \Delta_{k'}^2}} \left\{ \frac{1}{E_{k'} - E_k + \omega_q} + \frac{1}{E_{k'} + E_k + \omega_q} \right\} = 0$$

Noting that $\epsilon_k = \xi_k \gamma_k$ we may rearrange this to give the self-consistent gap equation

$$\Delta_k = (1/2\ \gamma_k) \sum_{k'}' |M_q|^2 \frac{\Delta_{k'}}{\sqrt{\xi_{k'}^2 + \Delta_{k'}^2}} \left\{ \frac{1}{E_{k'} - E_k + \omega_q} + \frac{1}{E_{k'} + E_k + \omega_q} \right\} = 0 \quad .$$

GLOSSARY

BCS — Bardeen, Cooper, and Schrieffer. The BCS theory was the first successful microscopic theory of superconductivity. The theory accounted for the properties common to superconductors: infinite conductivity, Meissner effect, critical field, persistent current, flux quantization, specific heat and isotope effect.

CI — Configuration Interaction. CI is a method for obtaining a more accurate ground-state wave function by adding excited-state functions to a trial ground-state function. Application of the variational principle determines the degree of admixture of excited states.

ISM — Interrupted Strand Model. This model seeks to explain the optical and conduction properties of one-dimensional systems by accounting for the effects of the finite chain length because of interruptions along the metal-atom chain.

KCP — Potassium Cyanoplatinate. KCP-Br and KCP-Cl denote the square-planar cyanide complexes of platinum that are partially oxidized by bromine and chlorine, respectively.

MGS — Magnus Green Salt. MGS consists of chains of alternating, square-planar, complexes of platinum with ammonia and with chloride ions.

MVP — Mixed Valency Planar, also Mixed Valency Platinum. MVP denotes the square-planar complexes of platinum with cyanide or oxalate ligands that have been partially oxidized because of cation deficiency or an excess of halogen.

RPA — Random Phase Approximation. Also known as the sum of ring diagrams, the RPA seeks to approximate the true interaction between fermions by accounting for the lowest-order polarization process in the many body system, the creation and propagation of a particle-hole pair.

WL — Weak Localization. The WL model seeks to explain the conduction properties of certain one-dimensional systems that have a random distribution of charges or dipoles along the periodic potential. Because of the non-periodic potential of the random distribution, electron states along the chain are localized.

ZDO-SCF-MO — Zero Differential Overlap-Self-Consistent Field-Molecular Orbital. The ZDO procedure for determining molecular orbitals is an approximation that includes electron-electron Coulomb repulsion except for those cases which depend on overlapping charge distributions of atomic orbitals on different atoms.

REFERENCES

1. H. K. Onnes, Commun. Phys. Lab. Univ. Leiden, Suppl., 34b (1913).
2. W. Meissner and R. Ochsenfeld, Naturwiss. 21, 787 (1933).
3. W. H. Keesom and J. A. Kok, Commun. Phys. Lab. Univ. Leiden 221e (1932).
4. C. A. Reynolds, B. Serin, W. H. Wright, and L. B. Nesbitt, Phys. Rev. 78, 487 (1950).
5. E. Maxwell, Phys. Rev. 78, 477 (1950).
6. J. Bardeen, L. N. Cooper, and J. R. Schrieffer, Phys. Rev. 108, 1175 (1957).
7. B. S. Deaver, Jr. and W. M. Fairbank, Phys. Rev. Letters 7, 43 (1961).
8. R. Doll and M. Näbauer, Phys. Rev. Letters 7, 51 (1961).
9. I. Giaever, Phys. Rev. Letters 5, 147 (1960).
10. J. A. Catterall, Metallurgical Rev. 11, 25 (1966).
11. J. R. Gavaler, Appl. Phys. Letters 23, 480 (1973).
12. L. Testardi, J. Wernick, and W. Royer, to be published.
13. W. A. Little, Phys. Rev. A134, 1416 (1964).
14. V. L. Ginsburg, Phys. Letters 13, 101 (1964).
15. V. L. Ginsburg and D. A. Kirzhnits, Soviet Phys. JETP 19, 269 (1964).
16. F. Kampas, J. Polymer Sci. C 29, 81 (1970).

17. R. A. Ferrell, Phys. Rev. Letters 13, 330 (1964).

18. T. M. Rice, Phys. Rev. A140, 1889 (1965).

19. P. C. Hohenberg, Phys. Rev. 158, 383 (1967).

20. W. A. Little, Phys. Rev. 156, 396 (1967).

21. See J. S. Langer, J. Polymer Sci. C 29, 87 (1970) and references cited therein.

22. I. E. Dzyaloshinskii and E. I. Katz, Soviet Phys. JETP 28, 178 (1969).

23. C. G. Kuper, Phys. Rev. 150, 189 (1966).

24. D. Davis, Phys. Rev. B, 7, 129 (1973).

25. For a review see, K. Krogmann, Angew. Chem. Int. Edit., 8, 35 (1969).

26. W. L. McMillan, Phys. Rev. 167, 331 (1968).

27. M. L. Cohen and P. W. Anderson in Superconductivity in d- and f-band Metals, ed. D. H. Douglas (AIP, New York, 1972), p.17.

28. D. Allender, J. Bray, and J. Bardeen, Phys. Rev. B, 7, 1020 (1973).

29. D. A. Kirzhnits, E. G. Maksimov, and D. I. Khomskii, J. Low Temp. Phys. 10, 79 (1973).

30. New Superconductors – First Annual Technical Report – CMR-71-15 (Center for Materials Research, Stanford, California, 1971).

31. E. B. Yagubskii and M. L. Khidekel, Russian Chemical Reviews 41, 1011 (1972).

32. New Superconductors – Fourth Semi-annual Technical Report – CMR-72-12 (Center for Materials Research, Stanford, California, 1972).

33. J. P. Collman, J. K. Hoyano, and D. W. Murphy, J. Am. Chem. Soc. 95, 3424 (1973).

34. New Superconductors – Fifth Semi-annual Technical Report – CMR-73-5 (Center for Materials Research, Stanford, California, 1973).

35. F. Bloch, Z. Phys. 52, 555 (1928).

36. R. de L. Kronig, and W. G. Penney, Proc. Roy. Soc. A, 130, 499 (1931).

37. E. G. Cox, F. W. Pinkard, W. Wardlaw, and G. H. Preston, J. Chem. Soc. (London) 2527 (1932).

38. S. Yamada, J. Am. Chem. Soc. 75, 1579 (1951).

39. S. Yamada, Bull. Chem. Soc. Japan. 24, 125 (1951).

40. R. E. Rundle, J. Phys. Chem. 61, 45 (1957).

41. J. R. Miller, J. Chem. Soc. (London) 4452 (1961).

42. J. Chatt, G. A. Gamlen, and L. E. Orgel, J. Chem. Soc.(London) 486 (1958).

43. R. F. Fenske, D. S. Martin, and K. Ruedenberg, Inorg. Chem. 1, 441 (1962).

44. H. B. Gray and C. J. Ballhausen, J. Am. Chem. Soc. 85, 260 (1963).

45. P. Day, A. F. Orchard, A. J. Thomson, and R.J.P. Williams, J. Chem. Phys. 42, 1973 (1965).

46. J. R. Miller, J. Chem. Soc. (London) 713 (1965).

47. J. Collman, Chem. and Eng. News, 50 (1967).

48. L. Atkinson, P. Day, and R.J.P. Williams, Nature 218, 668 (1968).

49. L. K. Monteith, C. G. Pitt, L. F. Ballard, and M. S. Fowler, Research Triangle Institute, Research Triangle Park, North Carolina, unpublished (1968).

50. F. A. Cotton and G. Wilkinson, Advanced Inorganic Chemistry, 2nd ed. (John Wiley and Sons, New York, 1966), p.713.

51. K. Krogmann and H. D. Hausen, Z. anorg. allg. Chem. 358, 67 (1968).

52. K. Krogmann and P. Dodel, Chem. Ber., 99, 3402 (1966).

53. K. Krogmann, Z. anorg. allg. Chem. 358, 97 (1968).

54. K. Krogmann, Z. Naturforsch. 23b, 1012 (1968).

55. K. Krogmann and H. D. Hausen, Z. Naturforsch. 23b, 1111 (1968).

56. K. Krogmann and G. Ringwald, Z. Naturforsch. 23b, 1112 (1968).

57. K. Krogmann and P. Dodel, Chem. Ber., 99, 3408 (1966).

58. S. B. Piepho, P. N. Schatz, and A. J. McCaffery, J. Am. Chem. Soc. 91, 5994 (1969).

59. M. J. Minot and J. H. Perlstein, Phys. Rev. Letters 26, 371 (1971).

60. A. S. Berenblyum, L. I. Buravov, M. D. Khidekel', I. F. Shchegolev, and E. B. Yakimov, JETP Letters 13, 440 (1971).

61. D. Kuse and H. R. Zeller, Phys. Rev. Letters 27, 1060 (1971).

62. P. Drude, Annalen der Physik 3, 369 (1900).

63. See for example, A. V. Sokolov, Optical Properties of Metals (Blackie and Son, London, 1967).

64. H. P. Geserich, H. D. Hausen, K. Krogmann, and P. Stampel, Phys. Stat. Sol. a10, 187 (1972).

65. P. Brüesch and F. Lehmann, Solid State Commun. 10, 579 (1972).

66. P. Brüesch, Helv. Phys. Acta 46, 427 (1973).

67. A. J. Epstein, S. Etemad, A. F. Garito, and A. J. Heeger, Phys. Rev. B, 5, 952 (1972).

68. N. F. Mott, Proc. Phys. Soc. (London) A62, 416 (1949).

69. J. Hubbard, Proc. Roy. Soc. (London) A276, 238 (1963); A277, 237 (1963); A281, 401 (1964).

70. E. H. Lieb and F. Y. Wu, Phys. Rev. Letters 20, 1445 (1968).

71. A. A. Ovchinnikov, Soviet Phys. JETP 30, 1160 (1970).

72. I. A. Musurkin and A. A. Ovchinnikov, Soviet Physics Solid State 12, 2031 (1970).

73. M. Takahashi, Progr. Theoret. Phys. (Kyoto) 43, 1619 (1970); 42, 1098 (1969); 43, 860(E) (1970).

74. W. Rüegg, D. Kuse, and H. R. Zeller, Phys. Rev. B, 8, 952 (1973).

75. A. N. Bloch, R. B. Weisman, and C. M. Varma, Phys. Rev. Letters 28, 753 (1972).

76. R. E. Borland, Proc. Phys. Soc. 78, 926 (1961).

77. N. F. Mott and W. D. Twose, Adv. Phys. 10, 107 (1971).

78. See for example, N. F. Mott, Adv. Phys. 16, 49 (1967).

79. W. A. Little, private communication.

80. R. L. Greene and W. A. Little, Phys. Rev. Letters 29, 718 (1972).

81. J. Bernasconi, D. Kuse, M. J. Rice, and H. R. Zeller, J. Phys. C, 5, L127 (1972).

82. M. J. Rice and J. Bernasconi, J. Phys. F, 2, 905 (1972); 3, 55 (1973).

83. M. J. Rice and J. Bernasconi, Phys. Letters 38A, 277 (1972).

84. R. E. Peierls, Quantum Theory of Solids (Clarendon Press, London, 1955), p.108-111.

85. W. Kohn, Phys. Rev. Letters 2, 393 (1959).

86. B. Renker, H. Rietschel, L. Pintschovius, W. Gläser, P. Brüesch, D. Kuse, and M. J. Rice, Phys. Rev. Letters 30, 1144 (1973).

87. B. R. Patton and L. J. Sham, Phys. Rev. Letters 31, 631 (1973).

88. P. A. Lee, T. M. Rice, and P. W. Anderson, Phys. Rev. Letters 31, 462 (1973).

89. I. F. Shchegolev, Phys. Stat. Sol. (a), 12, 9 (1972).

90. H. R. Zeller, Adv. in Solid State Phys. 13 (Oxford, England, Pergamon, 1973), p.31-58.

91. R. Comes, M. Lambert, and H. R. Zeller, Phys. Stat. Sol. 58, 587 (1973).

92. H. H. Rupp, Z. Naturforsch. 26a, 1937 (1971).

93. H. Nieboda, H. Launois, D. Brinkmann, R. Brugger, and H. R. Zeller, Phys. Stat. Sol. 58, 309 (1973).

94. F. Mehran and B. A. Scott, Phys. Rev. Letters 31, 1347 (1973).

95. F. Mehran and B. A. Scott, Phys. Rev. Letters 31, 99 (1973).

96. A. Abarbanel, Ph.D. Thesis, Stanford University (1973).

97. For a current review see K. H. Johnson, in Advances in Quantum Chemistry, Vol. 7, ed. P. O. Löwdin (Academic Press, New York, 1974), p.143.

98. J. Bernasconi, P. Brüesch, D. Kuse, and H. R. Zeller, J. Phys. Chem. Solids 35, 145 (1974).

99. P. B. Visscher and L. M. Falicov, Phys. Rev. B, 3, 2541 (1971).

100. B. Bush, Ph.D. Thesis, Stanford University (1973).

101. P. F. Williams, Phys. Rev. B, to be published.

102. J. Paldus and J. Cizek, J. Polymer Sci. C 29, 199 (1970).

103. N. F. Mott and H. Jones, The Theory of the Properties of Metals and Alloys (Dover, New York, 1958), p.48.

104. C. Kittel, Introduction to Solid-State Physics, 3rd. ed. (Wiley, New York, 1966), p.235.

105. F. Oberhettinger, Tabellen zur Fourier Transformation (Springer-Verlag, Berlin, 1957), p.87.

106. H. Gutfreund and W. A. Little, Chem. Phys. Letters 2, 589 (1968).

107. W. A. Little, J. Chem. Phys. 49, 420 (1968).

108. H. Gutfreund and W. A. Little, Phys. Rev. 183, 68 (1969).

109. H. Gutfreund and W. A. Little, J. Chem. Phys. 50, 4468 (1969).

110. H. Gutfreund and W. A. Little, J. Chem. Phys. 50, 4478 (1969).

111. W. A. Little and H. Gutfreund, Phys. Rev. B, 4, 817 (1971).

112. See for example, L. Salem, Molecular Orbital Theory of Conjugated Systems (W. A. Benjamin, Inc., New York, 1966).

113. C.E.K. Mees and T. H. James, The Theory of the Photographic Process, 3rd. ed. (Macmillan, New York, 1966), p.211.

114. A. Streitwieser, Molecular Orbital Theory (Wiley and Sons, New York, 1961), p.105.

115. R. Pariser and R. G. Parr, J. Chem. Phys. 21, 466 (1953).

116. R. Pariser and R. G. Parr, J. Chem. Phys. 21, 767 (1953).

117. J. A. Pople, Trans. Faraday Soc. 49, 1375 (1953).

118. K. Nishimoto and N. Mataga, Z. Physik. Chem. (Frankfurt) 13, 140 (1957).

119. M. Gell-Mann and Brueckner, Phys. Rev. 106, 364 (1957).

120. K. Sawada, Phys. Rev. 106, 372 (1957).

121. J. Hubbard, Proc. Roy. Soc. (London) A243, 336 (1957).

122. F. London and H. London, Proc. Roy. Soc. (London) A149, 71 (1935).

123. V. L. Ginzburg and L. D. Landau, Zh. Eksp. Teor. Fiz. 20, 1064 (1950); Eng. transl: Men of Physics: L. D. Landau, Vol. I, p. 138 (Pergamon Press, Oxford, 1965).

124. See for example, M. Tinkham, Superconductivity (Gordon and Breach, New York, 1965) p.70-82.

125. H. Frohlich, Phys. Rev. 79, 845 (1950).

126. L. N. Cooper, Phys. Rev. 104, 1189 (1956).

127. D. J. Scalapino, in Superconductivity, ed. R. D. Parks (Marcell Decker, Inc., New York, 1969), p.453.

128. J. R. Schrieffer, Superconductivity (W. A. Benjamin, Inc., New York, 1964), p.153.

129. T. Holstein and H. Primakoff, Phys. Rev. 58, 1098 (1940).

130. N. N. Bogoliubov, Soviet Phys. JETP 34, 41 (1958).

131. S. H. Liu, Phys. Rev. 125, 1244 (1962).

132. P. R. Auvil, Jr., Ph.D. Thesis, Stanford University (1962).

133. J. Bardeen, 1962 Cargèse Lectures in Theoretical Physics, (W. A. Benjamin, Inc., New York, 1963), Sec. VI.

134. N. N. Bogoliubov, V. V. Tolmachev, and D. V. Shirkov, A New Method in the Theory of Superconductivity (Consultants Bureau, New York, 1959), p.50ff.

135. P. Morel and P. W. Anderson, Phys. Rev. 125, 1263 (1962).

136. L. P. Gor'kov, Soviet Phys. JETP 34, 505 (1958).

137. G. M. Eliashberg, Soviet Phys. JETP 11, 696 (1960).

138. See for example, J. R. Schrieffer, op. cit., p.164ff.

139. Y. Nambu, Phys. Rev. 117, 648 (1960).

140. A. B. Migdal, Soviet Phys. JETP 7, 996 (1958).

141. D. J. Scalapino, J. R. Schrieffer, and J. W. Wilkins, Phys. Rev. 148, 263 (1966).

142. W. L. McMillan and J. M. Rowell, in Superconductivity, ed. R. D. Parks (Marcell Decker, Inc., New York, 1969), p.561-613.

143. J. C. Swihart, Phys. Rev. 131, 73 (1963).

144. J. Bardeen and D. Pines, Phys. Rev. 99, 1140 (1955).

145. For a discussion, see for example, A. L. Fetter and J. D. Walecka, Quantum Theory of Many-Particle Systems (McGraw-Hill, New York, 1971), p.72ff.

146. See for example, C. Kittel, Quantum Theory of Solids (John Wiley and Sons, New York, 1963), p.111.

147. G. M. Eliashberg, Soviet Phys. JETP 12, 1000 (1961).

148. H. Gutfreund, private communication.

149. A. Messiah, Quantum Mechanics, Vol. I (John Wiley and Sons, New York, 1958), p.469.

150. V. L. Ginsburg, Soviet Physics Uspekhi 13, 335 (1970).

151. See for example, reference 128, p.497.

152. J. C. Swihart, I.B.M. J. Res. Dev. 6, 14 (1962).

153. G. C. Culler, B. D. Fried, R. W. Huff, and J. R. Schrieffer, Phys. Rev. Letters 8, 399 (1962).

154. D. J. Scalapino, Y. Wada, and J. C. Swihart, Phys. Rev. Letters 14, 102 (1965).

155. C. R. Leavens and J. P. Carbotte, Can. J. Phys. 49, 724 (1971).

156. L. R. Testardi, Phys. Rev. B 3, 95 (1971).

157. H. Gutfreund, B. Horovits, and M. Weger, J. Phys. C: Solid State Phys. 7, 383 (1974).

158. D. Pines and P. Nozieres, Theory of Quantum Liquids (W.A. Benjamin, New York, 1966), p. 204-209.

159. V. L. Ginsburg, J. Polymer Sci. C 29, 3 (1970).

160. W. Gitzel, H. J. Keller, H. H. Rapp, and K. Seibold, Z. Naturforsch 27b, 365 (1972).

3781 Davis, D. H.
1974 Investigation of one-dimensional conducting
D systems: screening and exotonic superconductivity
in organometallic compounds.

NAME	ADDRESS	DATE (Stamp)
MARK MARKOCO	[illegible]	MAR 15 1975
	GD	2-14-77
MARK MARKOCO	[illegible]	MAR 08 1977
John T. McDevitt	SH [illegible]	MAR 31 1977
San Marking	GA. I, Rm 4	SEP 22 1984
Letter sent	[illegible]	DEC 17 [illegible]

SUL 54